Electronic Supplementary Material (ESI) for ChemComm.
This journal is © The Royal Society of Chemistry 2016

Supplementary Information

Salt Metathesis for Developing Injectable Supramolecular Metallohydrogelators as Multi-drug-self-delivery System

R. Roy,[a] M. Bhagyalalitha,[a] P. Choudhury[b] and P. Dastidar[a]*

[a]Department of Organic Chemistry and [b]Department of Biological Chemistry

Indian Association for the Cultivation of Science,

2A & 2B Raja S. C. Mullick Road, Jadavpur, Kolkata -700032, India.

E-mail: ocpd@iacs.res.in

Table of Content

Materials, Methods and Synthesis

Materials

Silica gel of 60-120 mesh, all the nonsteroidal anti-inflammatory drugs (NSAIDs), all the L-amino acids, amantadine hydrochloride (**AMN**·HCl), 2-Amino-2-(hydroxymethyl)-1,3-propanediol (**TRIS** or Trizma® base), N-hydroxysuccinimide (NHS), dicyclohexylcarbodiimide (DCC), anhydrous sodium carbonate, zinc nitrate hexahydrate [$Zn(NO_3)_2 \cdot 6H_2O$] were purchased from Sigma-Aldrich Chemical Company. All the chemicals were commercially available and used without further purification. Solvents were of analytical reagent grade (SRL, RANKEM, Merck, Sigma-Aldrich, Avra, S D Fine-Chem Limited, India) and used without further distillation. Gelatin, DMEM, heat inactivated FBS, trypsin from porcine pancreas and 3-(4,5-dimethyl-2-thiazolyl)-2,5-diphenyl-*2H*-tetrazolium bromide (MTT) were obtained from Sigma-Aldrich Chemical Company. PGE_2 assay was performed using Prostaglandin E_2 EIA Kit – Monoclonal (Cayman Chemicals, Ann Arbor, MI, USA). Reagents required for preparing the nutrient broth culture medium for bacterial experiments like peptone, yeast extract, and agar powder were purchased from Himedia Chemical Company, India.

Methods

Melting points of all the salts were determined by Veego programmable melting point apparatus, India. The elemental analyses of the salts were carried out using a Perkin–Elmer Precisely, Series-II, CHNO/S Analyser-2400. The mass spectra were collected using a QTOF Micro YA263 instrument. FT-IR spectra were obtained using instrument FTIR-8300, Shimadzu. NMR spectra (both ^{1}H and ^{13}C) were recorded using 300 MHz spectrometer (Bruker Ultrasheild Plus-300). TEM images were recorded using a JEOL instrument with 300 mesh copper TEM grid. SEM images were recorded using a JEOL JMS-6700F field-emission

scanning electron microscope. Rheology studies were carried out using an Anton Paar Modular Compact Rheometer MCR 102. Emission spectra were recorded with a Fluorolog Horiba Jobinyvon Fluoromax 4C Fluorescence Spectrometer. Single crystal X-ray diffraction data were collected using MoKα (λ = 0.7107 Å) radiation on a BRUKER APEX II diffractometer equipped with CCD area detector. Bruker AXS D8 Advance powder diffractometer equipped with super speed LYNXEYE detector (Cukα1 radiation, λ = 1.5406 Å) scan speed = 0.3 sec/step (step size = 0.02^{o}) was used to collect PXRD data. VARIAN CARY 50 Bio UV-Visible Spectrophotometer was used to measure the concentration of the hydrogelator in biostability, and leaching experiments. MTT and PGE_2 assay were conducted using a multiplate ELISA reader (Varioskan Flash Elisa Reader, Thermo Fisher).

Synthesis of salts

All the salts were prepared by reacting the corresponding acids and amines in 1:1 molar ratio in methanol at room temperature followed by evaporation of the solvent in a rotary evaporator. The resultant solid was isolated as the salt in near-quantitative yield. FT-IR spectra (KBr) of the salts showed the presence of stretching band of the carboxylate group (COO^-) and the absence of carbonyl stretching band (C=O) of COOH group indicating complete salt formation (for a specific example, see Figure S1).

Synthesis of peptides *i.e.* acid part

Indomethacin (3.0 mmol, 1073.37 mg) and N-hydroxysuccinimide (NHS) (3.3 mmol, 379.797 mg) were taken in a two-neck round-bottom flask and 50 mL dry THF was added into it to dissolve these into a homogeneous solution. The reaction mixture was stirred for 10 minutes in an ice-bath (0°-5 °C) in argon atmosphere and then dicyclohexylcarbodiimide (DCC) (4.5 mmol, 928.485 mg) was added into it dropwise taken in a solution of 20 mL dry THF. The reaction mixture was stirred overnight at room temperature. The white precipitate

obtained was filtered off and the filtrate was concentrated under reduced pressure. After evaporation of the solvent, the residue was again dissolved in 60 mL THF and then corresponding L-amino acid (3.0 mmol) dissolved in aqueous sodium carbonate (2.4 mmol, 254.372 mg) was added into it and was stirred for 24 h. THF was removed under reduced pressure and then the solution was acidified with cold aqueous HCl (1N) in a dropwise manner to obtain a white precipitate. The precipitate was filtered and washed with distilled water to remove the excess acid. The solid product thus obtained was dried in vacuum desiccator and was subjected to purify through column chromatography (using 2% MeOH in DCM) to give 73-82% pure product (see Scheme S1).

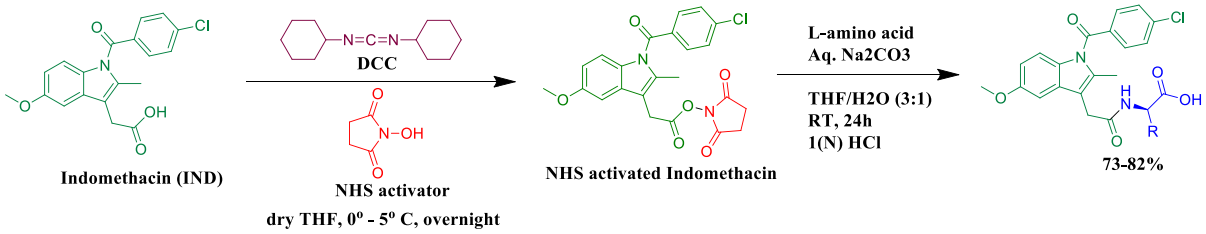

Scheme S1: Typical synthetic route of peptides.

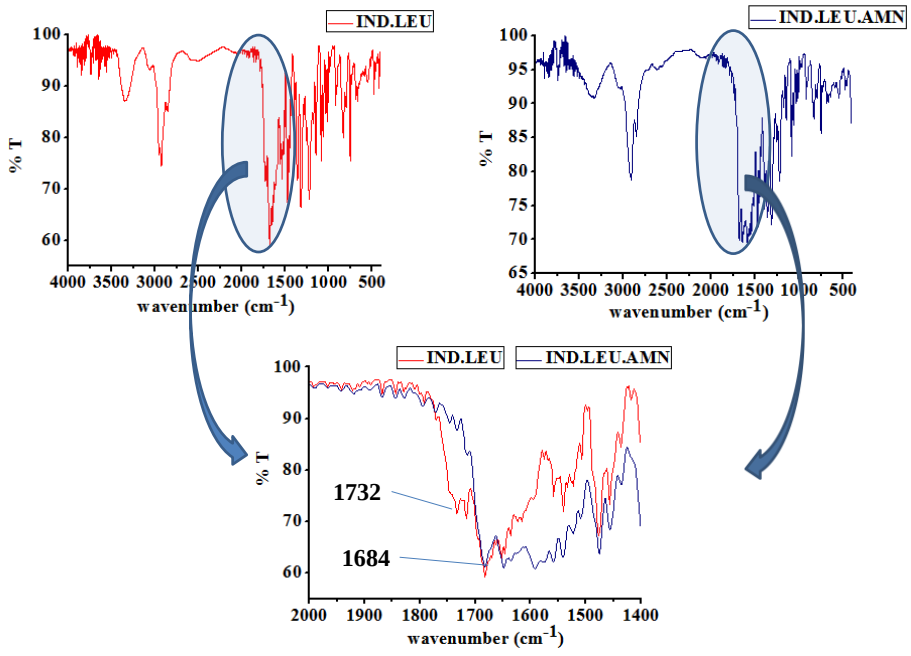

Figure S1: FTIR spectroscopy of **IND.LEU** (acid) and **IND.LEU.AMN** (salt).

Synthesis of metal complexes

Organic salts were reacted with zinc salts in 1:1 or 2:1 Ligand (organic salt):Metal ratio. In these reactions, salt-metathesis *i.e.* cation-anion exchange process happened and thus carboxylate anion of bio-conjugates or free NSAIDs made complex with positively charged zinc(II) metal center. The metal complexes were characterized by FTIR, ^{1}H NMR, CHN analysis; single crystal X-ray diffraction (SXRD) and X-ray powder diffraction (XRPD) (see Scheme S2-S5).

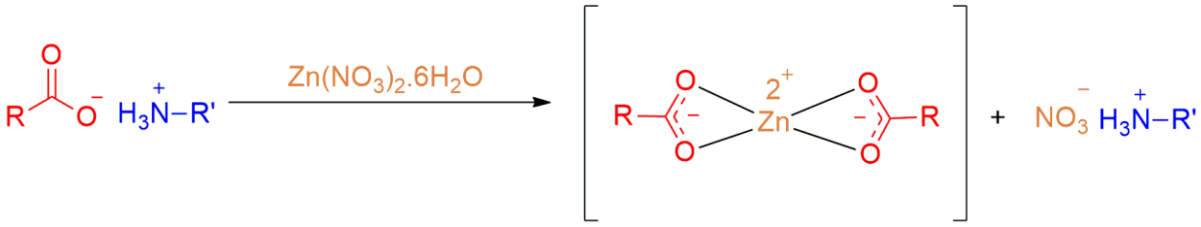

Scheme S2: Typical synthetic route of drug-zinc complexes by salt-metathesis process.

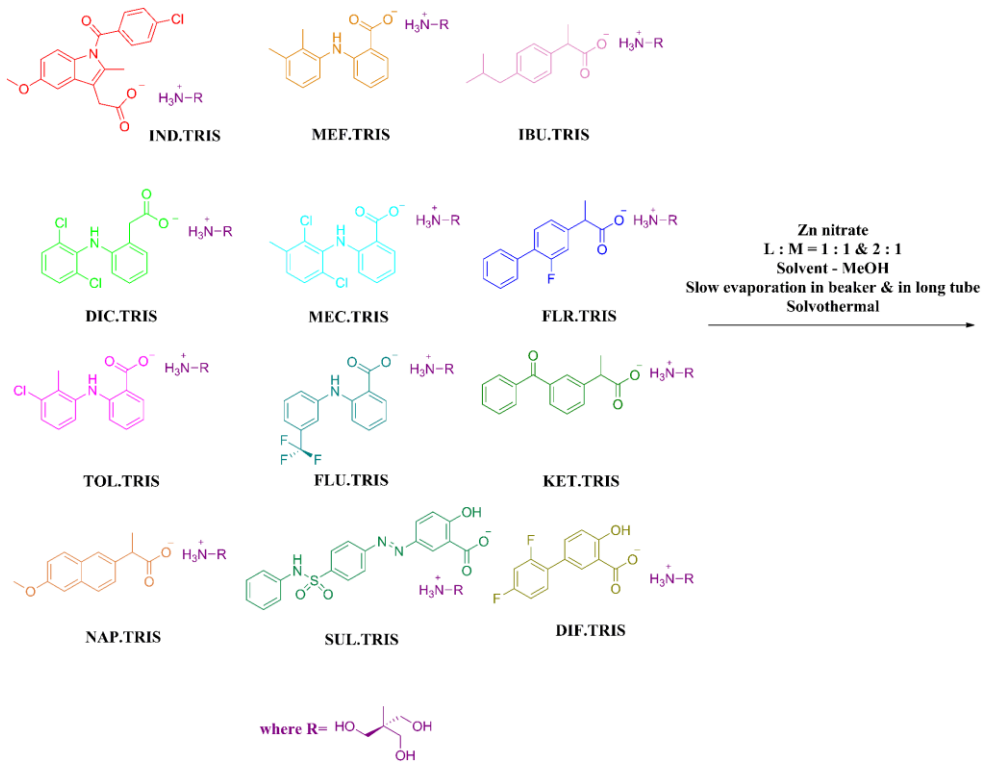

Scheme S3: Various metal complexes derived from the salts comprised of different NSAIDs and tris (**TRIS**).

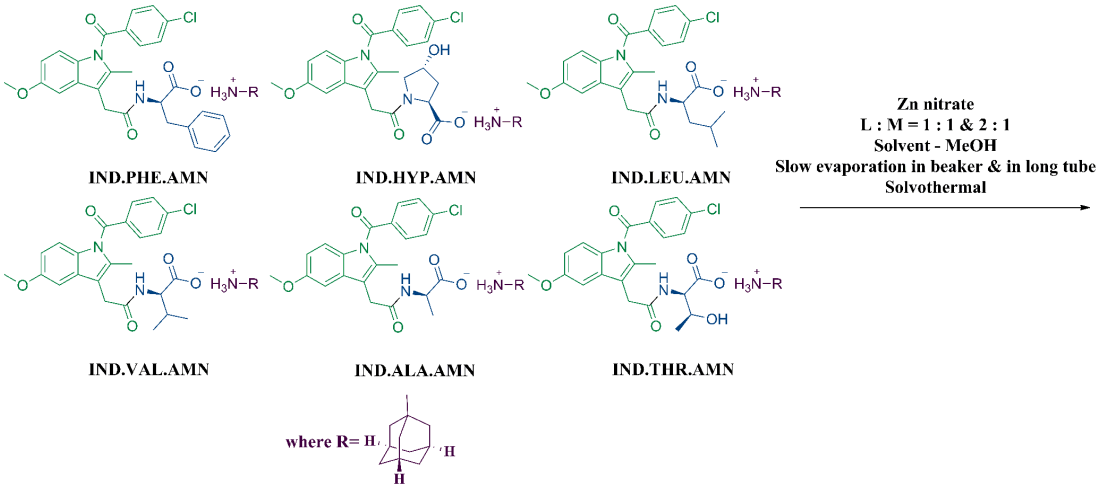

Scheme S4: Various metal complexes derived from the salts comprised of the peptide conjugates of NSAID indomethacin (**IND**) and amantadine (**AMN**).

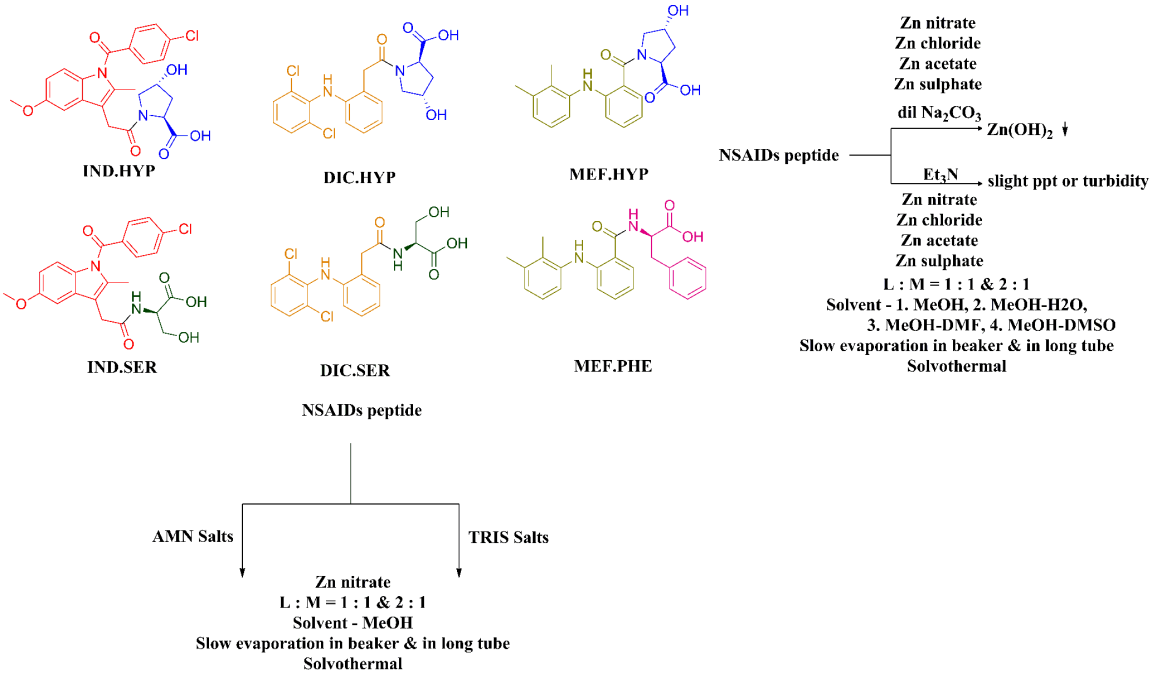

Scheme S5: Various metal complexes derived from the salts comprised of the peptide conjugates of different NSAIDs and amantadine (**AMN**) and tris (**TRIS**).

Characterization of metal complexes

$(IND)_2$.Zn complex: Elemental analysis calculated for $C_{38}H_{30}Cl_2N_2O_8Zn$ (%): C, 58.59; H, 3.88; N, 3.60; found: C, 58.26; H, 3.45; N, 3.24%; FT-IR (KBr pellet): 1679 (s, COO^- i.e. carboxylate C=O stretch) cm^{-1}.

$(DIC)_2$.Zn complex: Elemental analysis calculated for $C_{28}H_{20}Cl_4N_2O_4Zn$ (%): C, 51.29; H, 3.07; N, 4.27; found: C, 51.26; H, 3.34; N, 4.56%; FT-IR (KBr pellet): 1577 (s, COO^- i.e. carboxylate C=O stretch) cm^{-1}.

$(TOL)_2$.Zn complex: Elemental analysis calculated for $C_{28}H_{22}Cl_2N_2O_4Zn$ (%): C, 57.31; H, 3.78; Cl, 12.08; N, 4.77; found: C, 57.74; H, 3.52; N, 5.13%; FT-IR (KBr pellet): 1649 (s, COO^- i.e. carboxylate C=O stretch) cm^{-1}.

$(FLR)_2$.Zn complex: Elemental analysis calculated for $C_{30}H_{24}F_2O_4Zn$ (%): C, 65.29; H, 4.38; found: C, 65.88; H, 4.87%; FT-IR (KBr pellet): 1635 (s, COO^- i.e. carboxylate C=O stretch) cm^{-1}.

$(SUL)_2$.Zn complex: Elemental analysis calculated for $C_{38}H_{28}N_6O_{10}S_2Zn$ (%): C, 53.18; H, 3.29; N, 9.79; found: C, 52.69; H, 3.48; N, 9.37%; FT-IR (KBr pellet): 1604 (s, COO^- i.e. carboxylate C=O stretch) cm^{-1}.

$(DIF)_2$.Zn complex: Elemental analysis calculated for $C_{26}H_{14}F_4O_6Zn$ (%): C, 55.39; H, 2.50; found: C, 55.95; H, 3.14%; FT-IR (KBr pellet): 1631 (s, COO^- i.e. carboxylate C=O stretch) cm^{-1}.

$(IBU)_2$.Zn complex: Elemental analysis calculated for $C_{26}H_{34}O_4Zn$ (%): C, 65.61; H, 7.20; found: C, 62.06; H, 7.56; FT-IR (KBr pellet): 1639 (s, COO^- i.e. carboxylate C=O stretch) cm^{-1}.

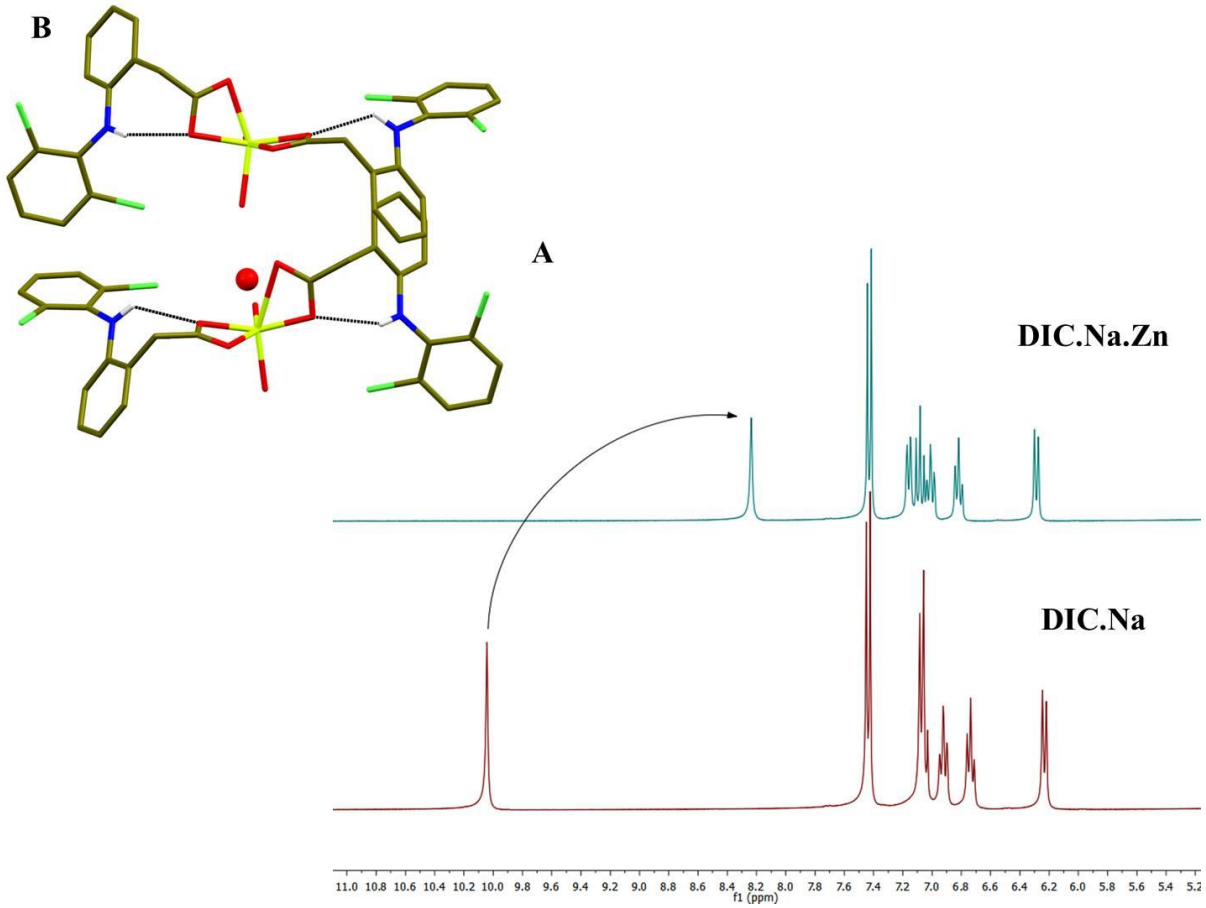

Figure S2: A) Change in δ value of N-H proton of **DIC.Na** and **DIC.Na.Zn** complex involved in intramolecular H-bonding depicted in ^{1}H NMR spectrum of **DIC.Na** and **DIC.Na.Zn** complex; B) intramolecular N-H···O H-bonding present in the crystal structure of **DIC.Na.Zn** complex.

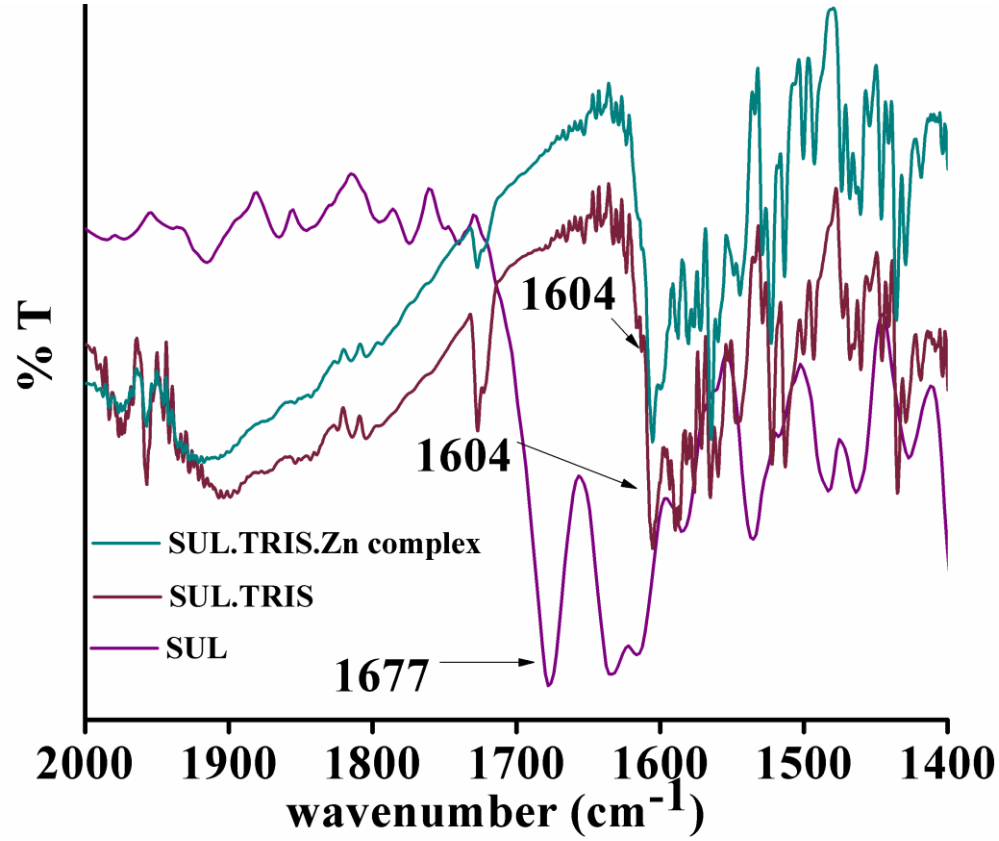

Figure S3: FTIR spectroscopy of **SUL**, **SUL.TRIS** and **SUL.TRIS.Zn** complex.

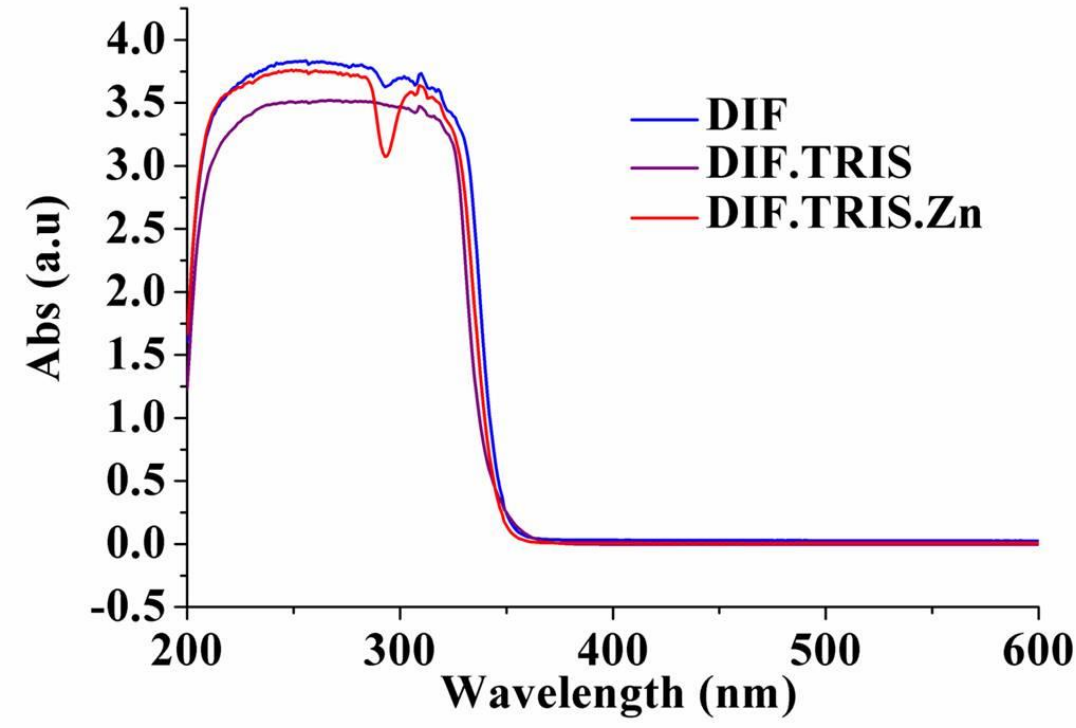

Figure S4: UV-Vis spectroscopy of **DIF**, **DIF.TRIS** and **DIF.TRIS.Zn** complex.

Physico-chemical data

IND.PHE.AMN : Light yellow solid. M.P: 173-174 °C; Elemental analysis calculated for $C_{38}H_{42}ClN_3O_5$ (%): C, 69.55; H, 6.45; N, 6.40; found: C, 69.91; H, 6.25; N, 6.76. ^{1}H NMR (300 MHz, Methanol-d4, 25 ^{o}C): δ = 7.63 – 7.55 (d, J = 8.6 Hz, 2H), 7.55 – 7.48 (d, J = 8.7 Hz, 2H), 7.10 – 7.04 (d, J = 9.0 Hz, 1H), 7.04 – 6.98 (s, 5H), 6.98 – 6.94 (d, J = 2.6 Hz, 1H), 6.74 – 6.66 (dd, J = 2.9, 2.6 Hz, 1H), 4.54 – 4.41 (t, J = 5.7 Hz, 1H), 3.84 – 3.72 (s, 3H), 3.63 – 3.50 (m, 2H), 3.20 – 3.07 (dd, J = 5.9, 4.9 Hz, 1H), 3.07 – 2.90 (dd, J = 6.0, 6.4 Hz, 1H), 2.18 – 2.02 (d, J = 12.7 Hz, 6H), 1.86 – 1.60 (m, 11H) ppm. ^{13}C NMR (75 MHz, Methanol-d4): δ = 170.5, 170.4, 168.4, 156.3, 138.6, 137.5, 136.3, 135.4, 134.2, 131.0, 130.9, 130.6, 129.1, 128.7, 127.6, 127.5, 125.7, 114.5, 113.2, 111.6, 100.8, 55.5, 54.7, 51.2, 48.1, 40.0, 37.3, 34.9, 31.0, 28.9, 12.2 ppm. (Fig. S5). FT-IR (KBr pellet): 1680 (s, salt stretch) cm^{-1}.

IND.HYP.AMN : Light yellow solid. M.P: 177-178 °C; Elemental analysis calculated for $C_{34}H_{40}ClN_3O_6 \cdot CH_3OH$ (%): C, 64.26; H, 6.78; N, 6.42; found: C, 64.81; H, 6.29; N, 6.76. ^{1}H NMR (300 MHz, Methanol-d4, 25 ^{o}C): δ = 7.78 – 7.61 (dd, *J* = 8.4, 9.0 Hz, 2H), 7.61 – 7.44 (m, 2H), 7.10 – 6.98 (dd, *J* = 3.0, 2.6 Hz, 1H), 6.99 – 6.86 (m, 1H), 4.65 – 4.44 (m, 1H), 3.91 – 3.73 (m, 4H), 3.73 – 3.48 (m, 3H), 2.45 – 2.29 (m, 1H), 2.28 – 2.16 (d, *J* = 8.1 Hz, 3H), 2.16 – 2.06 (m, 4H), 1.91 – 1.58 (m, 13H) ppm. ^{13}C NMR (75 MHz, Methanol-d4): δ = 172.7, 171.1, 167.0, 155.9, 135.1, 134.5, 132.2, 130.8, 130.7, 130.6, 128.7, 128.4, 123.7, 123.3, 114.3, 110.4, 109.5, 103.4, 100.9, 98.9, 69.4, 54.9, 54.7, 51.1, 40.2, 37.6, 35.0, 28.9, 12.2, 10.3 ppm. (Fig. S6). FT-IR (KBr pellet): 1683 (s, salt stretch) cm^{-1}.

IND.LEU.AMN : Light yellow solid. M.P: 167-168 °C; Elemental analysis calculated for $C_{35}H_{44}ClN_3O_5$ (%): C, 67.56; H, 7.13; N, 6.75; found: C, 68.01; H, 6.68; N, 6.79. ^{1}H NMR (300 MHz, Methanol-d4, 25 ^{o}C): δ = 7.78 – 7.62 (d, *J* = 8.3 Hz, 2H), 7.62 – 7.44 (d, *J* = 8.4 Hz, 2H), 7.14 – 6.86 (m, 2H), 6.76 – 6.55 (dd, *J* = 3.0, 2.6 Hz, 1H), 4.44 – 4.24 (dd, *J* = 3.0, 3.9 Hz, 1H), 3.89 – 3.71 (s, 3H), 3.71 – 3.56 (d, *J* = 2.2 Hz, 2H), 2.38 – 2.20 (s, 3H), 2.20 –

2.00 (t, *J* = 3.4 Hz, 3H), 1.94 – 1.36 (m, 16H), 1.02 – 0.66 (d, *J* = 5.8 Hz, 6H) ppm. ^{13}C NMR (75 MHz, Methanol-d4): δ = 170.7, 170.1, 168.4, 156.2, 138.6, 138.0, 135.5, 134.3, 130.9, 128.7, 114.5, 113.5, 111.5, 100.8, 54.6, 53.5, 51.0, 42.0, 40.2, 35.0, 33.3, 31.0, 28.9, 24.7, 22.3, 20.9, 12.2 ppm. (Fig. S7). FT-IR (KBr pellet): 1683 (s, salt stretch) cm^{-1}.

IND.VAL.AMN : Light yellow solid. M.P: 161-162 °C; Elemental analysis calculated for $C_{34}H_{42}ClN_3O_5$ (%): C, 67.15; H, 6.96; N, 6.91; found: C, 67.66; H, 7.34; N, 7.19. ^{1}H NMR (300 MHz, Methanol-d4, 25 ^{o}C): δ = 7.78 – 7.61 (d, *J* = 8.4 Hz, 2H), 7.61 – 7.45 (d, *J* = 8.6 Hz, 2H), 7.13 – 7.01 (d, *J* = 2.5 Hz, 1H), 7.01 – 6.87 (d, *J* = 9.1 Hz, 1H), 6.77 – 6.58 (dd, *J* = 3.0, 2.6 Hz, 1H), 4.33 – 4.09 (d, *J* = 4.8 Hz, 1H), 3.87 – 3.72 (s, 3H), 3.72 – 3.54 (d, *J* = 3.2 Hz, 2H), 2.40 – 2.20 (s, 3H), 2.21 – 2.04 (m, 3H), 1.94 – 1.55 (m, 9H), 0.96 – 0.86 (d, *J* = 6.9 Hz, 3H), 0.87 – 0.75 (d, *J* = 6.9 Hz, 3H) ppm. ^{13}C NMR (75 MHz, Methanol-d4): δ = 171.0, 170.9, 170.0, 156.2, 138.6, 135.5, 134.3, 130.9, 130.6, 128.7, 125.0, 114.5, 113.5, 112.8, 111.6, 100.7, 59.9, 54.7, 51.2, 40.1, 34.9, 31.3, 31.1, 28.9, 18.7, 16.8, 12.2 ppm. (Fig. S8). FT-IR (KBr pellet): 1683 (s, salt stretch) cm^{-1}.

IND.ALA.AMN : Light yellow solid. M.P: 158-159 °C; Elemental analysis calculated for $C_{32}H_{38}ClN_3O_5 \cdot H_2O$ (%): C, 64.26; H, 6.74; N, 7.03; found: C, 63.94; H, 7.14; N, 7.22. ^{1}H NMR (300 MHz, Methanol-d4, 25 ^{o}C): δ = 7.75 – 7.65 (d, *J* = 8.5 Hz, 2H), 7.61 – 7.51 (d, *J* = 8.5 Hz, 2H), 7.06 – 7.00 (d, *J* = 2.6 Hz, 1H), 7.00 – 6.93 (d, *J* = 9.0 Hz, 1H), 6.71 – 6.63 (dd, *J* = 2.4, 2.5 Hz, 1H), 4.32 – 4.13 (q, *J* = 7.1 Hz, 1H), 3.85 – 3.73 (s, 3H), 3.69 – 3.58 (s, 2H), 2.33 – 2.23 (s, 3H), 2.22 – 2.04 (d, *J* = 2.8 Hz, 3H), 1.92 – 1.56 (m, 9H), 1.41 – 1.27 (d, *J* = 7.0 Hz, 3H) ppm. ^{13}C NMR (75 MHz, Methanol-d4): δ = 177.2, 174.2, 168.5, 156.0, 138.4, 134.6, 134.3, 131.5, 130.9, 130.8, 128.6, 115.9, 114.3, 110.9, 108.9, 101.3, 58.4, 54.6, 51.2, 40.0, 36.1, 34.9, 32.3, 28.9, 12.2 ppm. (Fig. S9). FT-IR (KBr pellet): 1683 (s, salt stretch) cm^{-1}.

IND.THR.AMN : Yellow solid. M.P: 171-172 °C; Elemental analysis calculated for $C_{33}H_{40}ClN_3O_6 \cdot CH_3OH$ (%):C, 63.59; H, 6.91; N, 6.54; found: C, 63.94; H, 7.14; N, 7.22. ^{1}H NMR (300 MHz, Methanol-d4, 25 ^{o}C): δ = 7.79 – 7.62 (d, *J* = 8.5 Hz, 2H), 7.62 – 7.44 (d, *J* = 8.5 Hz, 2H), 7.12 – 6.92 (m, 2H), 6.74 – 6.60 (dd, *J* = 2.4, 2.5 Hz, 1H), 4.33 – 4.24 (d, *J* = 3.3 Hz, 1H), 4.24 – 4.12 (m, 1H), 3.90 – 3.75 (s, 3H), 3.75 – 3.61 (d, *J* = 2.9 Hz, 2H), 2.43 – 2.22 (s, 3H), 2.22 – 2.01 (t, *J* = 3.1 Hz, 3H), 1.97 – 1.53 (m, 10H), 1.17 – 0.95 (d, *J* = 6.3 Hz, 3H) ppm. ^{13}C NMR (75 MHz, Methanol-d4): δ = 173.5, 172.3, 168.7, 156.2, 138.6, 135.5, 134.4, 130.9, 130.6, 128.7, 128.4, 114.8, 111.7, 108.2, 100.7, 67.5, 56.0, 54.7, 50.4, 40.2, 35.0, 31.0, 28.9, 18.6, 12.2 ppm. (Fig. S10). FT-IR (KBr pellet): 1681 (s, salt stretch) cm^{-1}.

IND.HYP : Yellow solid. Yield: 73%. M.P: 168-169°C; Elemental analysis calculated for $C_{24}H_{23}ClN_2O_6 \cdot H_2O \cdot CH_3OH$ (%): C, 57.64; H, 5.61; N, 5.38%; found: C, 57.06; H, 5.12; N, 5.28%; ^{1}H NMR (300 MHz, CD_3OD, 25°C): δ = 7.69-7.64 (m, 2H), 7.55-7.51 (m, 2H), 7.00-6.90 (m, 2H), 6.65-6.61 (dd, *J* = 2.4, 2.4 Hz, 1H), 4.52-4.45 (dd, *J* = 3, 8.1 Hz, 1H), 3.85-3.80 (m, 1H), 3.79 (s, 3H), 3.78-3.55 (m, 4H), 2.43-2.27 (m, 1H), 2.23 (s, 3H), 2.20-2.04 (m, 1H) ppm.; ^{13}C NMR (75 MHz, CD_3OD): δ = 174.80, 170.41, 168.45, 156.04, 138.56, 135.34, 134.22, 130.91, 130.84, 130.74, 128.68, 114.31, 113.07, 111.22, 101.15, 69.57, 55.11, 54.70, 37.30, 29.81, 12.25 ppm. (Fig. S11); FT-IR (KBr pellet): 3367 (s, O-H stretch), 1712 (w, acid C=O stretch), 1683 (s, amide C=O stretch), 1624s, 1473m, 1456m, 1319s, 1224m, 833w, 754m cm^{-1}; HRMS, ESI (CH_3OH) *m/z* (100%): Calculated for $[(C_{24}H_{23}ClN_2O_6)][M+Na]^+$: 493.1142; found: 493.1142.

IND.SER : Yellow solid. Yield: 74%. M.P: 164-165°C; Elemental analysis calculated for $C_{22}H_{21}ClN_2O_6 \cdot CH_2Cl_2$ (%): C, 52.14; H, 4.38; N, 5.29%; found: C, 52.22; H, 3.87; N, 5.88%; ^{1}H NMR (300 MHz, CD_3OD, 25°C): δ = 7.65-7.62 (d, *J* = 8.4 Hz, 2H), 7.51-7.48 (d, *J* = 8.4 Hz, 2H), 7.05-7.04 (d, *J* = 2.1 Hz, 1H), 6.95-6.92 (d, *J* = 9 Hz, 1H), 6.64-6.60 (dd, *J* = 2.1, 2.1 Hz, 1H), 4.48 (s, 1H), 3.90-3.83 (dd, *J* = 4.5, 3.6 Hz, 2H), 3.78 (s, 3H), 3.68 (s, 2H), 2.25

(s, 3H) ppm.; ^{13}C NMR (75 MHz, CD_3OD): δ = 171.74, 171.69, 168.42, 156.10, 138.55, 135.49, 134.13, 130.83, 130.75, 130.61, 128.66, 114.39, 113.27, 111.49, 100.82, 61.51, 55.00, 54.67, 30.62, 12.19 ppm. (Fig. S12); FT-IR (KBr pellet): 3307 (s, O-H stretch), 1735 (m, acid C=O stretch), 1676 (s, amide C=O stretch), 1647s, 1604m, 1596m, 1541m, 1477s, 1363m, 1317m, 1222m cm^{-1}; HRMS, ESI (CH_3OH) *m/z* (100%): Calculated for $[(C_{22}H_{21}ClN_2O_6)][M+Na]^+$: 467.0986; found: 467.0986.

DIC.HYP : White solid. Yield: 78%. M.P: 143-144°C; Elemental analysis calculated for $C_{19}H_{18}Cl_2N_2O_4$ (%): C, 55.76; H, 4.43; N, 6.84%; found: C, 55.42; H, 4.62; N, 6.53%; ^{1}H NMR (300 MHz, DMSO-d_6) δ 7.49 (dd, *J* = 8.4, 3.9 Hz, 2H), 7.35 – 6.94 (m, 3H), 6.83 (q, *J* = 8.0 Hz, 1H), 6.27 (d, *J* = 7.8 Hz, 1H), 4.54 (t, *J* = 7.2 Hz, 1H), 4.44 – 4.15 (m, 2H), 3.76 (d, *J* = 7.5 Hz, 2H), 3.39 (s, 2H), 2.23 – 1.85 (m, 3H) ppm.; ^{13}C NMR (75 MHz, DMSO) δ 183.69, 171.06, 153.52, 153.41, 151.52, 147.45, 140.66, 139.92, 139.24, 137.38, 137.18, 135.75, 135.38, 134.89, 130.85, 130.74, 126.23, 78.95, 77.44, 75.31, 68.14, 65.44, 64.34, 48.07, 47.68 ppm. (Fig. S13); FT-IR (KBr pellet): 3319 (s, O-H stretch), 1716 (m, acid C=O stretch), 1618 (s, amide C=O stretch) cm^{-1}; HRMS, ESI (CH_3OH) *m/z* (100%): Calculated for $[(C_{19}H_{18}Cl_2N_2O_4)][M+Na]^+$: 431.0541; found: 431.0544.

DIC.SER : White solid. Yield: 82%. M.P: 140-141°C; Elemental analysis calculated for $C_{17}H_{16}Cl_2N_2O_4$ (%):C, 53.28; H, 4.21; N, 7.31%; found: C, 52.98; H, 4.53; N, 6.76%; ^{1}H NMR (300 MHz, DMSO-d_6) δ 8.65 – 8.06 (m, 2H), 7.47 (d, *J* = 8.1 Hz, 2H), 7.34 – 6.72 (m, 4H), 6.27 (d, *J* = 8.0 Hz, 1H), 4.24 – 4.14 (m, 2H), 3.65 (d, *J* = 27.4 Hz, 5H) ppm.; ^{13}C NMR (75 MHz, DMSO) δ 183.08, 181.69, 153.21, 147.42, 140.86, 139.60, 139.31, 137.32, 135.75, 135.14, 130.84, 126.11, 72.00, 65.46 ppm. (Fig. S14); FT-IR (KBr pellet): 3296 (s, O-H stretch), 1718 (m, acid C=O stretch), 1639 (s, amide C=O stretch) cm^{-1}; HRMS, ESI (CH_3OH) *m/z* (100%): Calculated for $[(C_{17}H_{16}Cl_2N_2O_4)][M+Na]^+$: 405.0385; found: 431.0394.

MEF.HYP : Light yellow solid. Yield: 75%. M.P: 137-138°C; Elemental analysis calculated for $C_{20}H_{22}N_2O_4 \cdot CH_3OH$ (%):C, 65.27; H, 6.78; N, 7.25%; found: C, 64.88; H, 6.68; N, 6.77%; ^{1}H NMR (300 MHz, DMSO-d_6) δ 7.37 – 6.98 (m, 4H), 6.97 – 6.84 (m, 1H), 6.84 – 6.50 (m, 2H), 4.47 (t, *J* = 7.9 Hz, 1H), 4.22 (s, 2H), 3.36 (d, *J* = 4.9 Hz, 1H), 3.18 (d, *J* = 10.9 Hz, 2H), 2.24 (s, 4H), 2.17 – 1.80 (m, 6H) ppm.; ^{13}C NMR (75 MHz, DMSO) δ 186.23, 178.22, 153.19, 150.01, 147.69, 140.86, 140.07, 137.50, 135.84, 135.38, 133.17, 131.08, 127.16, 123.22, 79.00, 75.79, 68.80, 66.46, 47.95, 30.41, 23.89 ppm. (Fig. S15); FT-IR (KBr pellet): 3446 (s, O-H stretch), 1649 (m, acid C=O stretch), 1612 (s, amide C=O stretch) cm^{-1}; HRMS, ESI (CH_3OH) *m/z* (100%): Calculated for $[(C_{20}H_{22}N_2O_4)][M+Na]^+$: 377.1477; found: 377.1475.

MEF.PHE : Light yellow solid. Yield: 76%. M.P: 157-158°C; Elemental analysis calculated for $C_{24}H_{24}N_2O_3 \cdot H_2O$ (%):C, 70.92; H, 6.45; N, 6.89%; found: C, 70.28; H, 6.92; N, 6.17%; ^{1}H NMR (300 MHz, DMSO-d_6) δ 9.36 (s, 1H), 9.02 – 8.55 (m, 1H), 8.34 (tt, *J* = 15.0, 8.0 Hz, 1H), 7.51 – 6.67 (m, 11H), 4.56 (dddd, *J* = 23.7, 19.1, 9.7, 5.2 Hz, 1H), 3.18 (tdd, *J* = 15.2, 9.7, 4.5 Hz, 2H), 3.02 (ddd, *J* = 21.8, 15.4, 9.8 Hz, 1H), 2.61 (d, *J* = 3.7 Hz, 1H), 2.29 – 2.01 (m, 3H) ppm.; ^{13}C NMR (75 MHz, DMSO) δ 181.20, 178.97, 149.22, 148.44, 147.76, 139.39, 139.25, 138.19, 138.15, 138.08, 136.29, 135.93, 135.26, 129.90, 126.76, 123.80, 71.73, 64.68, 64.07, 58.27, 46.98, 30.38, 23.62 ppm. (Fig. S16); FT-IR (KBr pellet): 3319 (s, O-H stretch), 1728 (m, acid C=O stretch), 1631 (s, amide C=O stretch) cm^{-1}; HRMS, ESI (CH_3OH) *m/z* (100%): Calculated for $[(C_{24}H_{24}N_2O_3)][M+Na]^+$: 411.1685; found: 411.1486.

IND.TRIS : Yellow solid. M.P: 178-179 °C; Elemental analysis calculated for $C_{23}H_{27}ClN_2O_7$ (%):C, 57.68; H, 5.68; N, 5.85; found: C, 57.31; H, 6.14; N, 5.37. ^{1}H NMR (300 MHz, Methanol-d_4) δ 7.79 – 7.63 (m, 2H), 7.63 – 7.44 (m, 2H), 7.17 – 7.03 (d, *J* = 2.6 Hz, 1H), 7.03 – 6.90 (d, *J* = 9.1 Hz, 1H), 6.71 – 6.59 (dd, *J* = 8.9, 2.5 Hz, 1H), 3.91 – 3.75 (s, 3H), 3.70 – 3.60 (s, 6H), 3.60 – 3.51 (s, 2H), 2.37 – 2.19 (s, 3H). ^{13}C NMR (75 MHz, MeOD) δ

178.7, 169.6, 157.0, 139.3, 135.6, 135.3, 132.5, 131.8, 129.6, 117.0, 115.3, 111.9, 102.2, 61.9, 60.7, 55.6, 48.5, 33.5, 13.2 (Fig. S17). FT-IR (KBr pellet): 1676 (s, salt stretch) cm^{-1}.

MEF.TRIS : White solid. M.P: 198-199 °C; Elemental analysis calculated for $C_{19}H_{26}N_2O_5$ (%):C, 62.97; H, 7.23; N, 7.73; found: C, 63.18; H, 7.71; N, 7.58. ^{1}H NMR (300 MHz, Methanol-d_4) δ 8.01 – 7.84 (dd, *J* = 7.7, 1.7 Hz, 1H), 7.19 – 7.04 (m, 2H), 7.04 – 6.93 (t, *J* = 7.7 Hz, 1H), 6.93 – 6.82 (d, *J* = 7.3 Hz, 1H), 6.82 – 6.70 (d, *J* = 8.2 Hz, 1H), 6.70 – 6.54 (t, *J* = 7.4 Hz, 1H), 3.78 – 3.56 (s, 6H), 2.34 – 2.23 (s, 3H), 2.23 – 2.09 (s, 3H). ^{13}C NMR (75 MHz, MeOD) δ 176.1, 148.4, 141.1, 138.3, 132.5, 131.9, 131.1, 126.2, 125.6, 121.2, 120.3, 116.7, 114.0, 61.9, 60.8, 48.5, 20.2, 13.6 (Fig. S18). FT-IR (KBr pellet): 1639 (s, salt stretch) cm^{-1}.

DIC.TRIS : White solid. M.P: 218-219 °C; Elemental analysis calculated for $C_{18}H_{22}Cl_2N_2O_5 \cdot CH_3OH$ (%):C, 50.79; H, 5.83; N, 6.23; found: C, 51.31; H, 6.34; N, 6.16. ^{1}H NMR (300 MHz, DMSO-d_6) δ 9.45 – 9.19 (s, 1H), 7.54 – 7.37 (d, *J* = 8.0 Hz, 1H), 7.17 – 7.02 (dd, *J* = 9.5, 6.8 Hz, 1H), 7.02 – 6.90 (td, *J* = 7.7, 1.5 Hz, 1H), 6.88 – 6.70 (m, 1H), 6.38 – 6.18 (d, *J* = 7.5 Hz, 1H), 3.55 – 3.32 (d, *J* = 3.7 Hz, 5H), 2.15 – 1.98 (s, 1H). ^{13}C NMR (75 MHz, DMSO) δ 176.1, 143.0, 137.8, 130.3, 129.1, 127.4, 126.2, 124.2, 120.2, 115.7, 60.6, 59.7, 43.2, 39.5, 30.7 (Fig. S19). FT-IR (KBr pellet): 1647 (s, salt stretch) cm^{-1}.

MEC.TRIS : White solid. M.P: 225-226 °C; Elemental analysis calculated for $C_{18}H_{22}Cl_2N_2O_5$ (%):C, 51.81; H, 5.31; N, 6.71; found: C, 52.18; H, 5.84; N, 7.25. ^{1}H NMR (300 MHz, Methanol-d_4) δ 8.05 – 7.78 (d, *J* = 7.8 Hz, 1H), 7.42 – 7.23 (d, *J* = 8.2 Hz, 1H), 7.21 – 6.98 (dd, *J* = 15.4, 7.9 Hz, 2H), 6.79 – 6.53 (t, *J* = 7.5 Hz, 1H), 6.28 – 6.08 (d, *J* = 8.3 Hz, 1H), 3.83 – 3.49 (s, 7H), 2.54 – 2.11 (s, 3H). ^{13}C NMR (75 MHz, MeOD) δ 175.8, 146.9, 137.3, 137.1, 134.3, 132.1, 131.6, 128.4, 120.4, 117.5, 113.5, 61.9, 60.9, 48.5, 20.2 (Fig. S20). FT-IR (KBr pellet): 1612 (s, salt stretch) cm^{-1}.

TOL.TRIS : White solid. M.P: 162-163 °C; Elemental analysis calculated for $C_{18}H_{23}ClN_2O_5 \cdot 2H_2O$ (%):C, 51.61; H, 6.50; N, 6.69; found: C, 51.55; H, 7.04; N, 7.13. ^{1}H NMR (300 MHz, Methanol-d_4) δ 8.04 – 7.85 (dd, *J* = 7.9, 1.7 Hz, 1H), 7.34 – 7.22 (dd, *J* = 7.5, 1.7 Hz, 1H), 7.22 – 7.11 (ddd, *J* = 8.7, 7.1, 1.8 Hz, 1H), 7.11 – 6.99 (m, 2H), 6.99 – 6.89 (d, *J* = 8.0 Hz, 1H), 6.80 – 6.63 (t, *J* = 7.5 Hz, 1H), 3.71 – 3.63 (s, 6H), 2.43 – 2.22 (s, 3H). ^{13}C NMR (75 MHz, MeOD) δ 175.7, 146.8, 143.3, 135.7, 132.6, 131.8, 129.1, 127.3, 123.6, 121.7, 119.5, 118.0, 114.7, 61.9, 60.8, 57.8, 48.5, 17.9, 14.6 (Fig. S21). FT-IR (KBr pellet): 1608 (s, salt stretch) cm^{-1}.

FLU.TRIS : Pale yellow solid. M.P: 154-155 °C; Elemental analysis calculated for $C_{18}H_{21}F_3N_2O_5$ (%):C, 53.73; H, 5.26; N, 6.96; found: C, 53.36; H, 5.77; N, 7.18. ^{1}H NMR (300 MHz, Methanol-d_4) δ 8.02 – 7.91 (dd, *J* = 7.8, 1.4 Hz, 1H), 7.46 – 7.36 (d, *J* = 2.8 Hz, 3H), 7.36 – 7.21 (m, 2H), 7.20 – 7.07 (td, *J* = 5.7, 4.7, 3.1 Hz, 1H), 6.91 – 6.71 (m, 1H), 3.76 – 3.57 (s, 6H). ^{13}C NMR (75 MHz, MeOD) δ 174.2, 144.2, 143.5, 131.7, 130.8, 129.6, 126.1, 122.0, 121.6, 118.3, 116.6, 114.4, 61.1, 59.7, 47.5, 29.2 (Fig. S22). FT-IR (KBr pellet): 1606 (s, salt stretch) cm^{-1}.

IBU.TRIS : White solid. M.P: 184-185 °C; Elemental analysis calculated for $C_{17}H_{29}NO_5$ (%):C, 62.36; H, 8.93; N, 4.28; found: C, 62.95; H, 8.57; N, 4.87. ^{1}H NMR (300 MHz, Methanol-d_4) δ 7.32 – 7.15 (m, 2H), 7.12 – 6.94 (m, 2H), 3.69 – 3.60 (s, 5H), 3.60 – 3.49 (q, *J* = 7.2 Hz, 1H), 2.49 – 2.31 (d, *J* = 7.2 Hz, 2H), 1.99 – 1.62 (dp, *J* = 13.5, 6.8 Hz, 1H), 1.48 – 1.27 (d, *J* = 7.1 Hz, 3H), 0.98 – 0.73 (d, *J* = 6.6 Hz, 6H). ^{13}C NMR (75 MHz, MeOD) δ 181.7, 140.9, 139.0, 128.4, 126.8, 60.8, 59.9, 47.5, 46.7, 44.6, 30.0, 21.2, 18.4 (Fig. S23). FT-IR (KBr pellet): 1645 (s, salt stretch) cm^{-1}.

FLR.TRIS : White solid. M.P: 171-172 °C; Elemental analysis calculated for $C_{19}H_{24}FNO_5$ (%):C, 62.45; H, 6.62; N, 3.83; found: C, 62.31; H, 6.83; N, 4.31. ^{1}H NMR (300 MHz,

Methanol-d_4) δ 7.56 – 7.44 (m, 2H), 7.44 – 7.26 (m, 4H), 7.26 – 7.14 (m, 2H), 3.66 – 3.63 (s, 6H), 3.63 – 3.59 (s, 1H), 1.53 – 1.37 (d, J = 7.3 Hz, 3H). ^{13}C NMR (75 MHz, MeOD) δ 180.7, 157.7, 145.6, 135.8, 129.9, 128.4, 127.9, 126.9, 126.4, 123.4, 114.3, 60.9, 59.8, 47.5, 46.6, 18.2 (Fig. S24). FT-IR (KBr pellet): 1627 (s, salt stretch) cm^{-1}.

KET.TRIS : White solid. M.P: 187-188 °C; Elemental analysis calculated for $C_{20}H_{25}NO_6$· CH_3OH· H_2O (%):C, 59.28; H, 7.34; N, 3.29; found: C, 58.82; H, 7.27; N, 3.82. ^{1}H NMR (300 MHz, Methanol-d_4) δ 7.82 – 7.73 (m, 3H), 7.70 – 7.38 (m, 7H), 3.65 – 3.64 (s, 1H), 3.64 – 3.62 (s, 6H), 1.54 – 1.38 (d, J = 7.1 Hz, 4H). ^{13}C NMR (75 MHz, MeOD) δ 197.4, 180.7, 144.2, 137.5, 137.2, 132.2, 131.7, 129.6, 128.8, 128.0, 127.4, 60.8, 59.8, 47.5, 46.6, 18.3 (Fig. S25). FT-IR (KBr pellet): 1656 (s, salt stretch) cm^{-1}.

NAP.TRIS : White solid. M.P: 153-154 °C; Elemental analysis calculated for $C_{18}H_{25}NO_6$· CH_3OH (%):C, 59.52; H, 7.62; N, 3.65; found: C, 60.04; H, 7.64; N, 3.29. ^{1}H NMR (300 MHz, Methanol-d_4) δ 7.76 – 7.60 (m, 3H), 7.54 – 7.41 (dd, J = 8.5, 1.8 Hz, 1H), 7.22 – 7.11 (d, J = 2.5 Hz, 1H), 7.11 – 6.98 (dd, J = 8.9, 2.5 Hz, 1H), 3.95 – 3.80 (s, 3H), 3.78 – 3.65 (q, J = 7.1 Hz, 1H), 3.65 – 3.54 (s, 7H), 1.57 – 1.36 (d, J = 7.0 Hz, 3H). ^{13}C NMR (75 MHz, MeOD) δ 176.2, 157.2, 138.9, 133.3, 129.0, 128.6, 126.4, 126.1, 125.0, 117.9, 105.0, 60.3, 60.2, 54.2, 48.1, 47.5, 46.6, 18.4 (Fig. S26). FT-IR (KBr pellet): 1654 (s, salt stretch) cm^{-1}.

SUL.TRIS : Orange solid. M.P: 163-164 °C; Elemental analysis calculated for $C_{22}H_{25}N_5O_8S$ (%):C, 50.86; H, 4.85; N, 13.48; found: C, 50.31; H, 4.66; N, 12.96. ^{1}H NMR (300 MHz, DMSO-d_6) δ 8.08 (d, J = 2.7 Hz, 1H), 7.87 – 7.72 (m, 3H), 7.71 – 7.57 (m, 3H), 7.53 (ddd, J = 8.8, 7.0, 1.9 Hz, 1H), 6.99 (d, J = 8.7 Hz, 1H), 6.69 – 6.53 (m, 2H), 3.29 (s, 7H). ^{13}C NMR (75 MHz, DMSO-d_6) δ 180.8, 179.9, 164.1, 152.6, 137.8, 137.1, 136.8, 132.2, 129.3, 128.1, 124.4, 71.0, 69.4, 50.3, 50.1, 49.8, 49.5, 49.2, 48.9, 48.7 (Fig. S27). FT-IR (KBr pellet): 1649 (s, salt stretch) cm^{-1}.

DIF.TRIS : White solid. M.P: 214-215 °C; Elemental analysis calculated for $C_{17}H_{19}F_2NO_6$ (%):C, 54.99; H, 5.16; N, 3.77; found: C, 55.38; H, 5.19; N, 3.33. ^{1}H NMR (300 MHz, DMSO-d_6) δ 7.85 (d, *J* = 2.5 Hz, 2H), 7.75 (s, 1H), 7.49 (td, *J* = 8.9, 6.6 Hz, 2H), 7.39 – 7.19 (m, 3H), 7.12 (td, *J* = 8.5, 2.7 Hz, 1H), 6.75 (d, *J* = 8.4 Hz, 1H), 5.34 (s, 2H), 3.51 (s, 11H), 2.50 (s, 2H). ^{13}C NMR (75 MHz, DMSO-d_6) δ 181.5, 172.7, 142.1, 140.4, 132.2, 130.1, 126.4, 121.7, 114.3, 71.1, 69.4, 50.3, 50.1, 49.8, 49.5, 49.2, 48.9, 48.7 (Fig. S28). FT-IR (KBr pellet): 1620 (s, salt stretch) cm^{-1}.

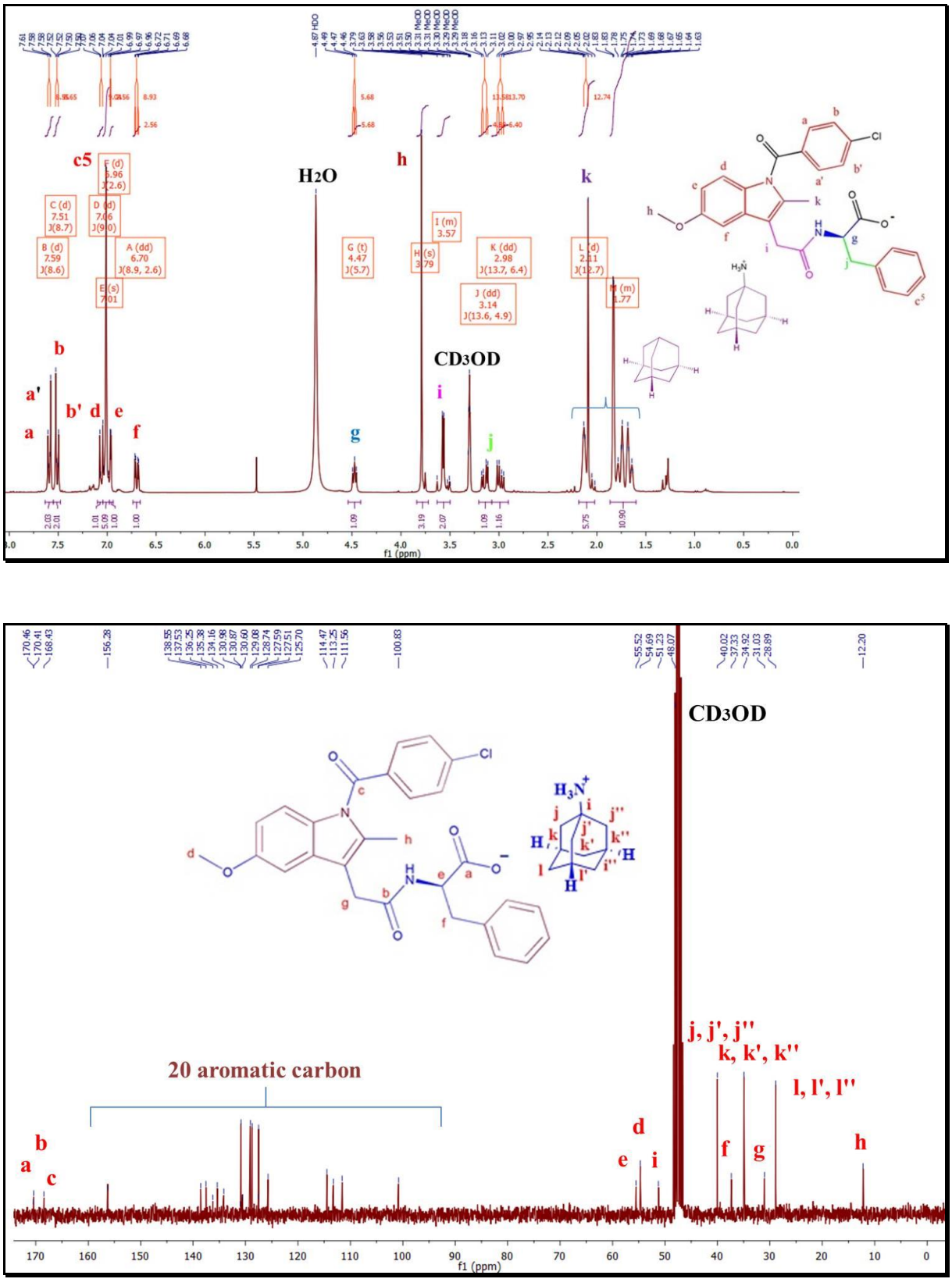

Figure S5: ^{1}H NMR and ^{13}C NMR spectra of **IND.PHE.AMN** in CD_3OD.

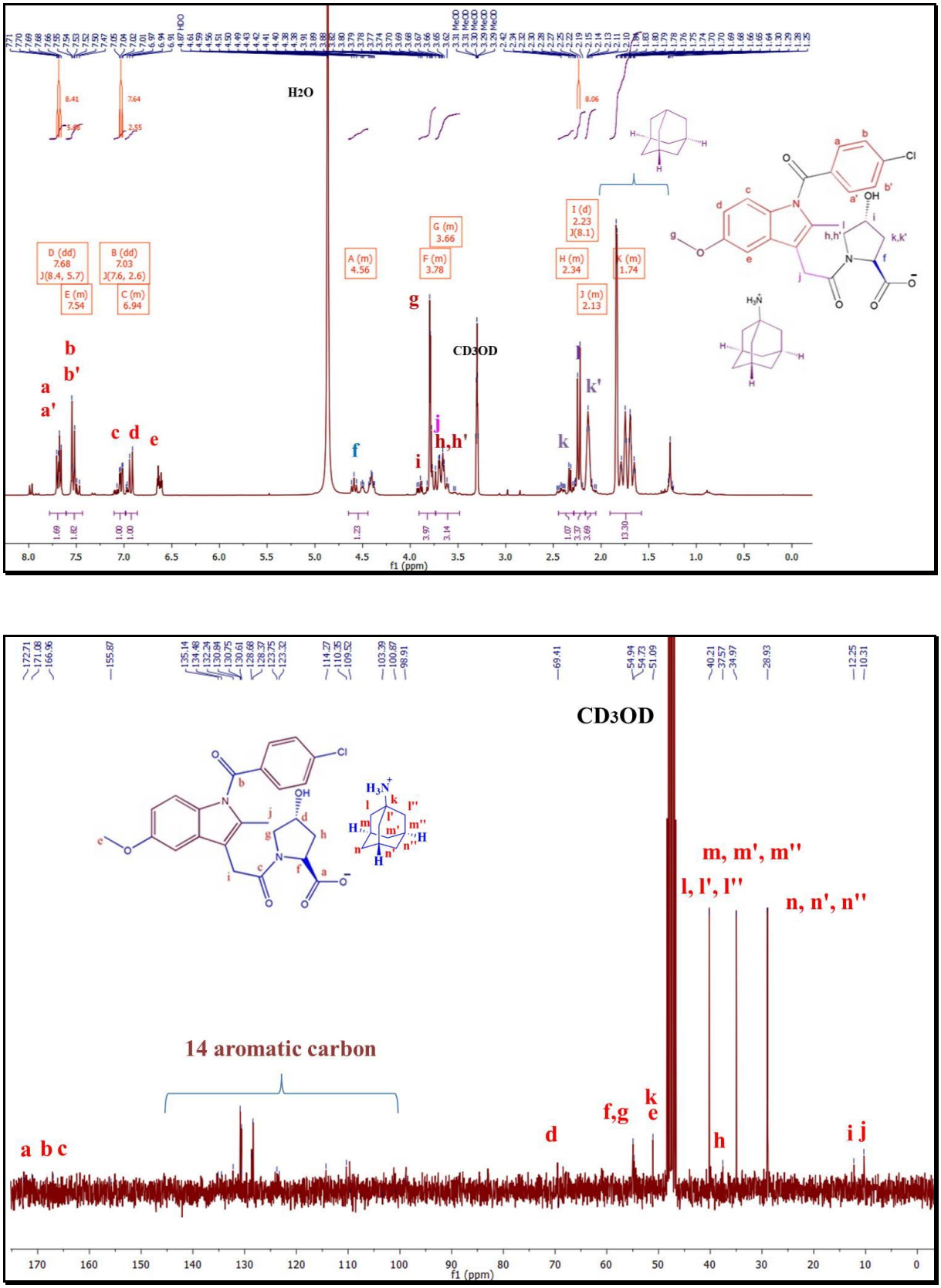

Figure S6: ^{1}H NMR and ^{13}C NMR spectra of **IND.HYP.AMN** in CD_3OD.

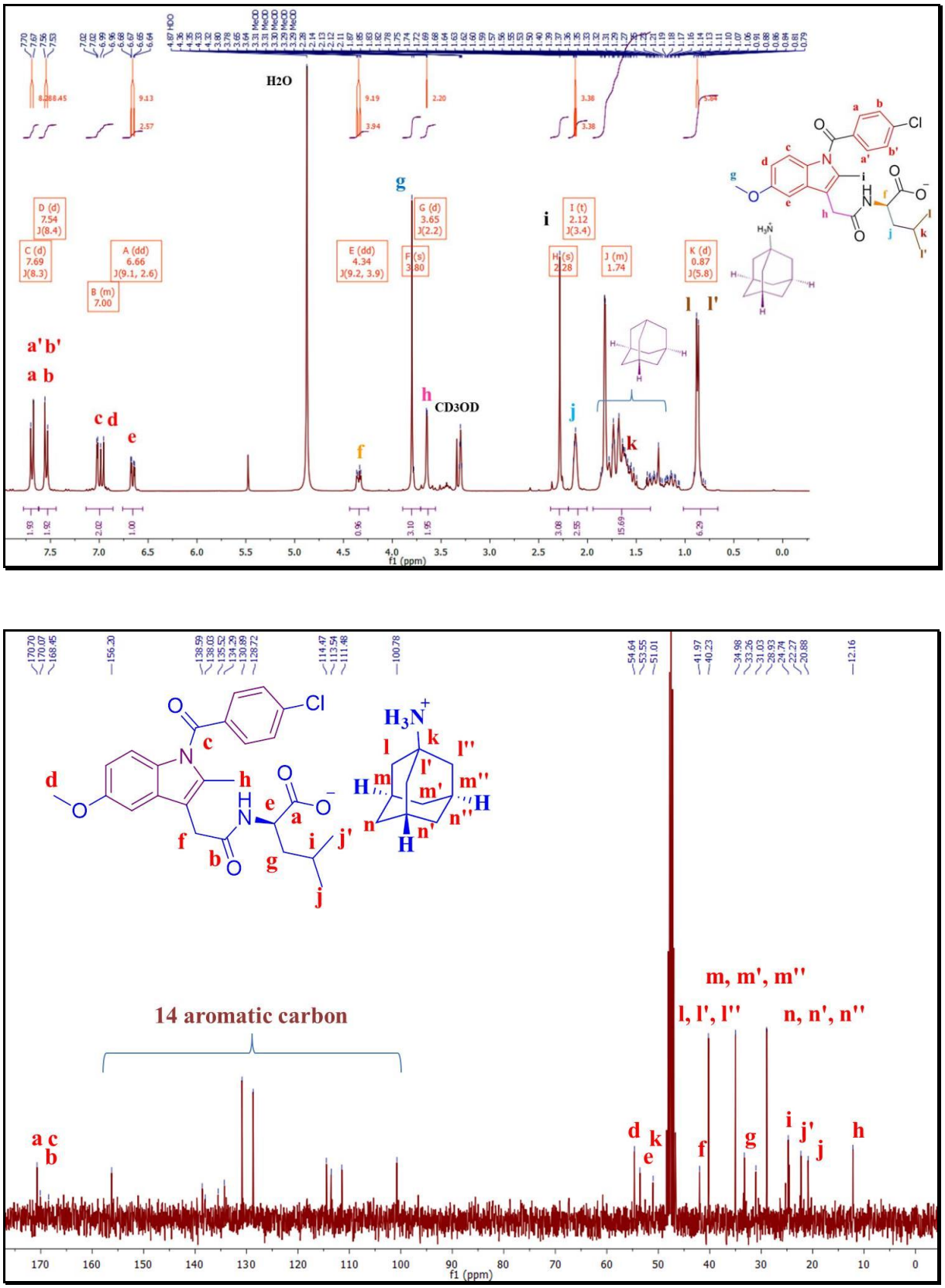

Figure S7: ^{1}H NMR and ^{13}C NMR spectra of **IND.LEU.AMN** in CD_3OD.

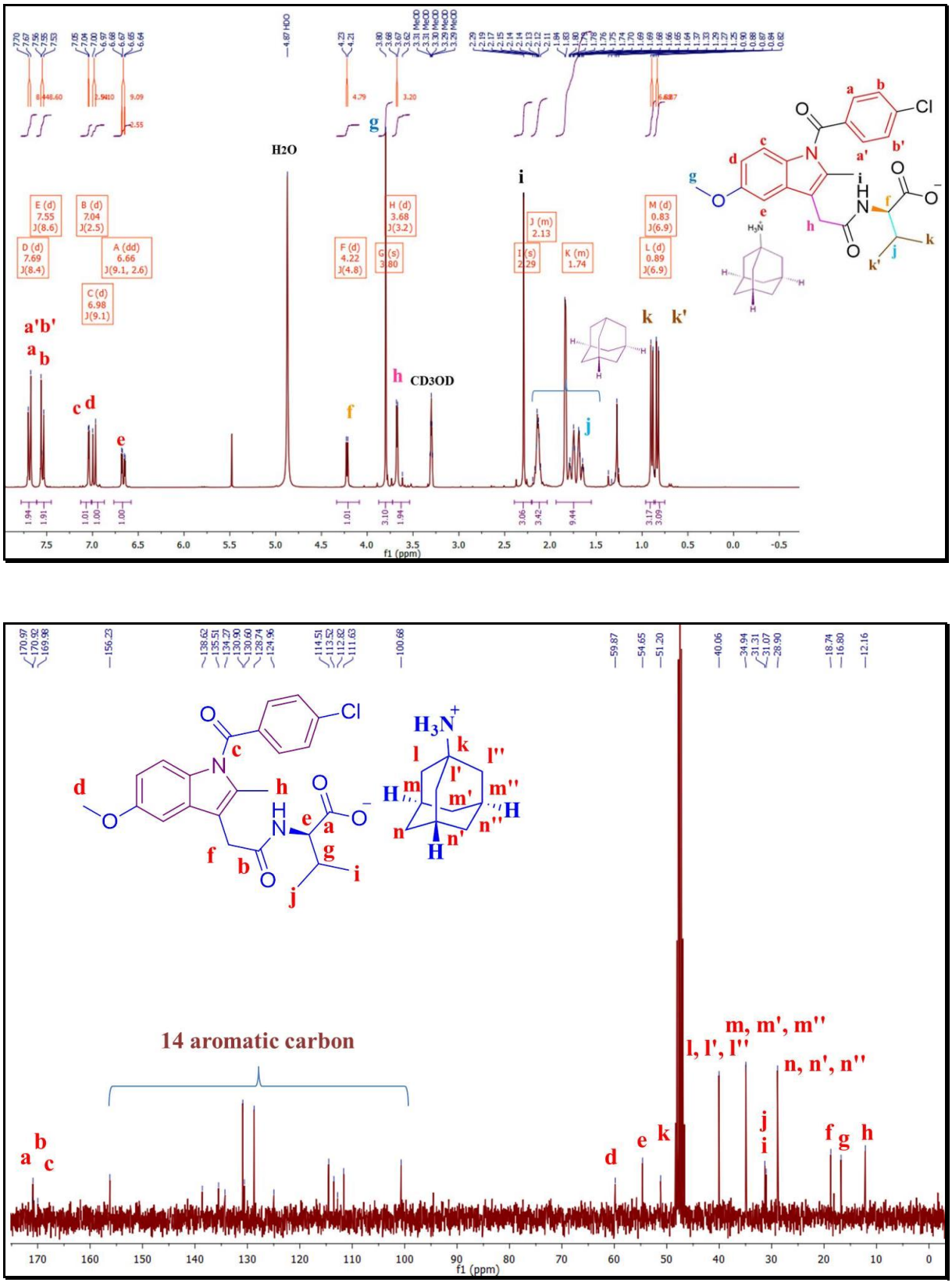

Figure S8: ^{1}H NMR and ^{13}C NMR spectra of **IND.VAL.AMN** in CD_3OD.

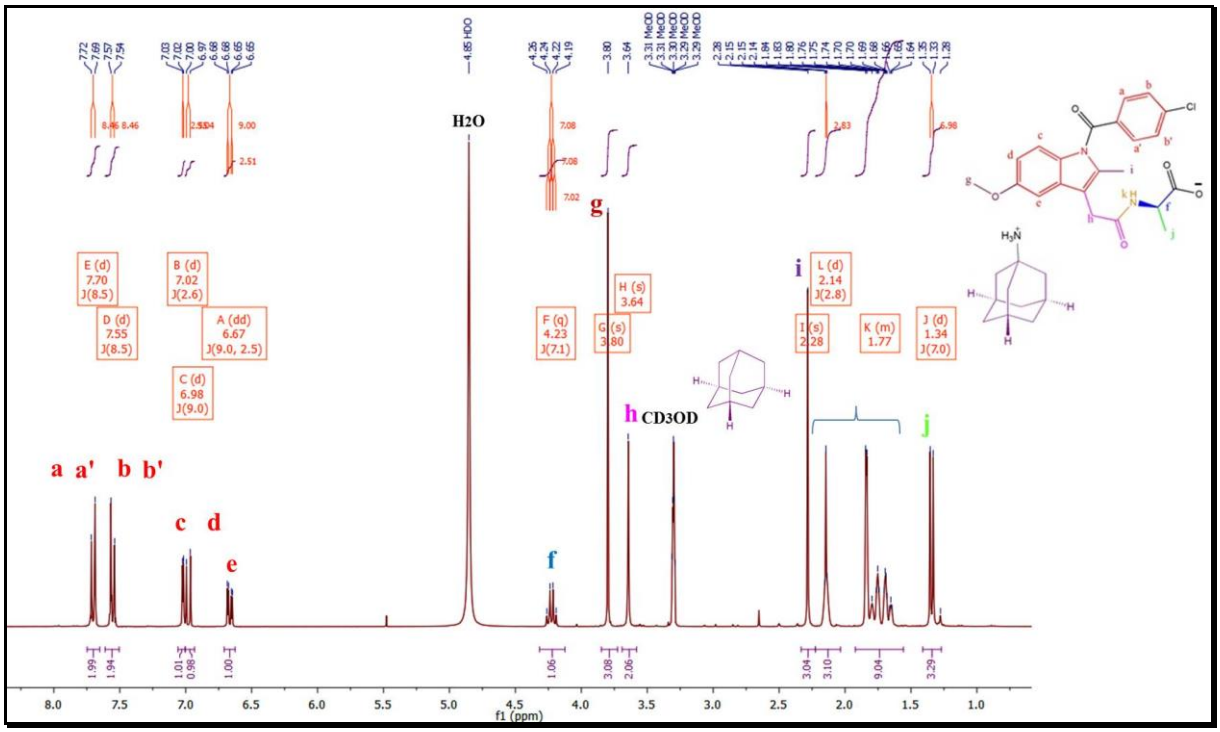

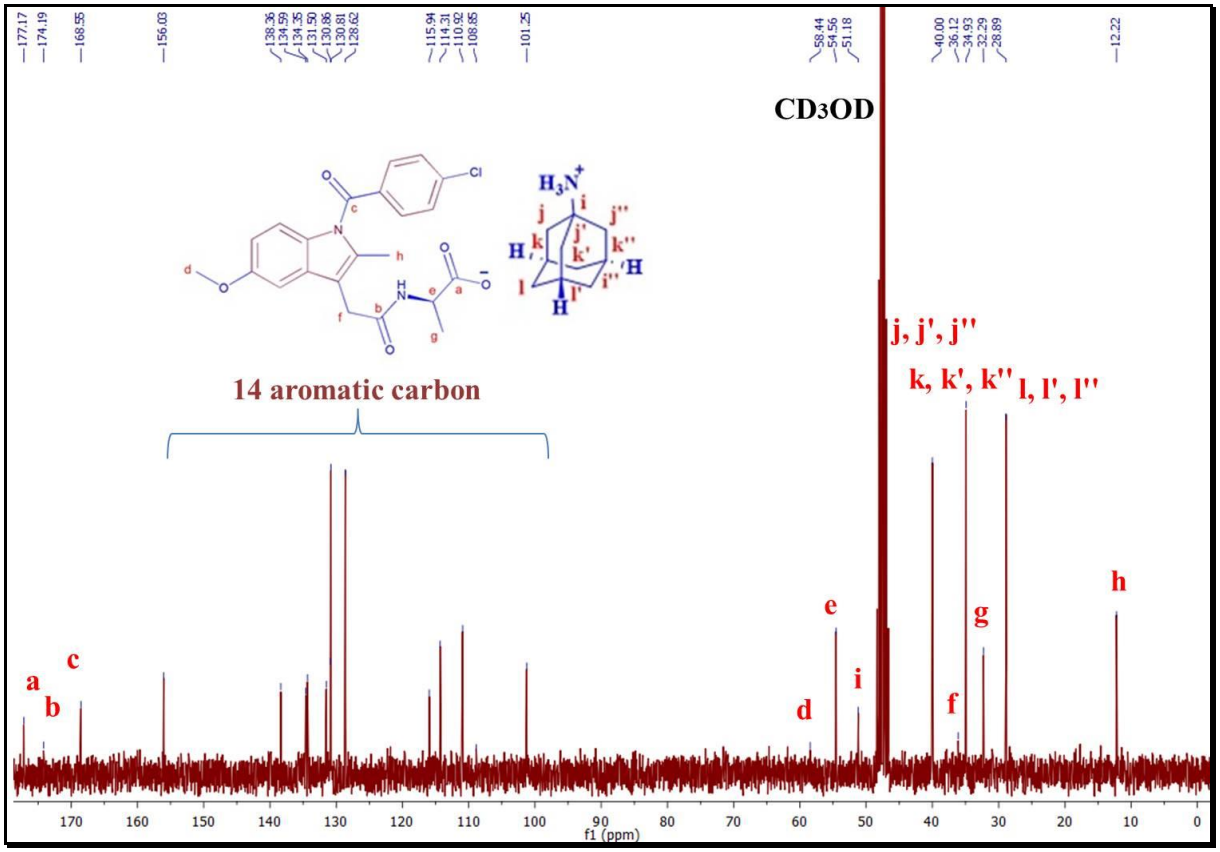

Figure S9: ^{1}H NMR and ^{13}C NMR spectra of **IND.ALA.AMN** in CD_3OD.

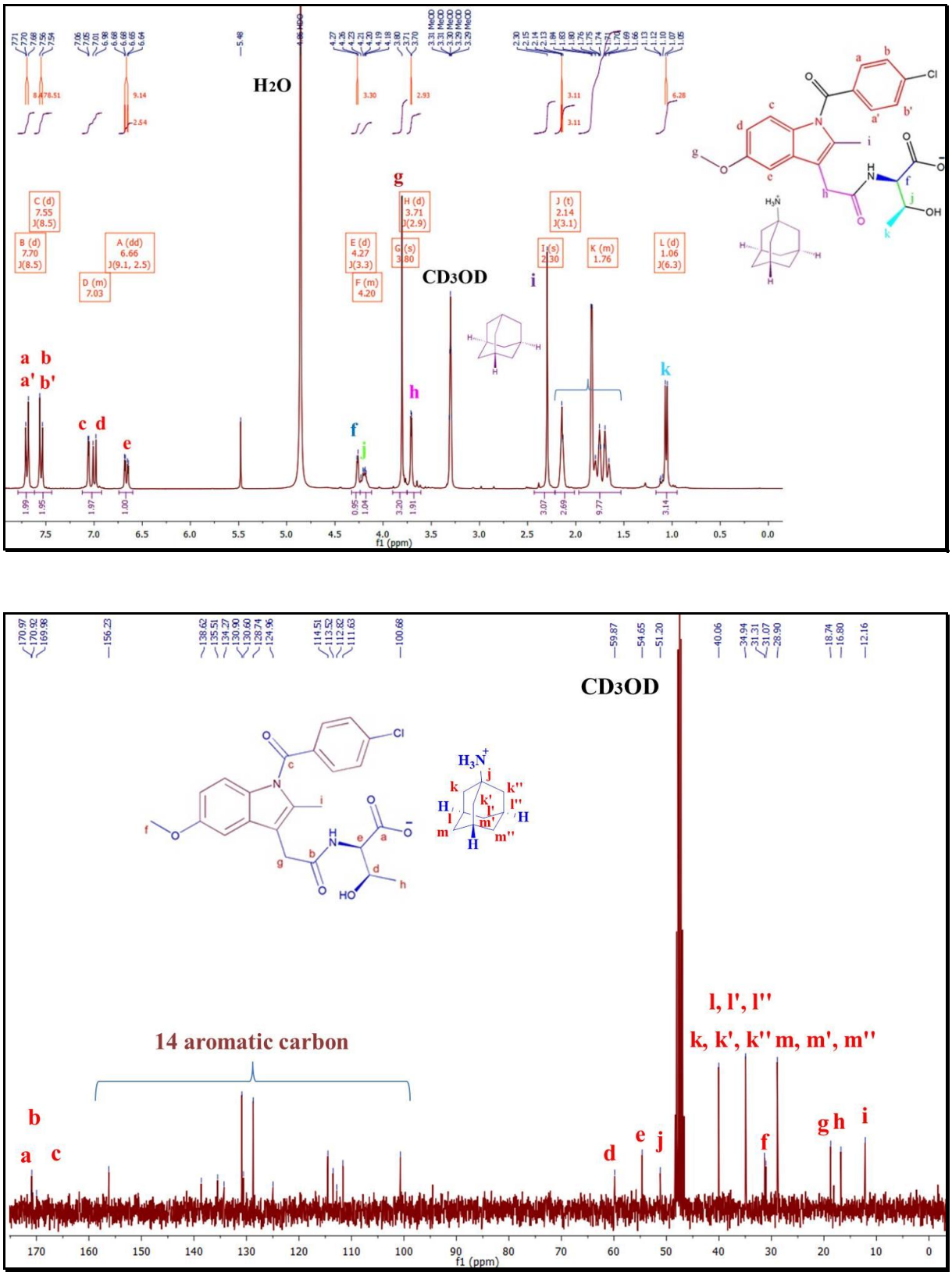

Figure S10: ^{1}H NMR and ^{13}C NMR spectra of **IND.THR.AMN** in CD_3OD.

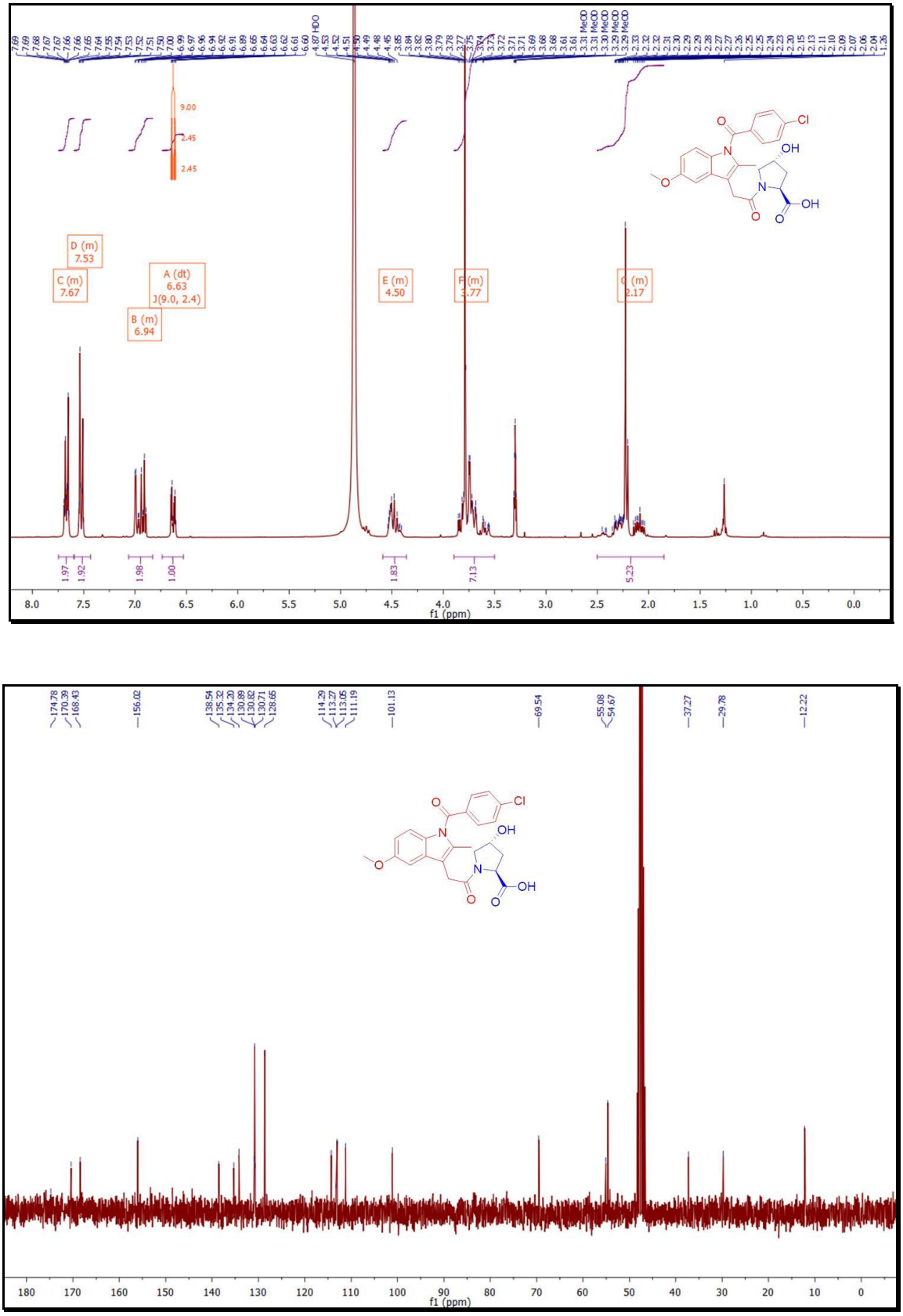

Figure S11: ^{1}H NMR and ^{13}C NMR spectra of **IND.HYP** in CD_3OD.

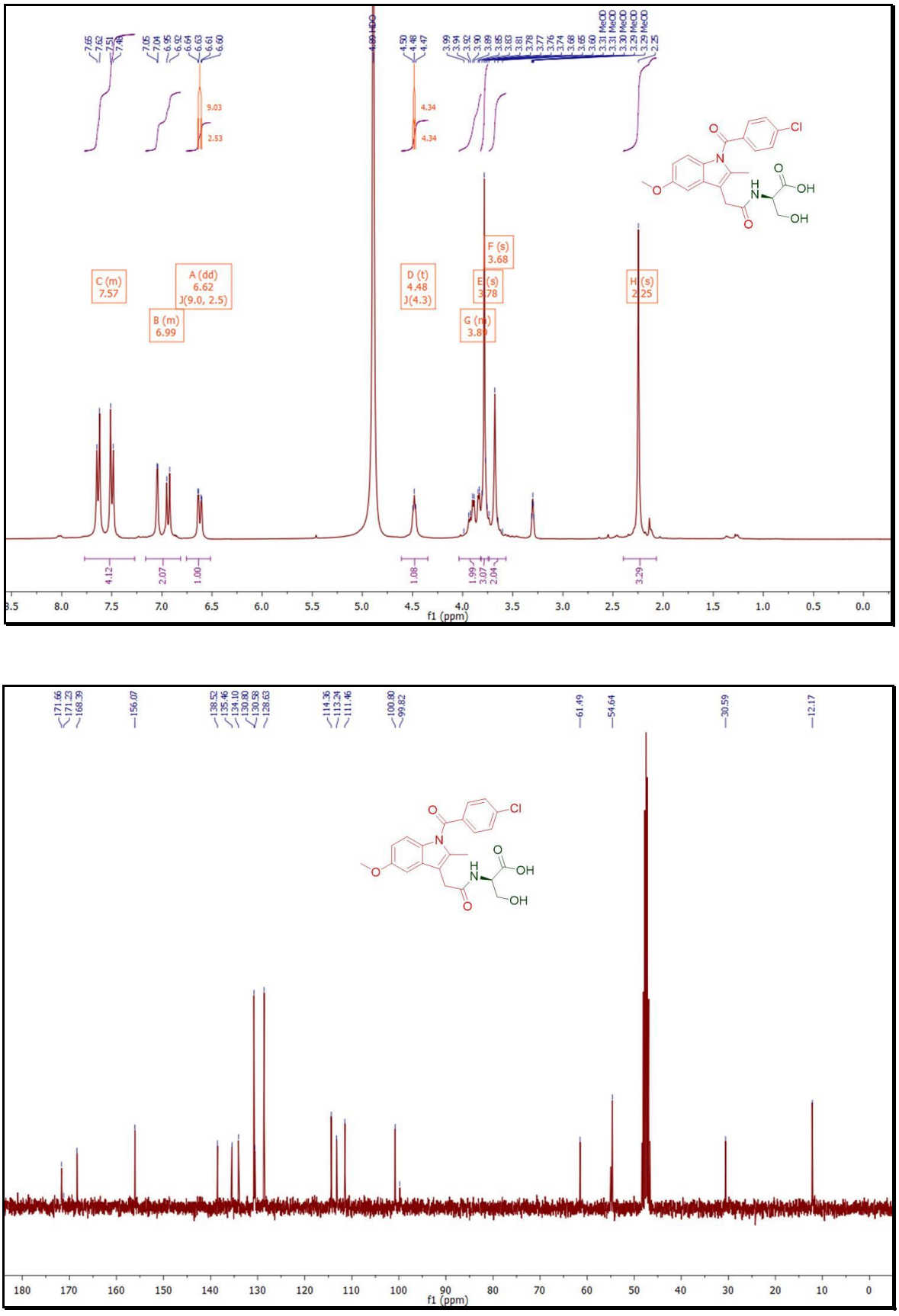

Figure S12: ^{1}H NMR and ^{13}C NMR spectra of **IND.SER** in CD_3OD.

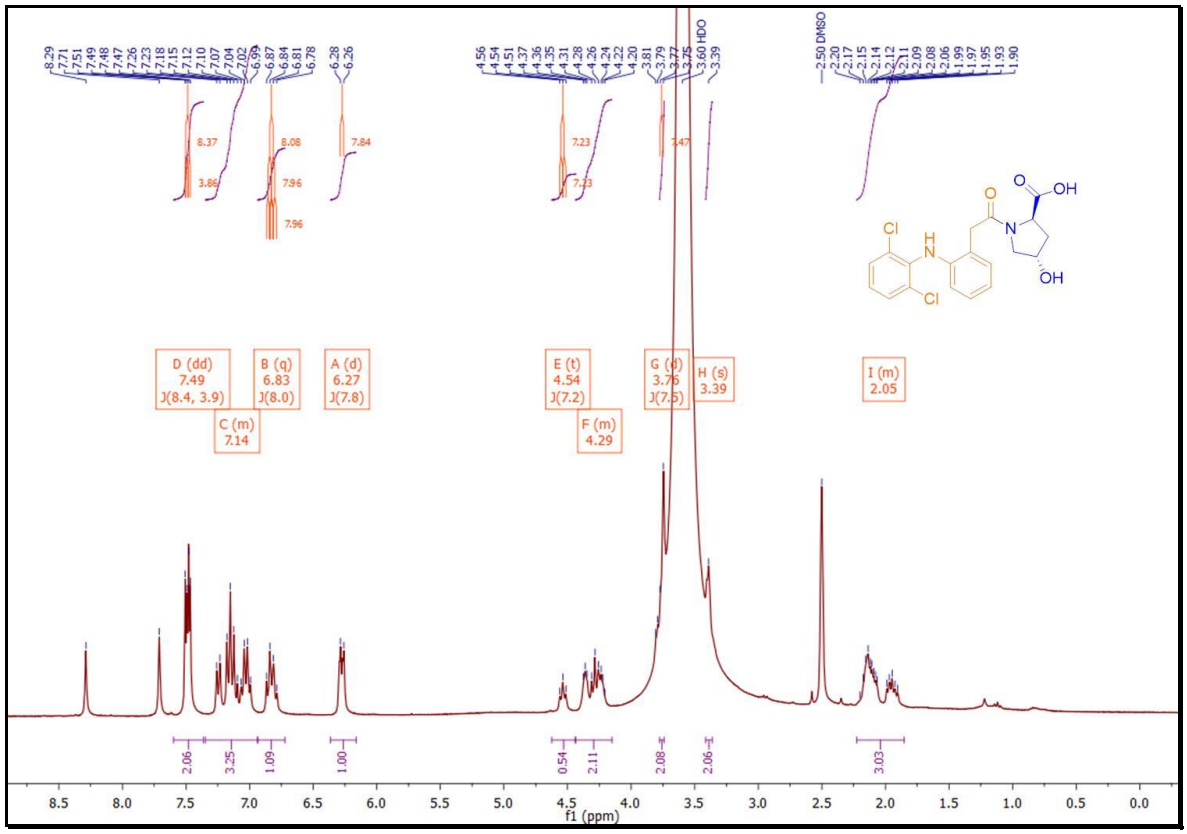

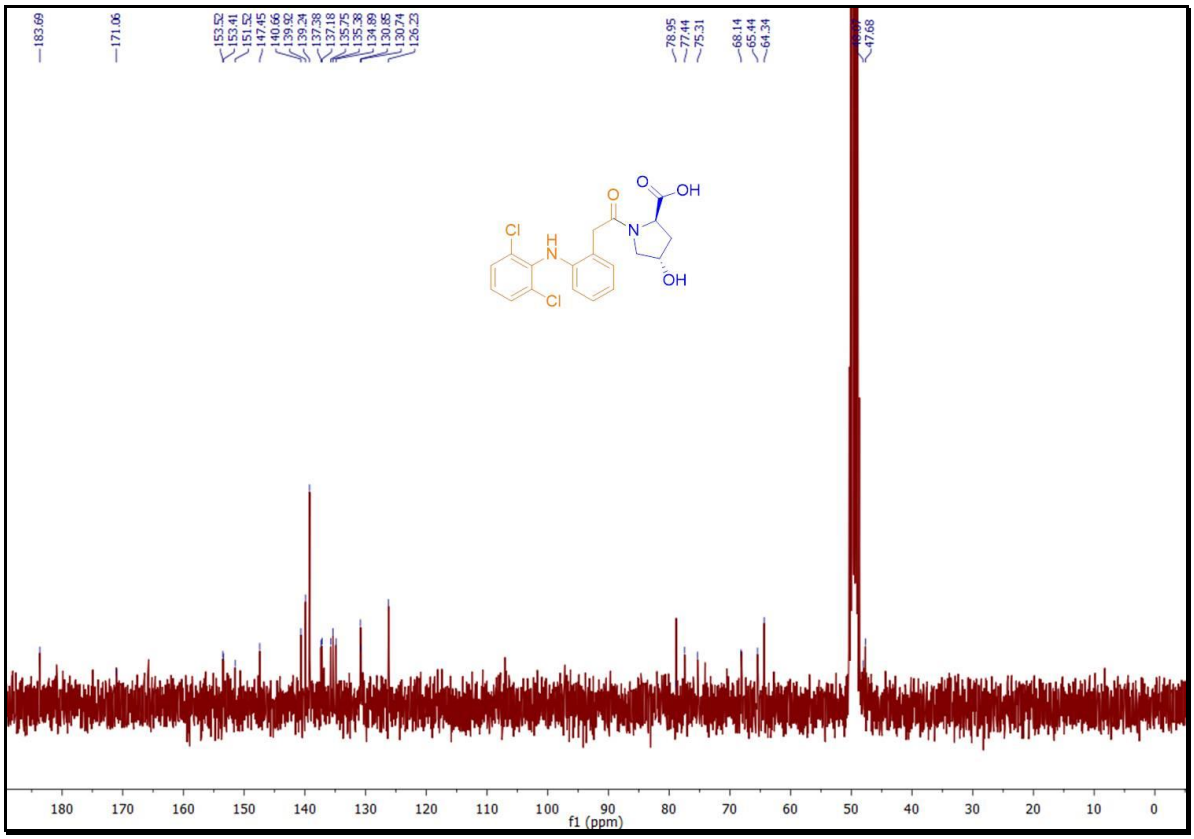

Figure S13: ^{1}H NMR and ^{13}C NMR spectra of **DIC.HYP** in DMSO-d_6.

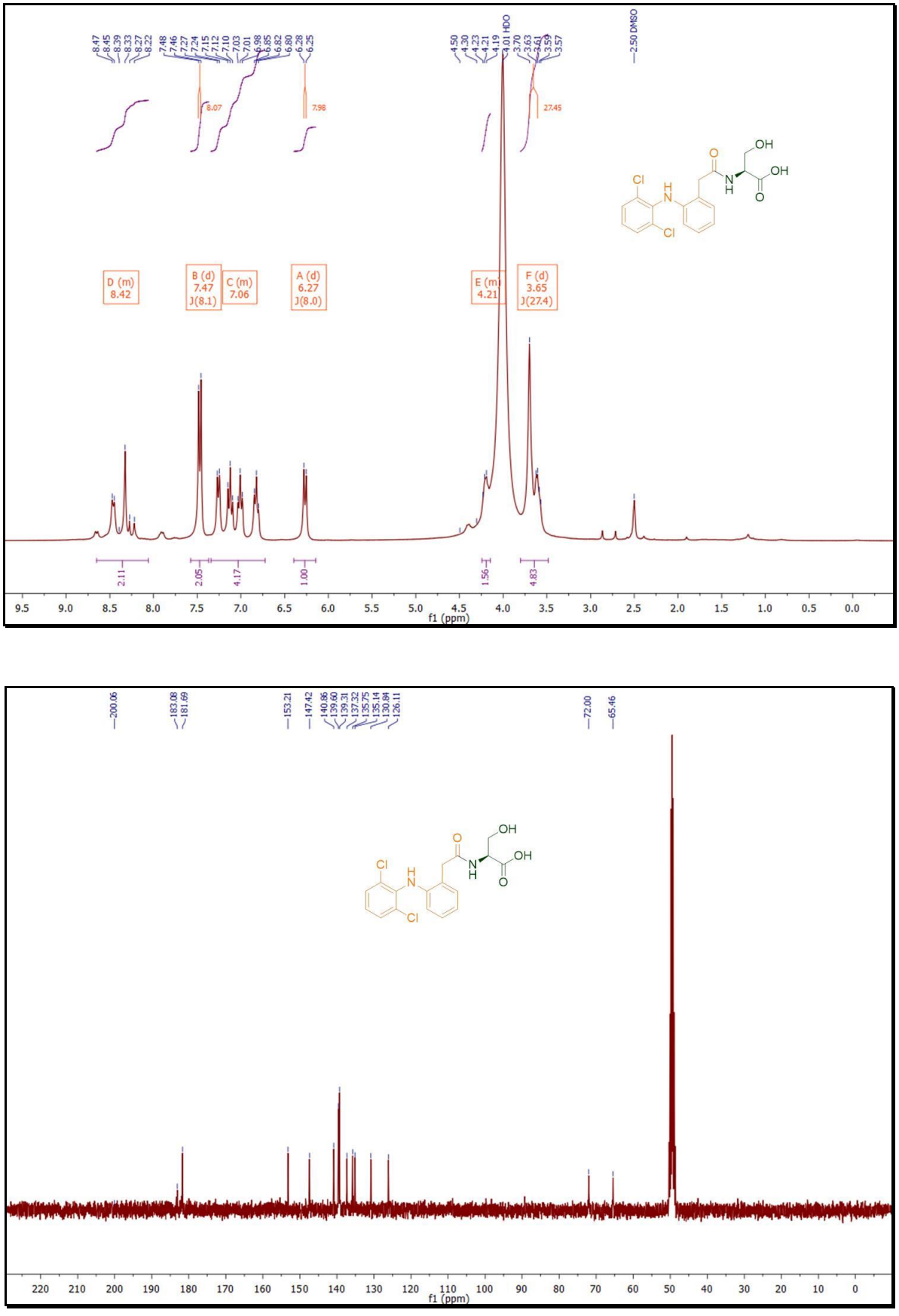

Figure S14: ^{1}H NMR and ^{13}C NMR spectra of **DIC.SER** in DMSO-d_6.

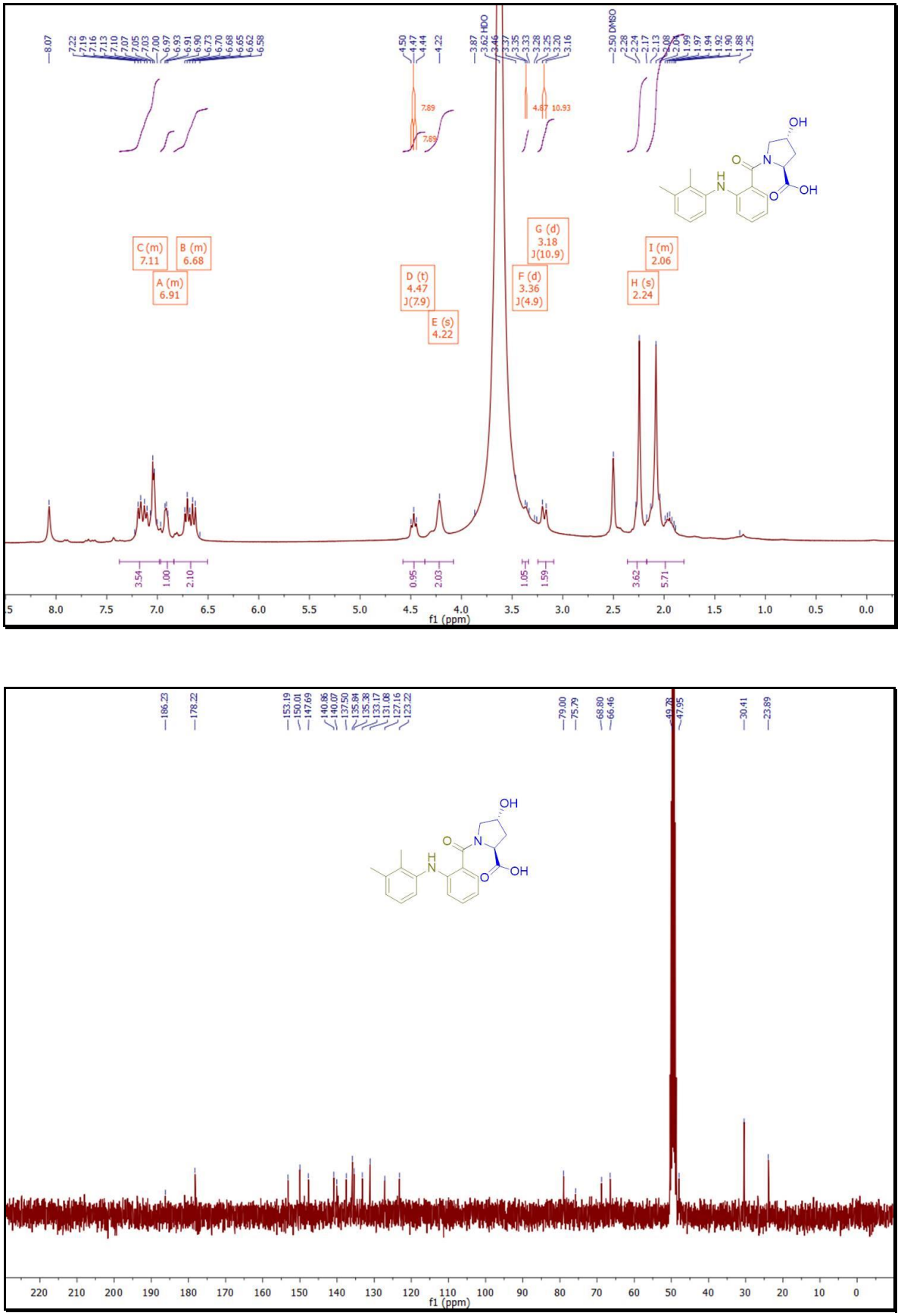

Figure S15: ^{1}H NMR and ^{13}C NMR spectra of **MEF.HYP** in DMSO-d_6.

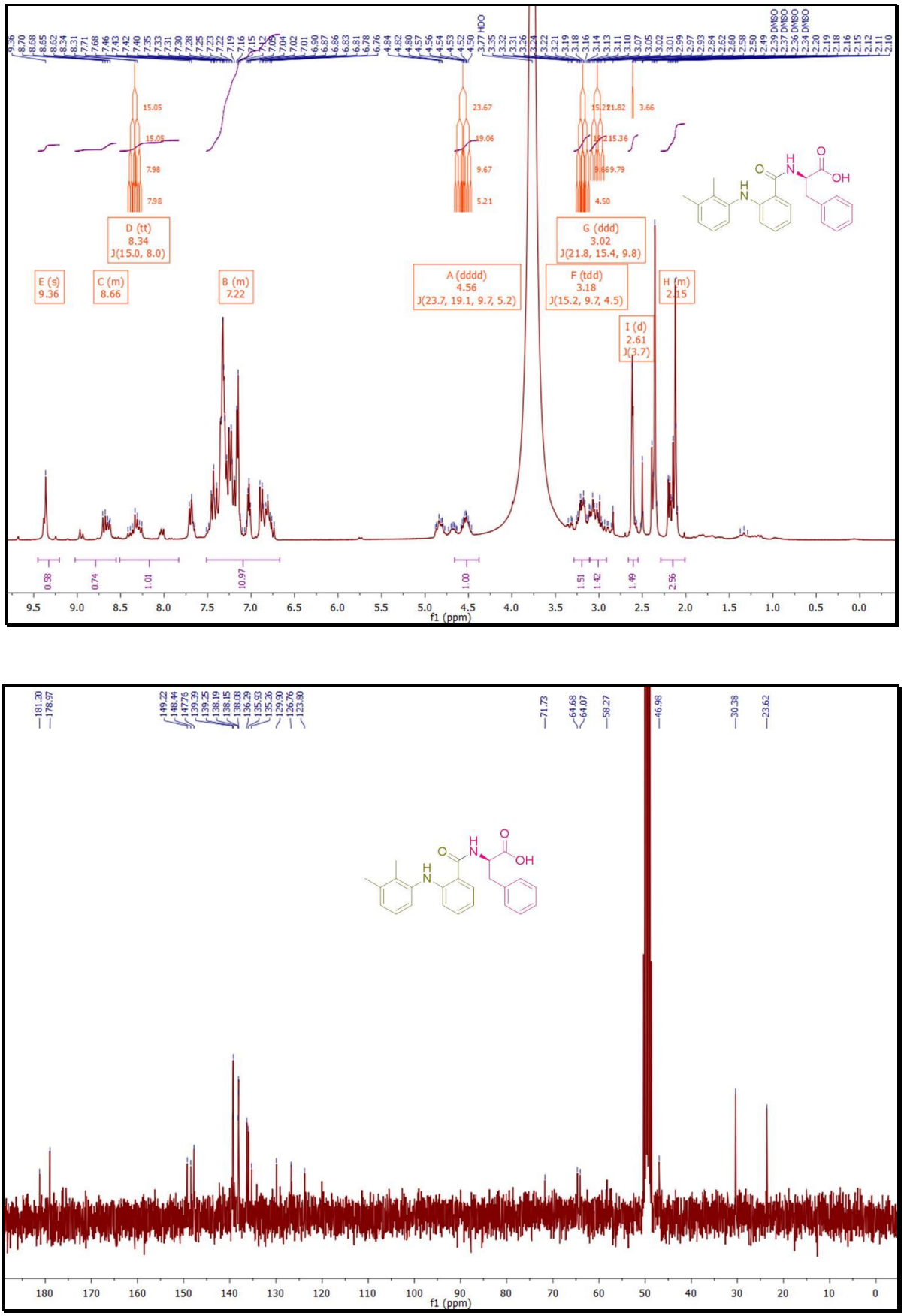

Figure S16: ^{1}H NMR and ^{13}C NMR spectra of **MEF.PHE** in DMSO-d_6.

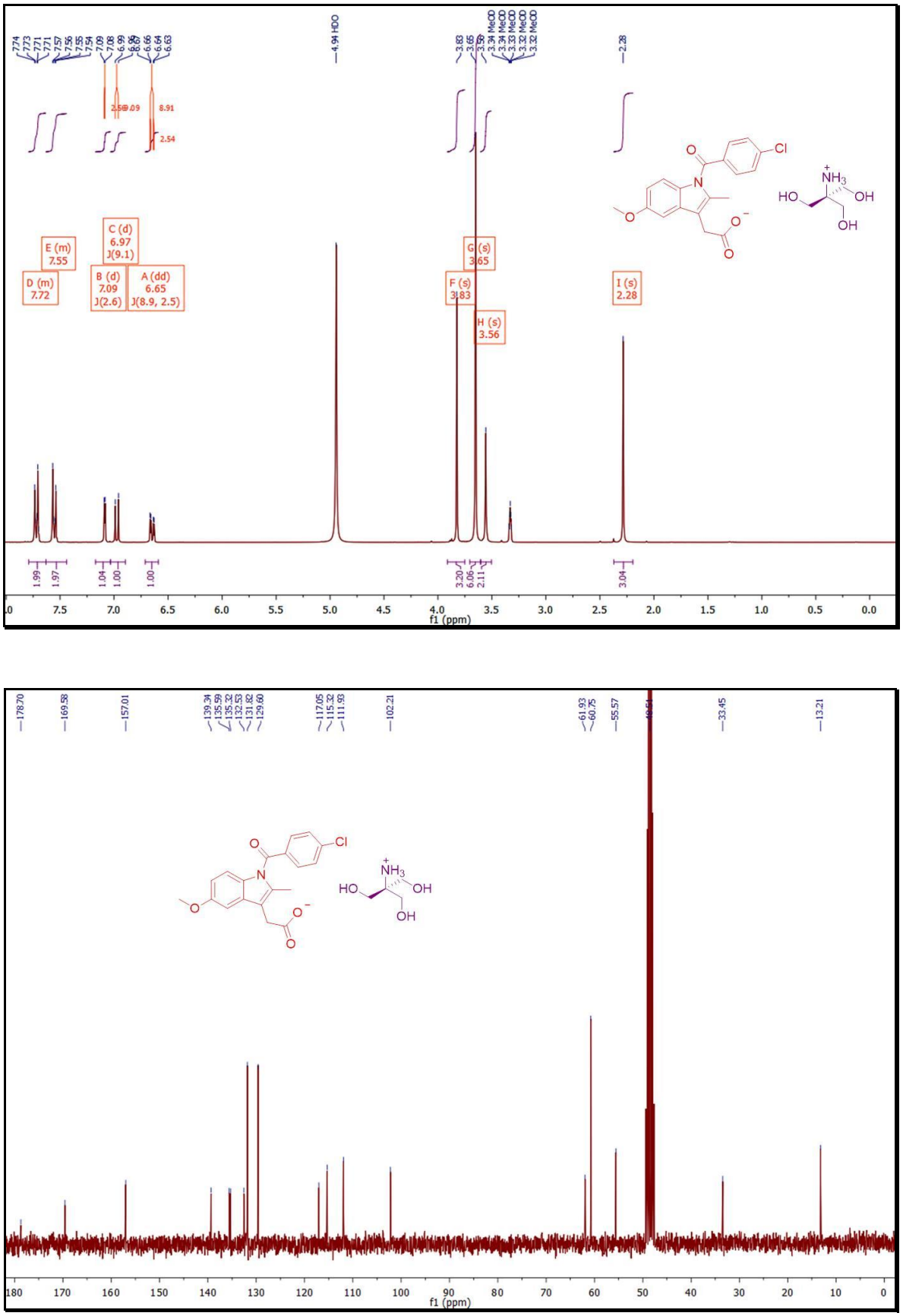

Figure S17: ^{1}H NMR and ^{13}C NMR spectra of **IND.TRIS** in CD_3OD.

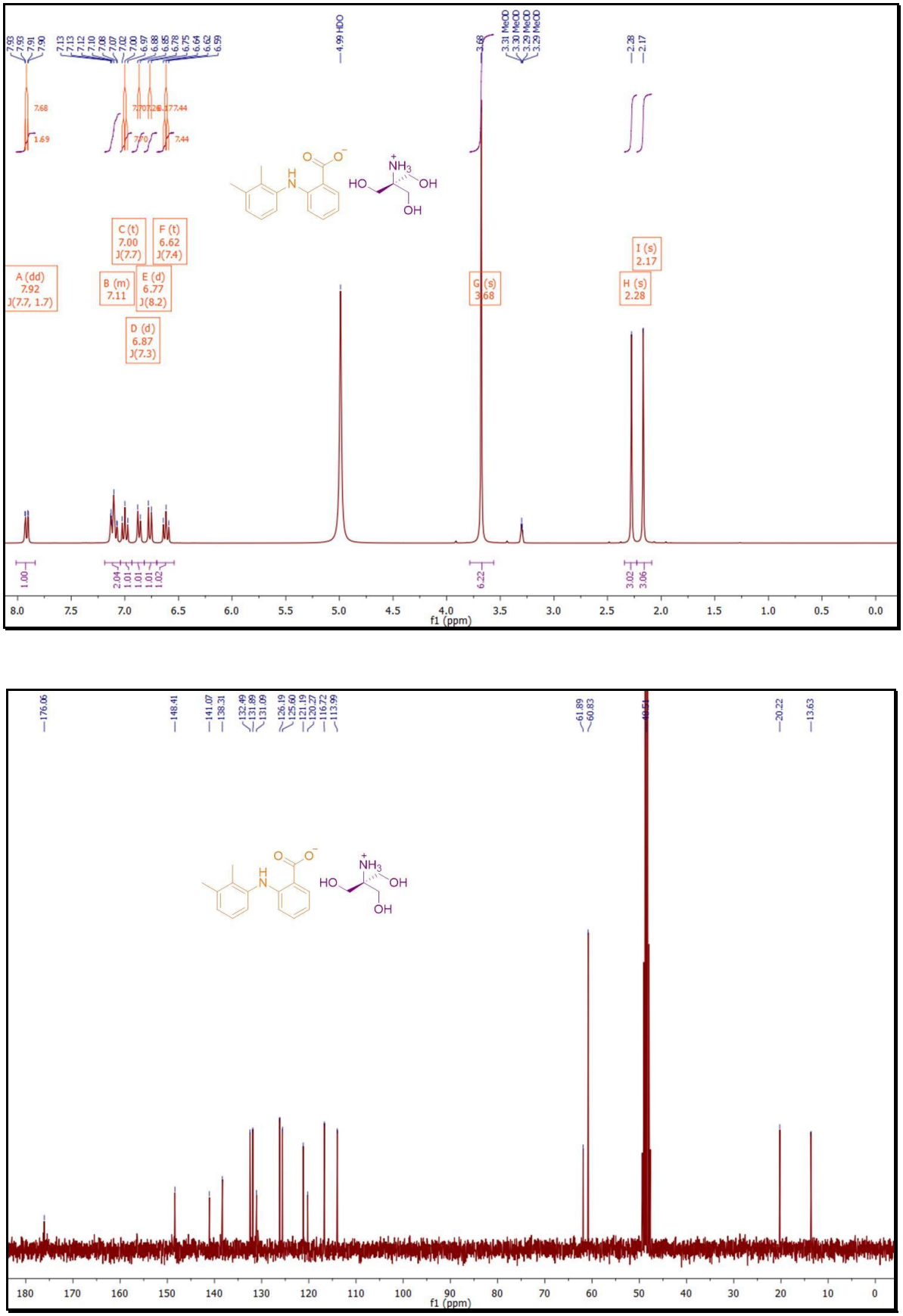

Figure S18: ^{1}H NMR and ^{13}C NMR spectra of **MEF.TRIS** in CD_3OD.

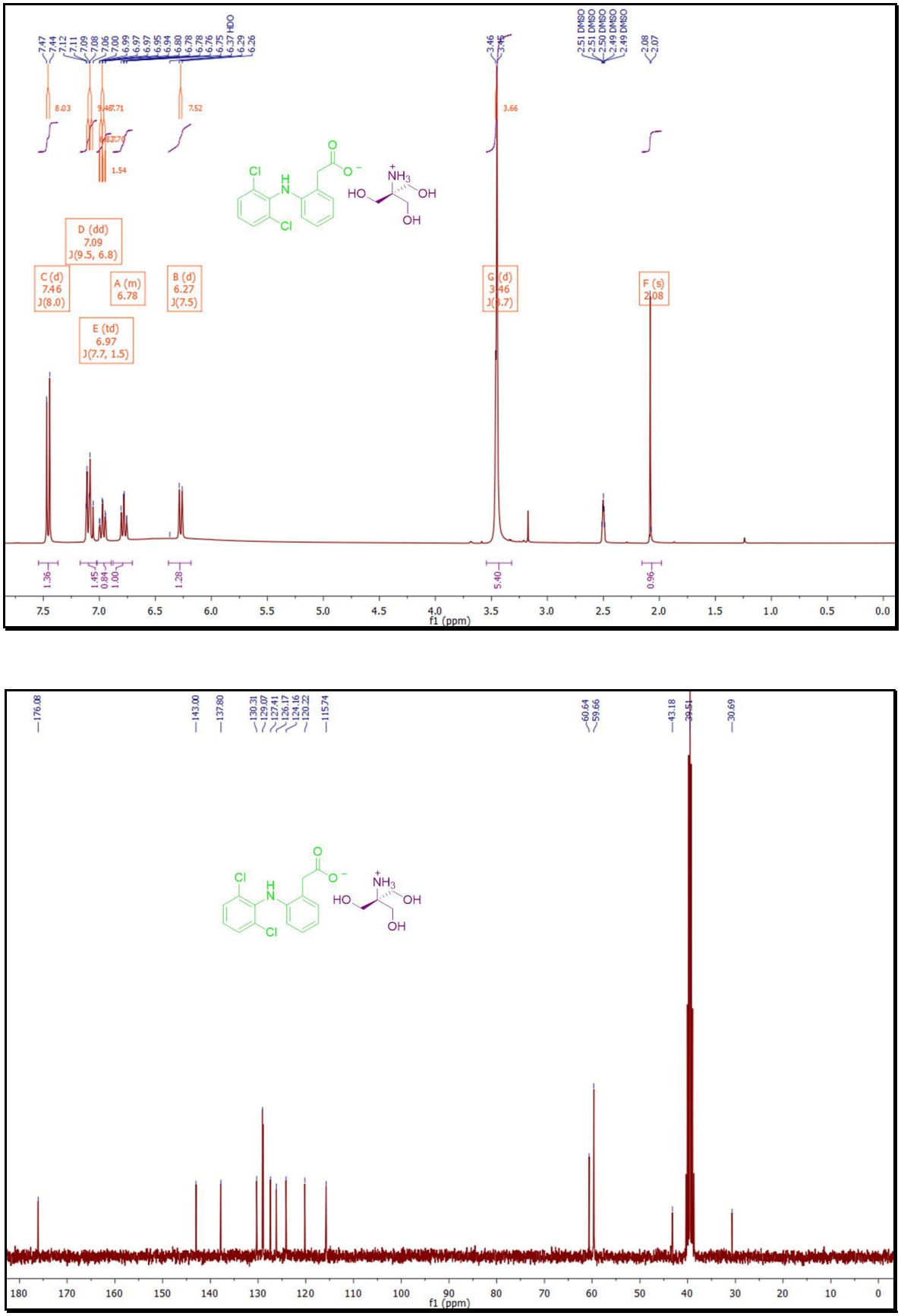

Figure S19: ^{1}H NMR and ^{13}C NMR spectra of **DIC.TRIS** in DMSO-d_6.

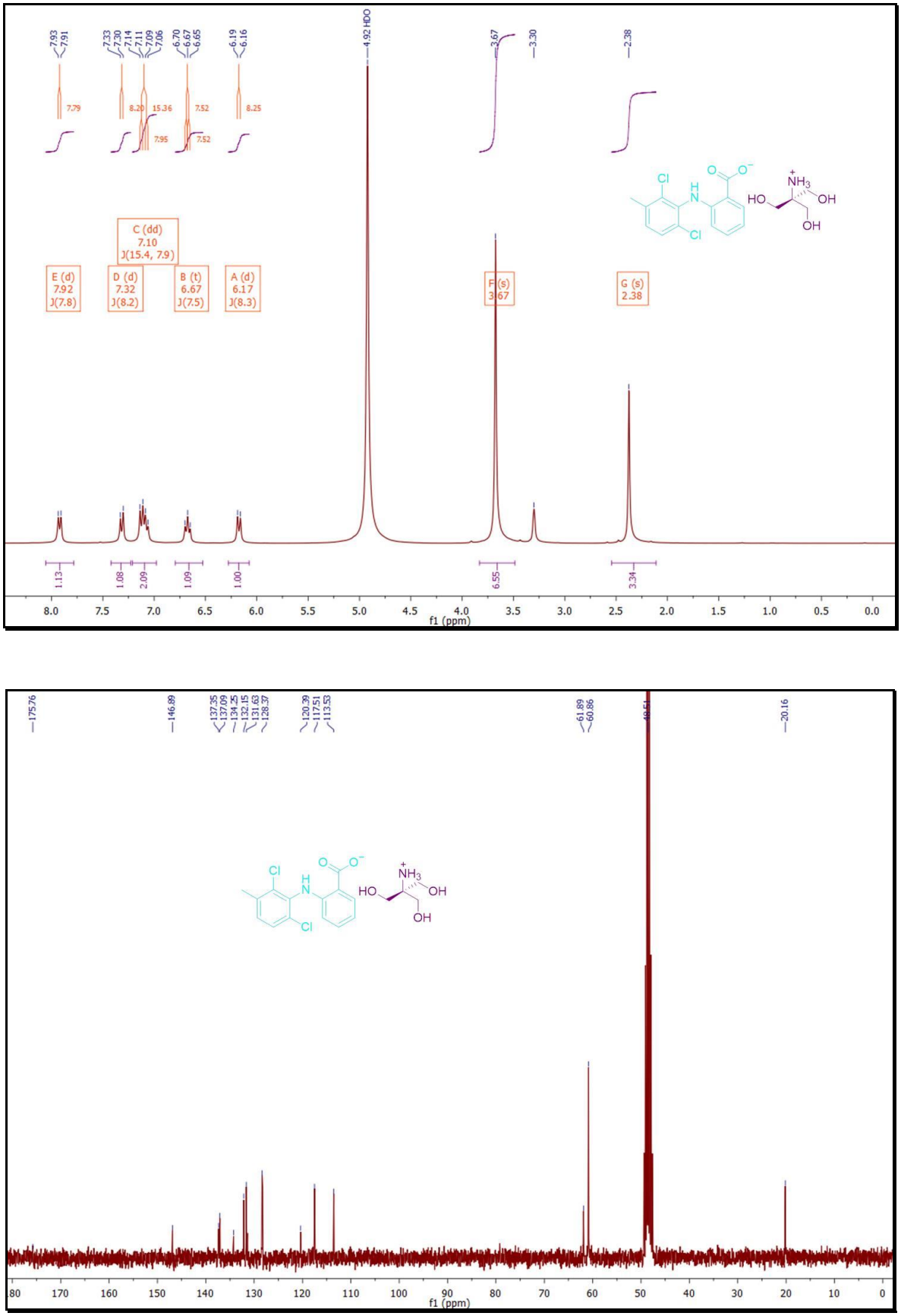

Figure S20: ^{1}H NMR and ^{13}C NMR spectra of **MEC.TRIS** in CD_3OD.

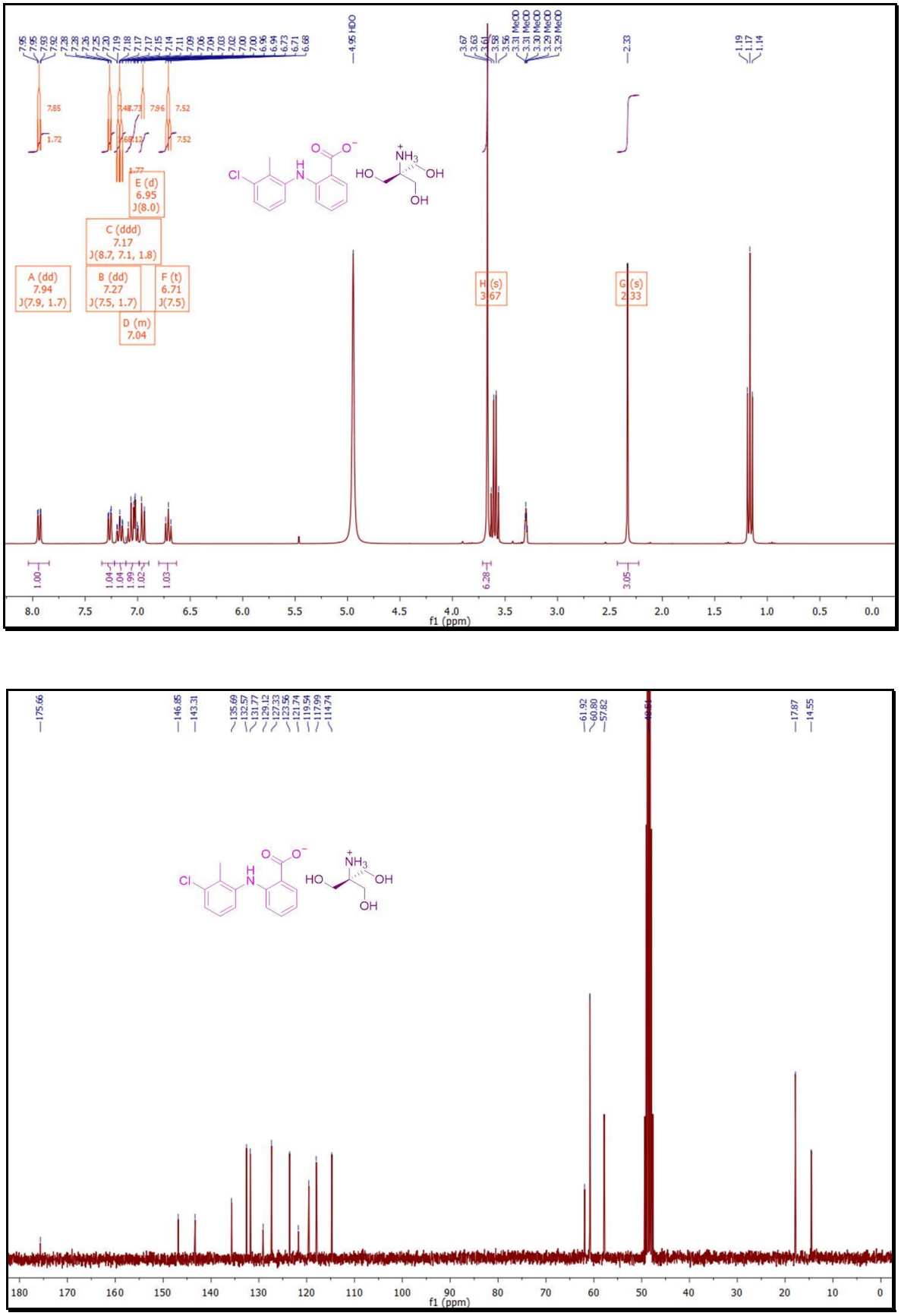

Figure S21: ^{1}H NMR and ^{13}C NMR spectra of **TOL.TRIS** in CD_3OD.

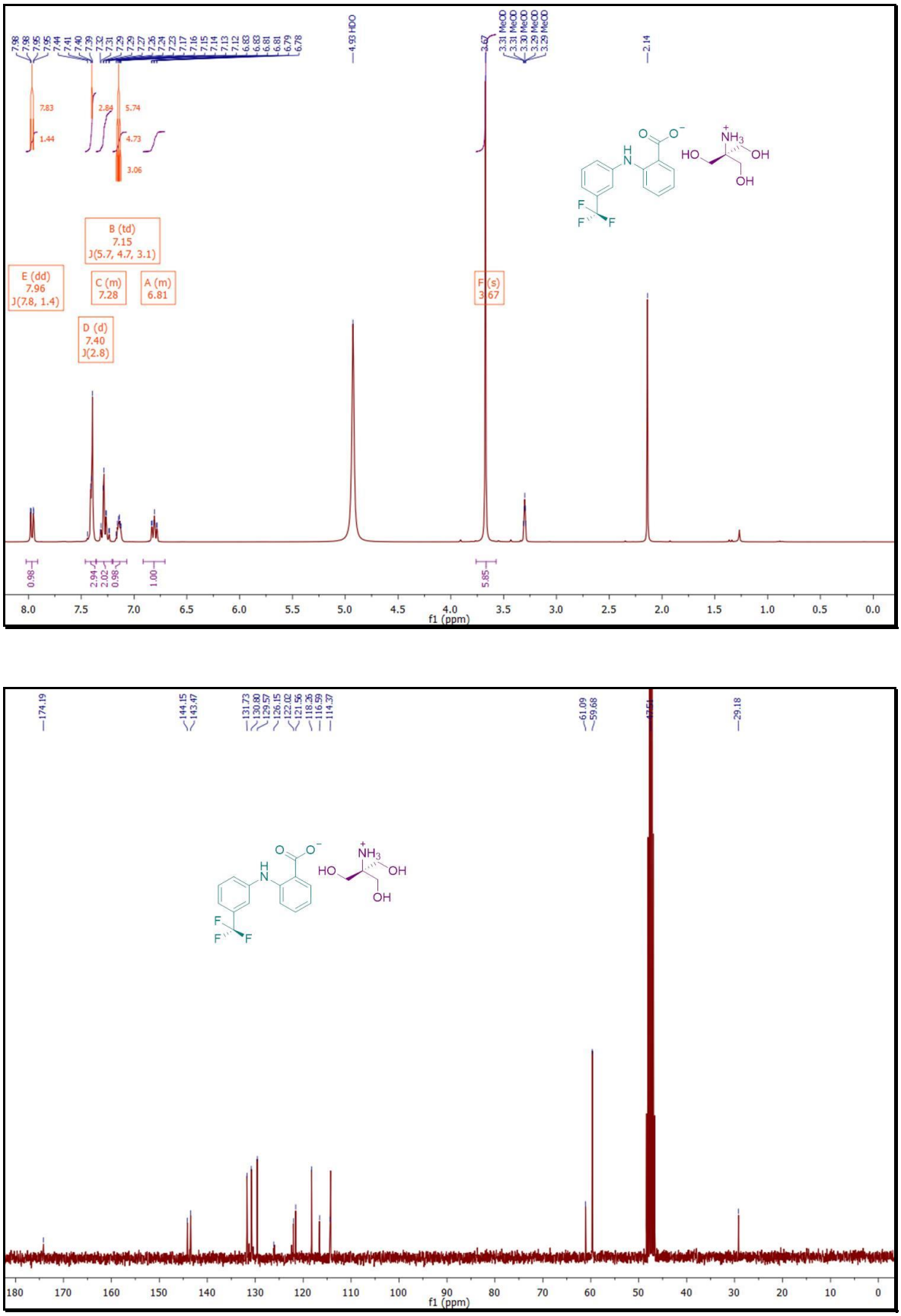

Figure S22: ^{1}H NMR and ^{13}C NMR spectra of **FLU.TRIS** in CD_3OD.

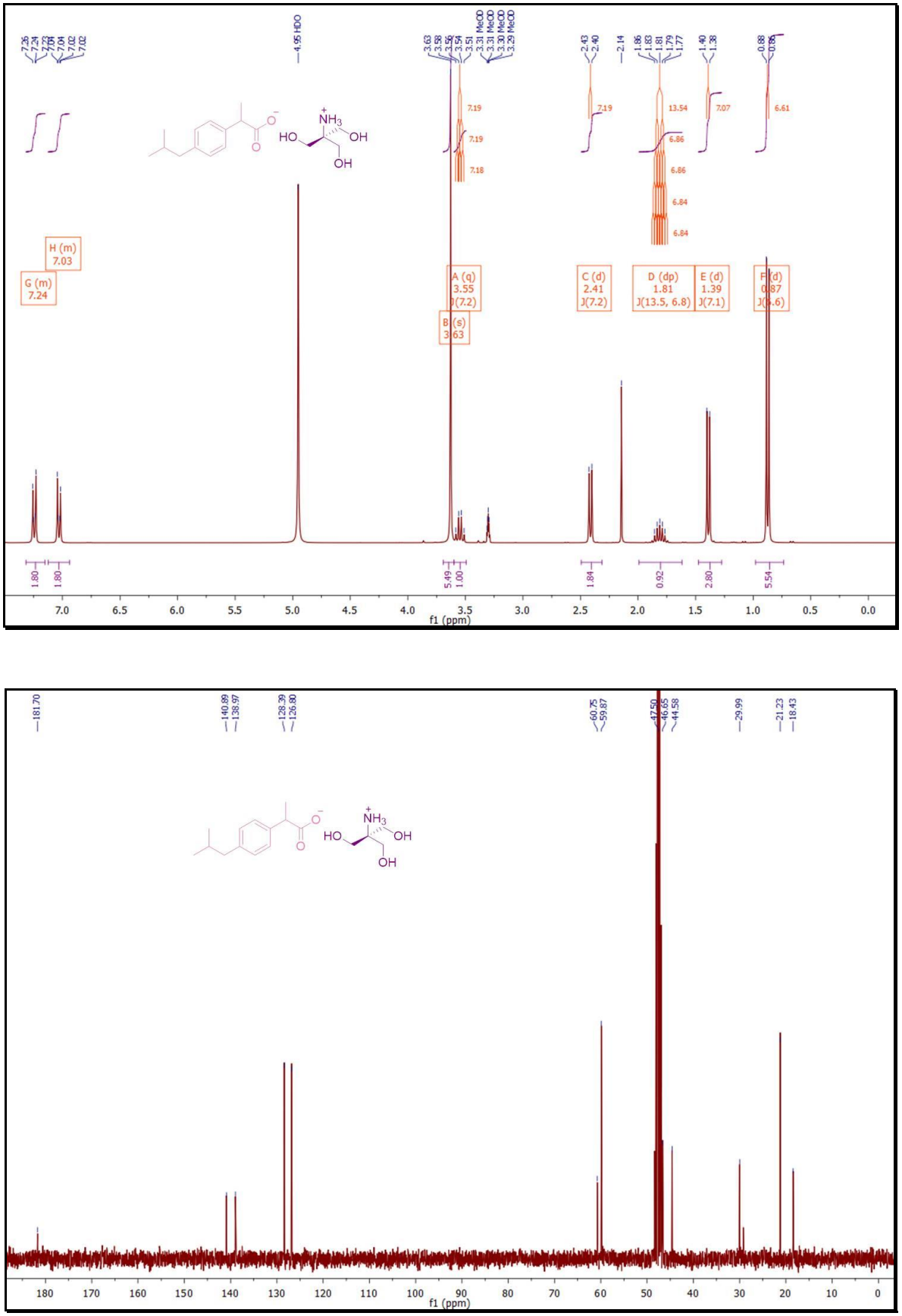

Figure S23: ^{1}H NMR and ^{13}C NMR spectra of **IBU.TRIS** in CD_3OD.

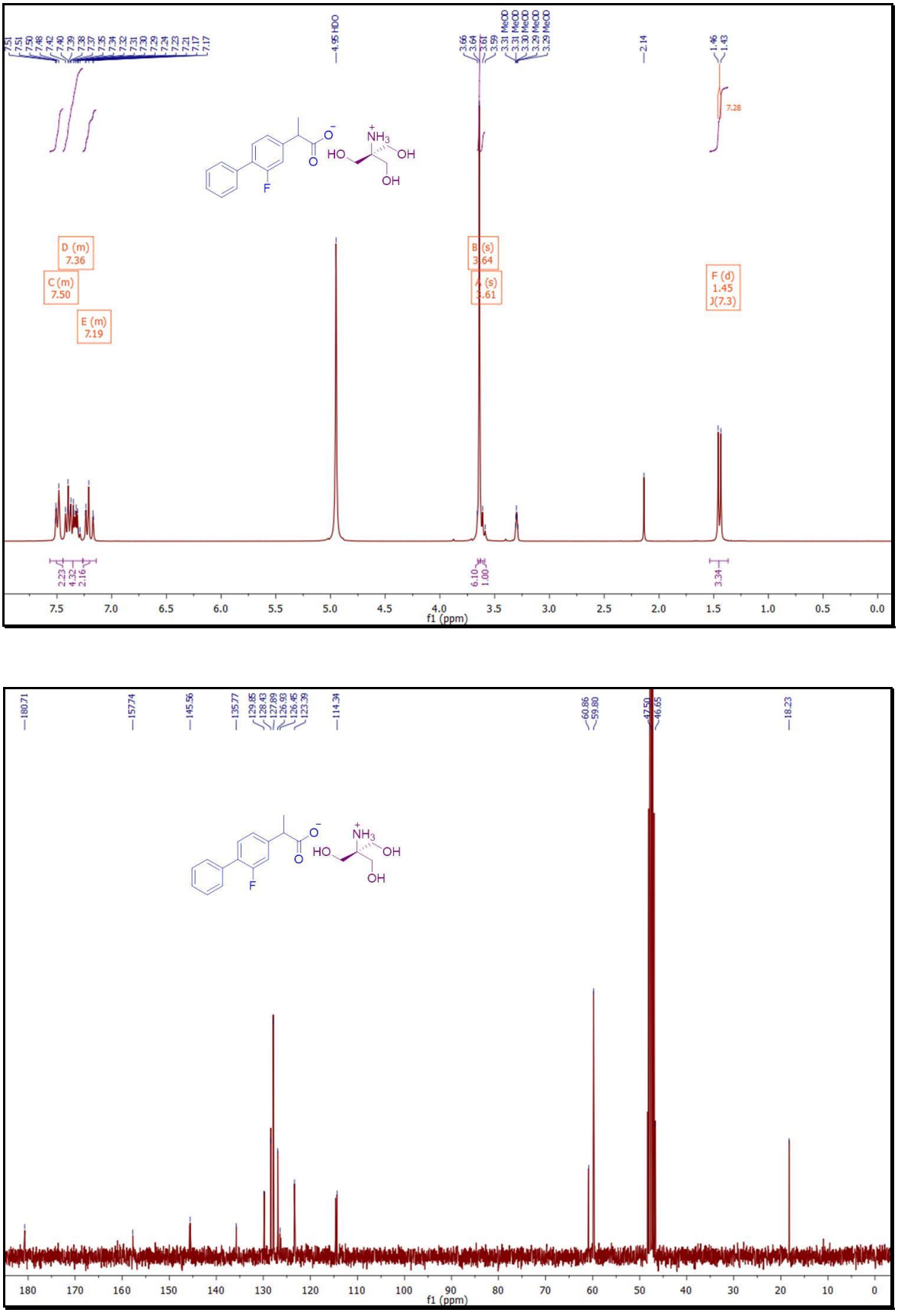

Figure S24: ^{1}H NMR and ^{13}C NMR spectra of **FLR.TRIS** in CD_3OD.

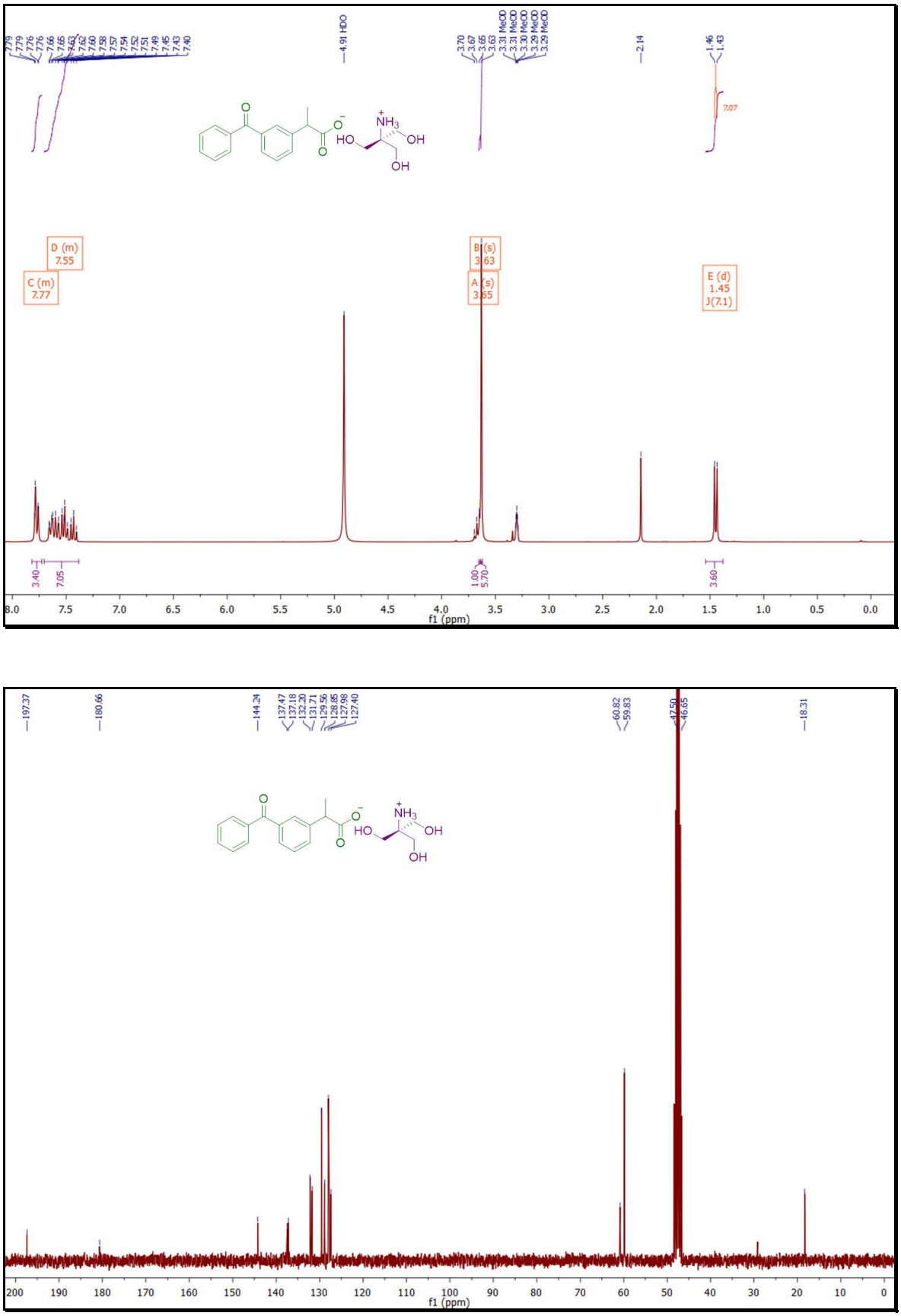

Figure S25: ^{1}H NMR and ^{13}C NMR spectra of **KET.TRIS** in CD_3OD.

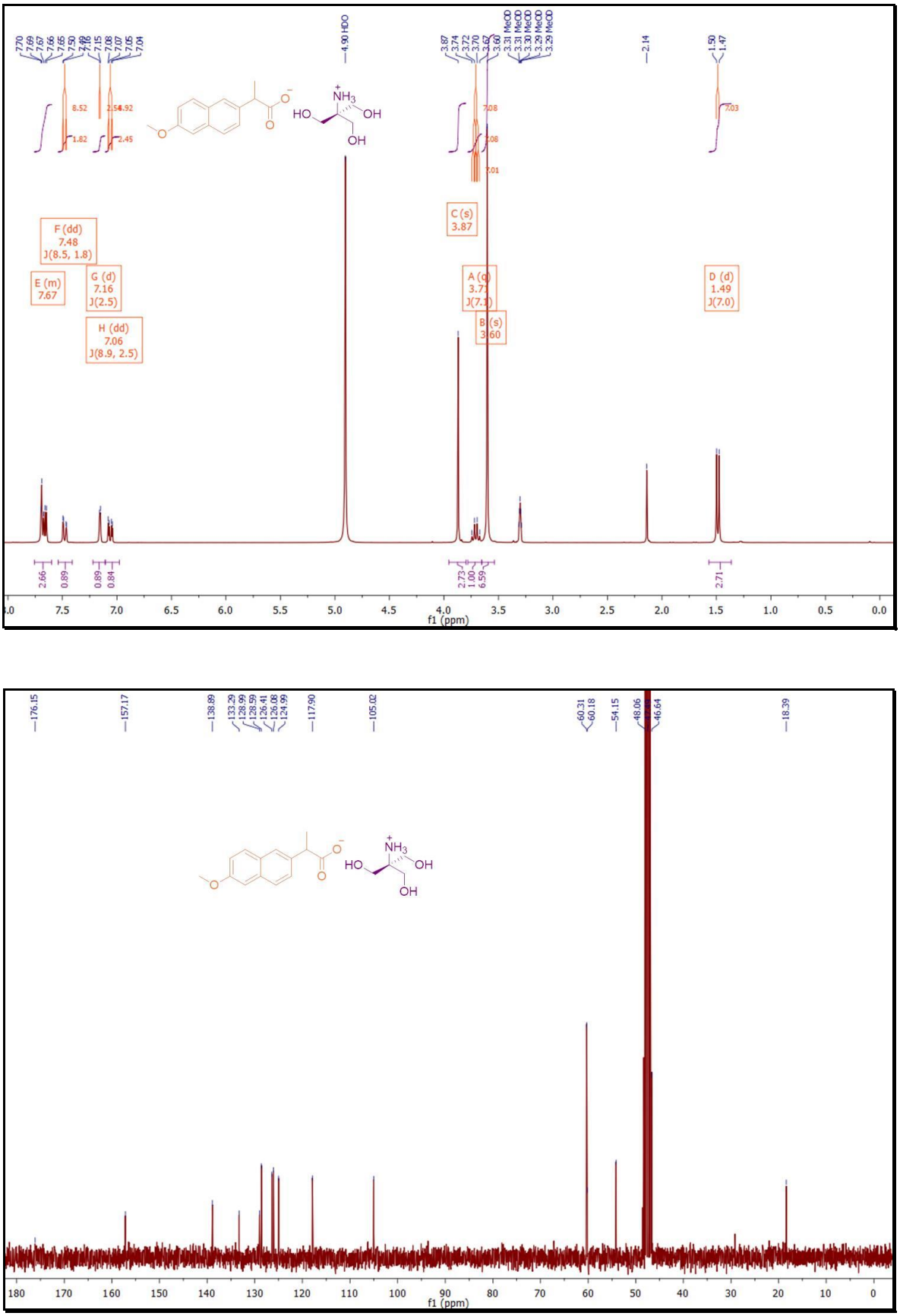

Figure S26: ^{1}H NMR and ^{13}C NMR spectra of **NAP.TRIS** in CD_3OD.

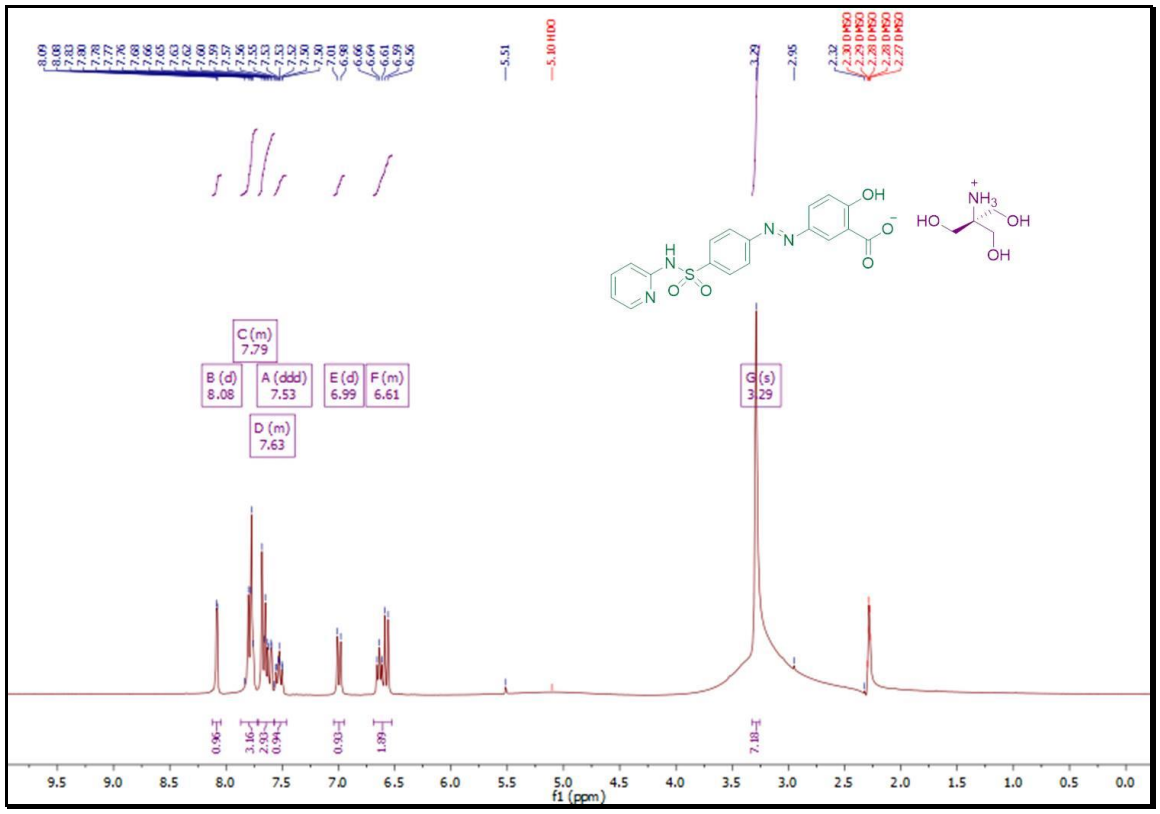

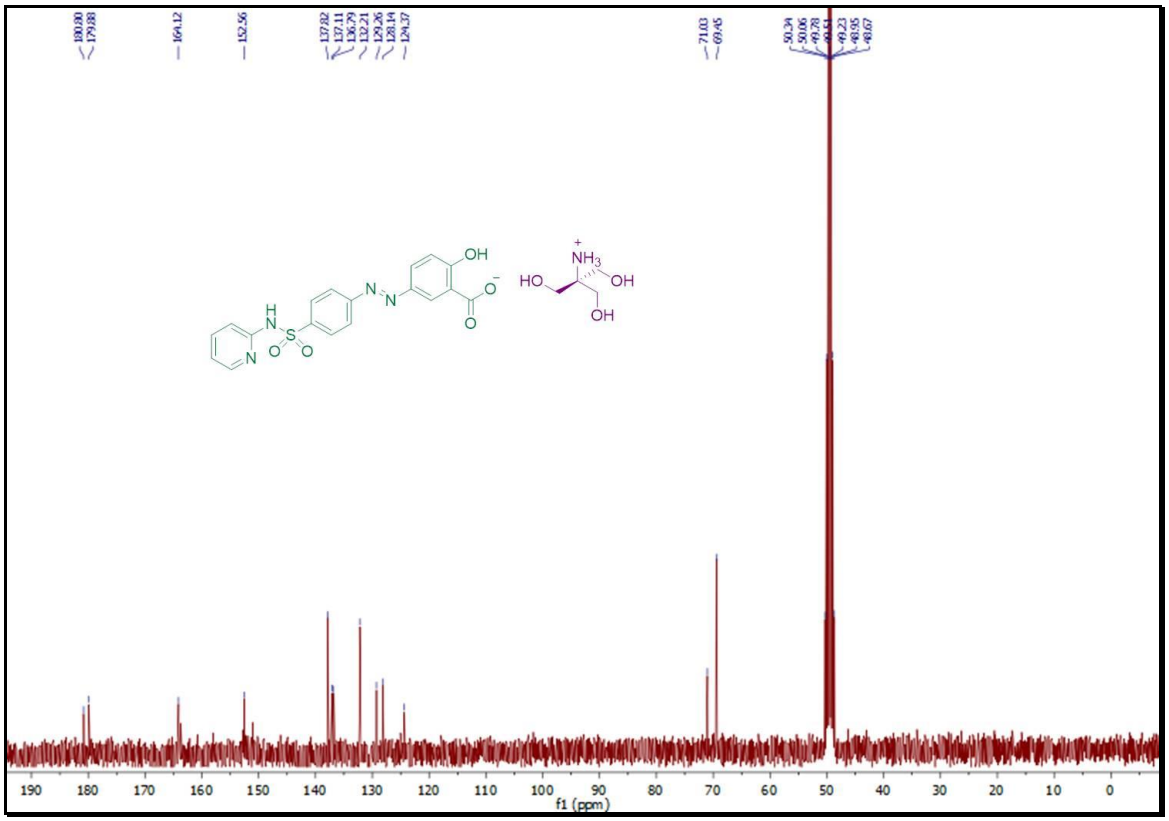

Figure S27: ^{1}H NMR and ^{13}C NMR spectra of **SUL.TRIS** in DMSO-d_6.

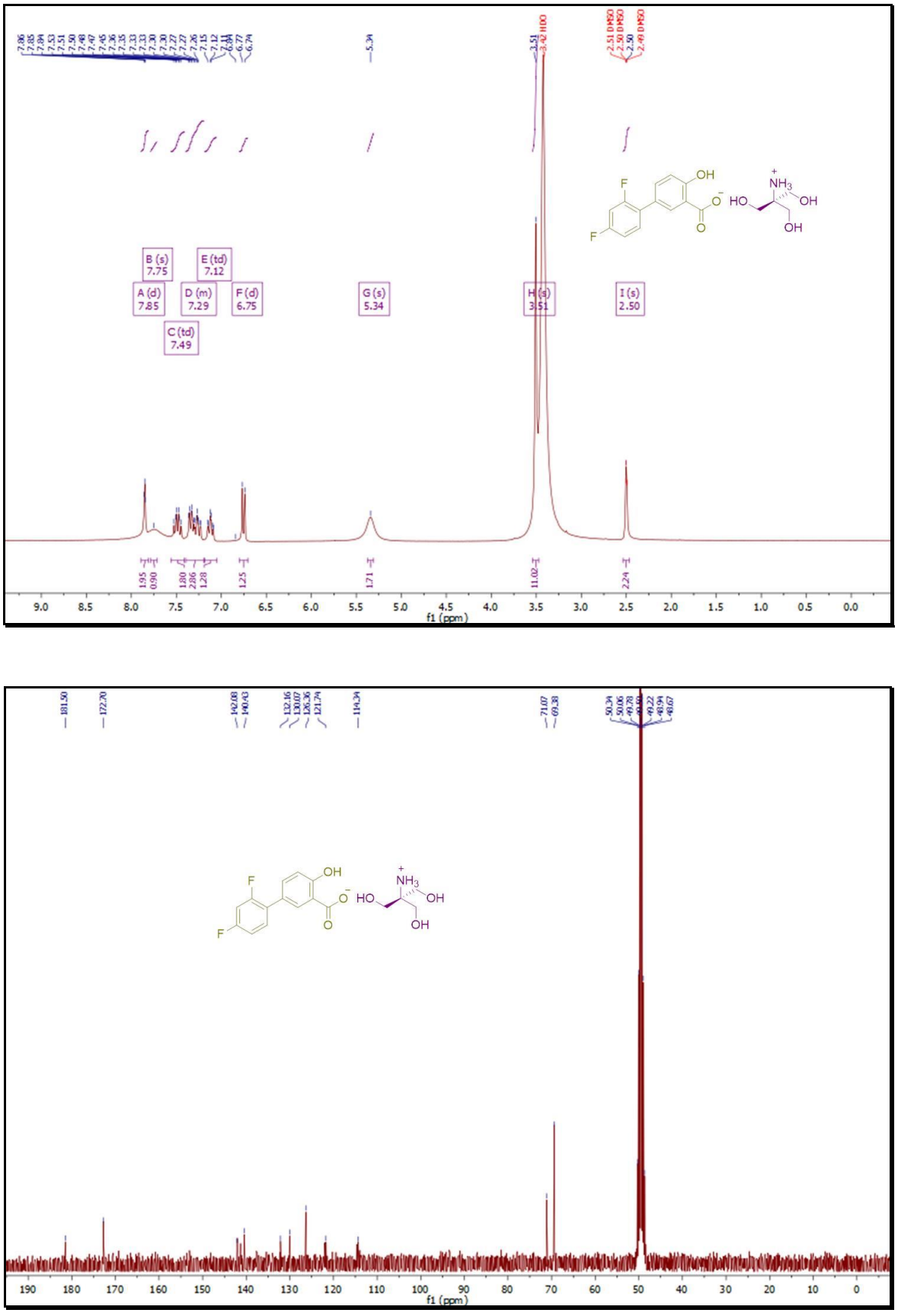

Figure S28: ^{1}H NMR and ^{13}C NMR spectra of **DIF.TRIS** in DMSO-d_6.

Gelation experiment

In a typical gelation experiment, 20 mg of the compound [in proper Ligand (organic salt):Metal ratio] was taken in a test tube (10x100 mm) and then first the ligands were dissolved in 50 µL of the targeted solvent (for aqueous solvents – the organic solvent) by heating until a clear hot solution was formed. Then the remaining 450 µL metal salt containing water was added into the hot clear solution. The solution was then allowed to cool to room temperature for the formation of a stable gel which was confirmed by test tube inversion (see Figure S29).

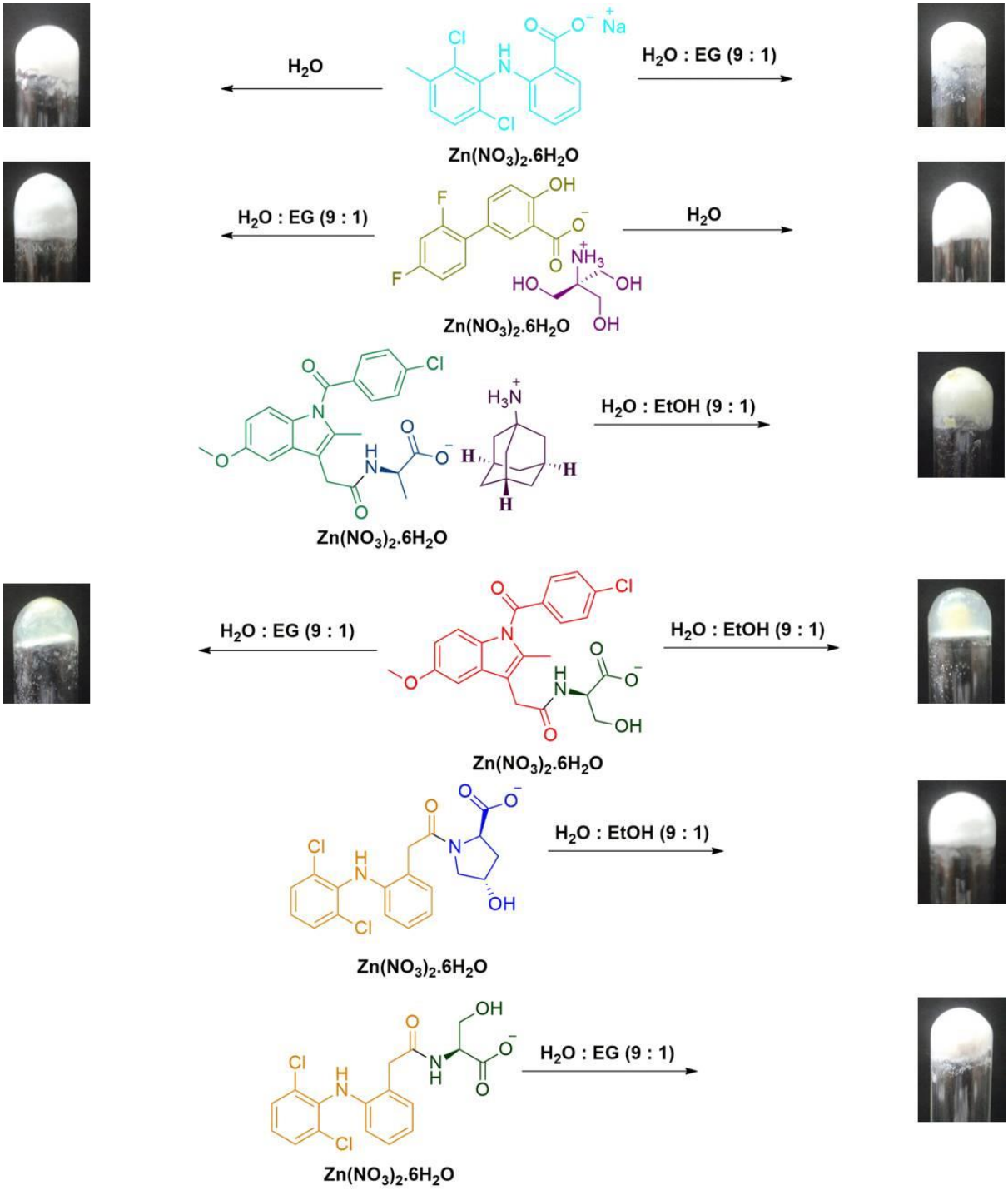

Figure S29: Optical images of the metallohydrogels.

After reacting with different zinc metal salts, the organic salts and bioconjugates were tested for metallogelation. Out of all the compounds; **MEC.Na.Zn**, **IND.SER.TRIS.Zn**, **DIC.HYP.TRIS.Zn**, **DIC.SER.TRIS.Zn**, **IND.ALA.AMN.Zn** and **DIF.TRIS.Zn** turned out to be gelators of four different aqueous solvents and that of **MEC.Na.Zn** and

DIF.TRIS.Zn are pure hydrogelators with the MGC range of 4-8 wt% (W/V) (see Table S1). Variation of Ligand (organic salt):Metal and anion variation on gelation for the gelator molecule in $Zn(NO_3)_2 \cdot 6H_2O$ [Ligand (organic salt):Metal = 2:1] were also performed (see Table S2).

Table S1: Gelation data of the compounds.

Compounds	Gelation solvents			
	H_2O	H_2O : DMSO (9 : 1)	H_2O : EtOH (9 : 1)	H_2O : EG (9 : 1)
DIC.Na.Zn	CS	INS	CS	INS
MEC.Na.Zn	**G (8.0[a])**	SG	SG	**G (8.0[a])**
IBU.Na.Zn	CS	CS	CS	CS
NAP.Na.Zn	INS	INS	INS	INS
IND.TRIS.Zn	INS	INS	INS	INS
MEF.TRIS.Zn	CS	INS	INS	CS
DIC.TRIS.Zn	INS	INS	INS	INS
MEC.TRIS.Zn	CS	CS	CS	CS
TOL.TRIS.Zn	INS	INS	CS	CS
FLU.TRIS.Zn	CS	CS	INS	INS
IBU.TRIS.Zn	CS	INS	SG	SG
FLR.TRIS.Zn	CS	INS	INS	CS
KET.TRIS.Zn	INS	INS	INS	INS
NAP.TRIS.Zn	INS	INS	INS	INS
SUL.TRIS.Zn	CS	CS	INS	INS
DIF.TRIS.Zn	**G (8.0[a])**	INS	INS	**G (8.0[a])**
IND.PHE.AMN.Zn*	INS	INS	INS	INS
IND.ALA.AMN.Zn*	INS	INS	**G (4.0[a])**	INS
IND.HYP.AMN.Zn*	INS	INS	INS	INS
IND.THR.AMN.Zn*	INS	INS	INS	INS
IND.VAL.AMN.Zn*	INS	INS	INS	CS
IND.LEU.AMN.Zn*	GP	INS	INS	GP
IND.HYP.TRIS.Zn*	CS	INS	CS	INS
IND.SER.TRIS.Zn*	SG	SG	**G (4.0[a])**	**G (4.0[a])**
DIC.HYP.TRIS.Zn*	SG	INS	**G (4.0[a])**	SG
DIC.SER.TRIS.Zn*	GP	INS	CS	**G (4.0[a])**
MEF.HYP.TRIS.Zn*	INS	INS	INS	INS
MEF.PHE.TRIS.Zn*	INS	INS	INS	INS

Gelator concentration = 8 wt%, *Gelator concentration = 4 wt%, Metal salt is $Zn(NO_3)_2 \cdot 6H_2O$. Ligand : Metal = 2 :1. [a]The minimum gelator concentration, (MGC) in wt % (w/v). CS= Colloidal Solution. INS= Insoluble. SG= Semi Gel. GP= Gelatinous Precipitate. G= Gel.

To study the role of counter anion as well as NSAID salt:metal salt ratio on gelation, we reacted the gel producing NSAID salts (**MEC.Na**, **DIF.TRIS**, **IND.ALA.AMN**, **IND.SER.TRIS**, **DIC.SER.TRIS** and **DIC.HYP.TRIS**) with Zn(II) salts having various counter anions (NO_3^-,SO_4^{2-}, AcO^-, ClO_4^-, F^-, Cl^-, Br^- and I^-) with 2:1 and 1:1 ratio in the corresponding gelling solvents.

Table S2: Gelation data of the compounds.

Compounds	Gelation Solvents	Metal salt (L:M)															
		$Zn(NO_3)_2 \cdot 6H_2O$		$ZnSO_4 \cdot 7H_2O$		$Zn(OAc)_2 \cdot 2H_2O$		$Zn(ClO_4)_2 \cdot 6H_2O$		ZnF_2		$ZnCl_2$		$ZnBr_2$		ZnI_2	
	L : M	(2:1)	(1:1)	(2:1)	(1:1)	(2:1)	(1:1)	(2:1)	(1:1)	(2:1)	(1:1)	(2:1)	(1:1)	(2:1)	(1:1)	(2:1)	(1:1)
MEC.Na.Zn*	H_2O	G	CS	INS	INS	CS	INS	INS	INS	CS	SG	CS	CS	SG	INS	SG	GP
	H_2O : EG (9:1)	G	G	G	CS	G	G	G	CS	CS	SG	G	SG	G	SG	G	SG
IND.SER.TRIS.Zn	H_2O : EtOH (9:1)	G	G	G	G	G	G	G	G	G	G	G	G	G	G	G	G
	H_2O : EG (9:1)	G	G	G	G	G	G	G	CS	G	G	G	G	G	G	G	G
DIC.SER.TRIS.Zn	H_2O : EG (9:1)	G	G	G	G	INS	GF	G	GP	CS	CS	G	CS	CS	G	G	G
DIC.HYP.TRIS.Zn	H_2O : EtOH (9:1)	G	G	G	CS	INS	INS	G	GP	CS	CS	CS	CS	CS	GP	CS	CS
DIF.TRIS.Zn	H_2O	G	G	INS	INS	G	SG	INS	INS	GP	GP	INS	INS	SG	SG	SG	SG
	H_2O : EG (9:1)	G	G	INS	INS	CS	CS	GP	CS	GP	GP	SG	SG	GP	INS	GP	GP
IND.ALA.AMN.Zn	H_2O : EtOH (9:1)	G	G	G	G	G	G	G	G	G	G	INS	G	G	G	G	G

Gelator concentration = 4 wt%, *Gelator concentration = 8 wt%, [a]The minimum gelator concentration, (MGC) in wt % (w/v). CS= Colloidal Solution. INS= Insoluble. SG= Semi Gel. GP= Gelatinous Precipitate. G= Gel. GF= Gelatinous fibre.

Table S3: Gelation data of the crystals of Zn complexes in aqueous solvents.

Compounds	Aqueous solvents
$(DIC)_2.Zn$	Colloidal precipitate
$(IND)_2.Zn$	Soluble
$(TOL)_2.Zn$	Insoluble
$(IBU)_2.Zn$	Soluble
$(FLR)_2.Zn$	Soluble
$(TOL)_2.Zn$	Soluble
$(DIF)_2.Zn$	Gelatinous Precipitate

Gelator concentration = 8 wt%

Microscopy

Microscopical measurement of the gel was done by TEM (transmission electron microscopy). The sample for TEM was prepared by painting a small portion gel on a carbon coated Cu (300 mesh) TEM grid. The grid was dried under vacuum at room temperature for one day and used for recording TEM images using an accelerating voltage of 100 kV without staining. To study the morphology of the gel network, we then performed high-resolution transmission electron microscopy (HR-TEM) on selected gels (see Figure S30-S32). Highly entangled 1D objects were obtained in all cases. HR-TEM images of the xerogels of **MEC.Na.Zn**, **DIF.TRIS.Zn, DIC.SER.TRIS.Zn** and **IND.ALA.AMN.Zn** revealed the highly entangled fibrous nature present in the gel state.

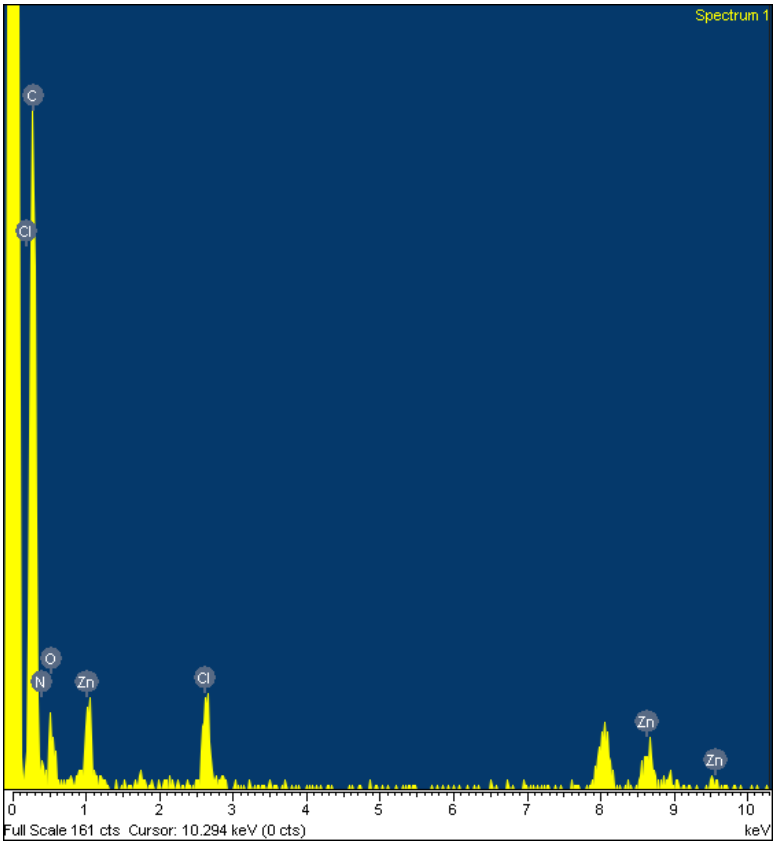

Figure S30: EDX spectrum of H_2O : EtOH (9 : 1) gel of **IND.ALA.AMN.Zn**.

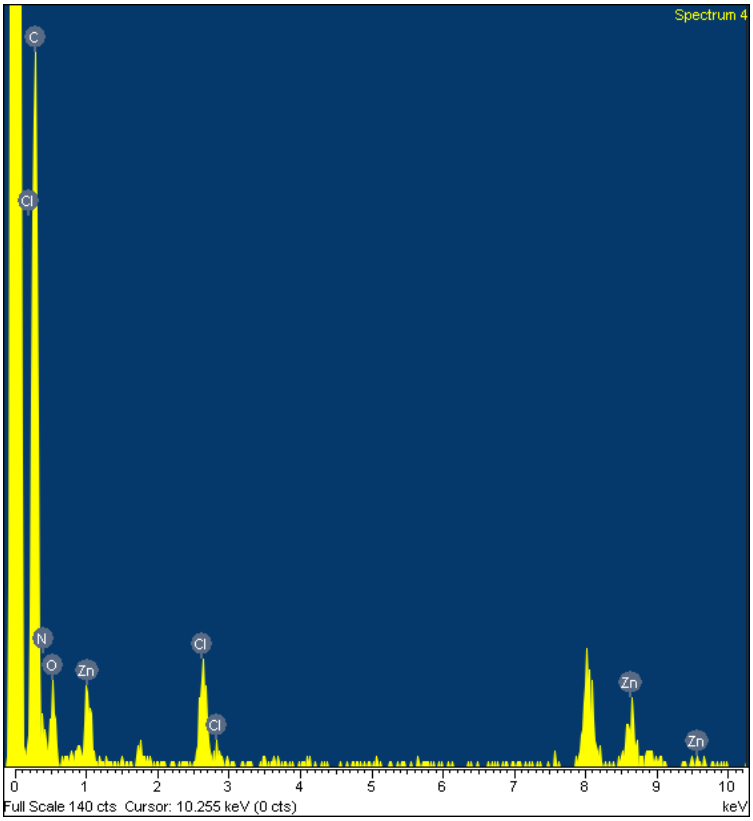

Figure S31: EDX spectrum of H_2O : EG (9 : 1) gel of C. **DIC.SER.TRIS.Zn**.

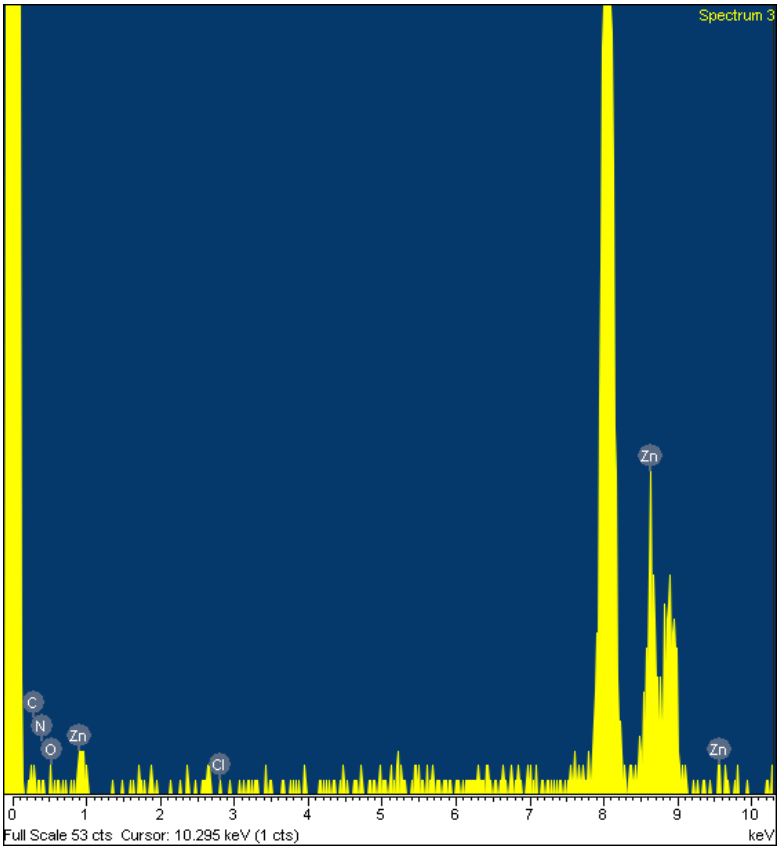

Figure S32: EDX spectrum of hydrogel of **DIF.TRIS.Zn**.

Rheological studies

Rheology studies were carried out using an Anton Paar Modular Compact Rheometer MCR 102. 4 wt % of different gels were taken in this experiments and these were carried out at 25 ^{o}C using parallel plate geometry (25 mm diameter, 1 mm gap). Rheology or flow study is a technique suitable for studying the flow behaviour of non-Newtonian fluid like supramolecular gels. Since supramolecular gels are visco-elastic material, they are expected to display both viscous (liquid like) as well as elastic (solid like) behaviour. Dynamic rheology wherein elastic modulus G´ and viscous modulus G´´ are plotted against angular frequency ω (rad s^{-1}) with a constant strain (predetermined by amplitude sweep experiment) provides characteristic plot that clearly establishes the visco-elastic nature of the material under study (frequency sweep); in such plot, G´ should be larger than G´´ and frequency invariant the entire range of frequency ω specially in the longer time scale. Thus, we first carried out amplitude sweep experiment on the hydrogel (8 wt %) in order to determine the strain required for carrying out frequency sweep experiment. The results recommended 0.1 % strain for frequency sweep for the gel. Thus, the plot of G´ and G´´ of the hydrogels against angular frequency ω with a constant strain of 0.1 % revealed that G´s were much larger than G´´s and were frequency invariant over the entire range of frequency ω meaning that the hydrogel displayed visco-elastic response. The amplitude sweep experiments already carried out on these gels also provided important information about the yield stress (the stress at which the crossover point of G´/G´´ lies) of the gels; it was observed that the hydrogel had a yield stress in between 10-100 Kpa.

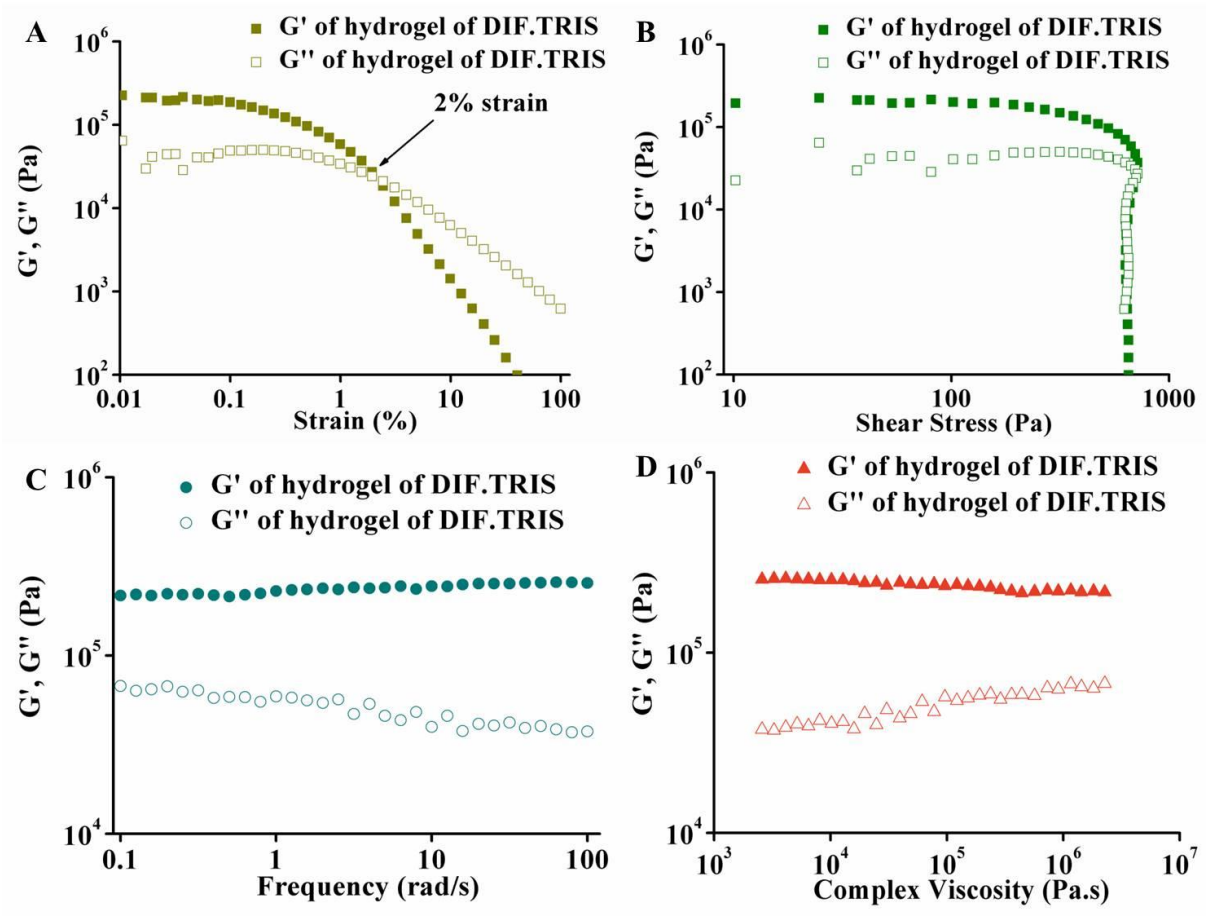

Figure S33: Different rheological responses: (A) oscillatory amplitude strain sweep; (B) oscillatory amplitude stress sweep; C) oscillatory frequency sweep and D) oscillatory complex viscosity sweep of hydrogel of **DIF.TRIS.Zn**.

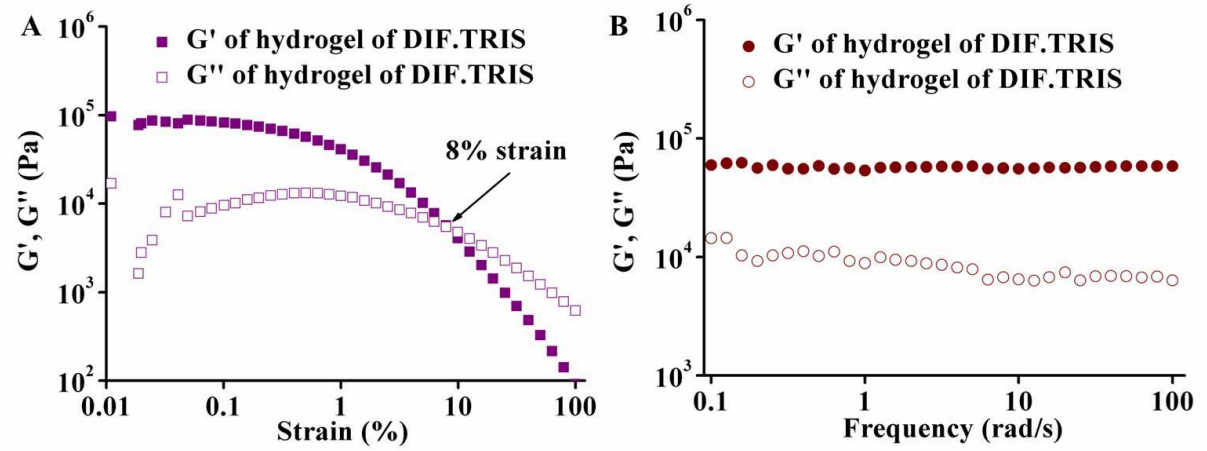

Figure S34: Different rheological responses: (A) oscillatory amplitude strain sweep and (B) oscillatory frequency sweep of H_2O : EG (9 : 1) gel of **DIF.TRIS.Zn**.

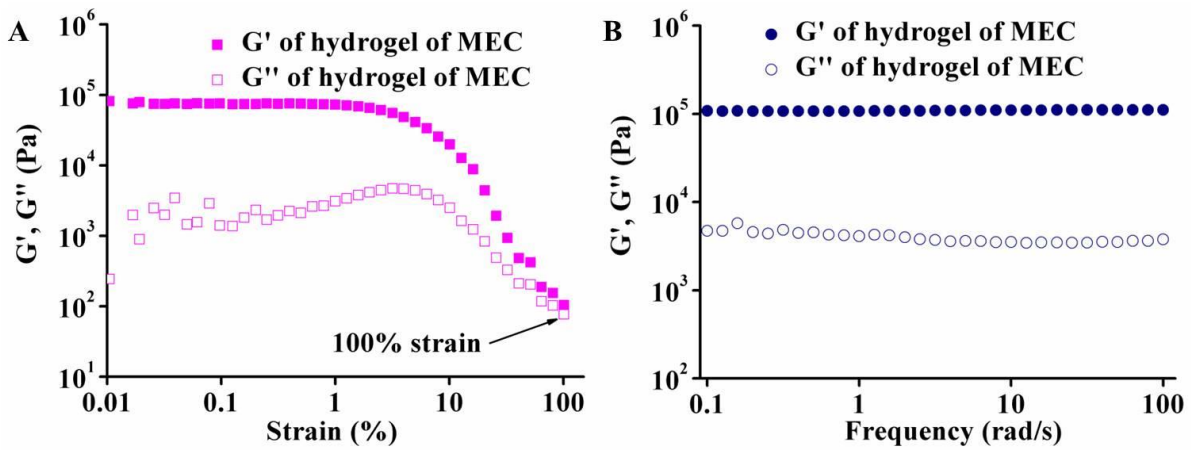

Figure S35: Different rheological responses: (A) oscillatory amplitude strain sweep and (B) oscillatory frequency sweep of hydrogel of **MEC.Na.Zn**.

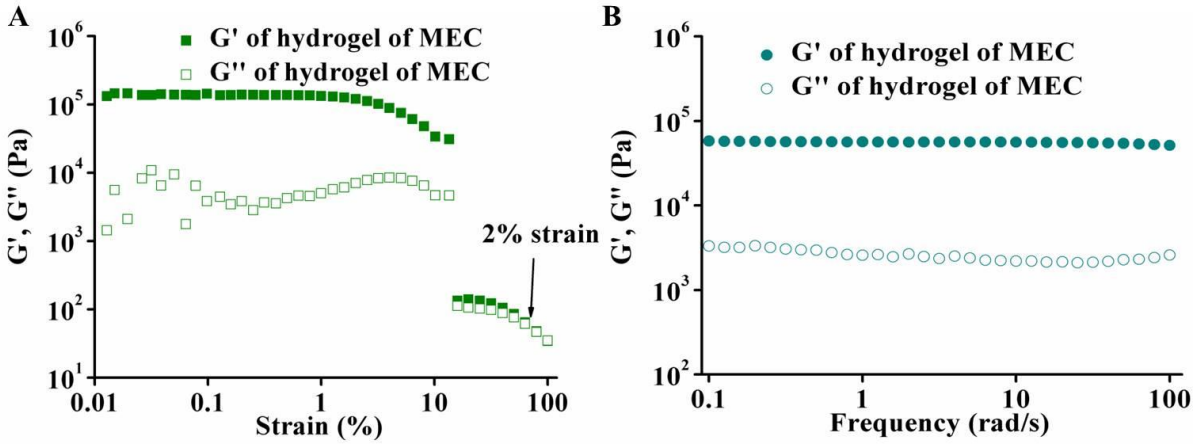

Figure S36: Different rheological responses: (A) oscillatory amplitude strain sweep and (B) oscillatory frequency sweep of H_2O : EG (9 : 1) gel of **MEC.Na.Zn**.

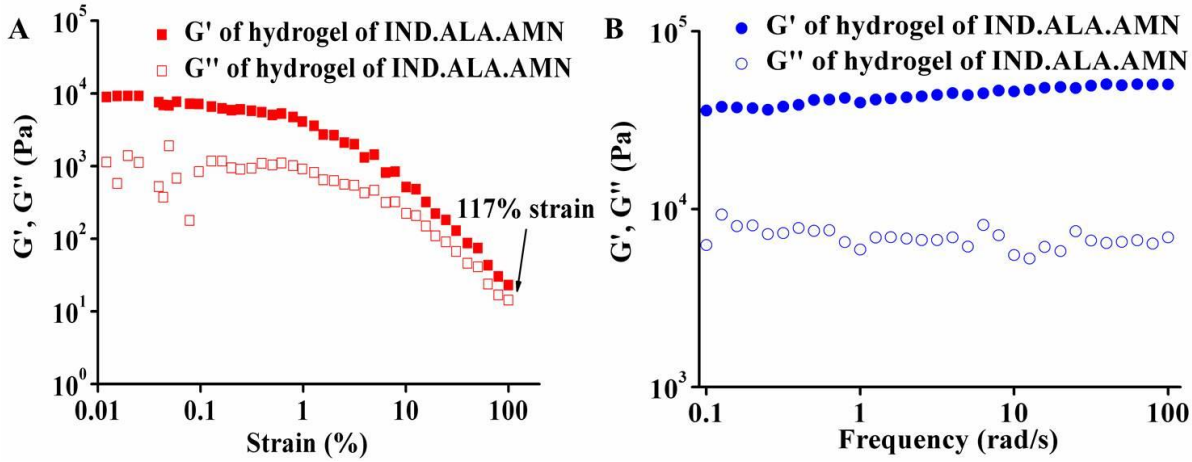

Figure S37: Different rheological responses: (A) oscillatory amplitude strain sweep and (B) oscillatory frequency sweep of H_2O : EtOH (9 : 1) gel of **IND.ALA.AMN.Zn**.

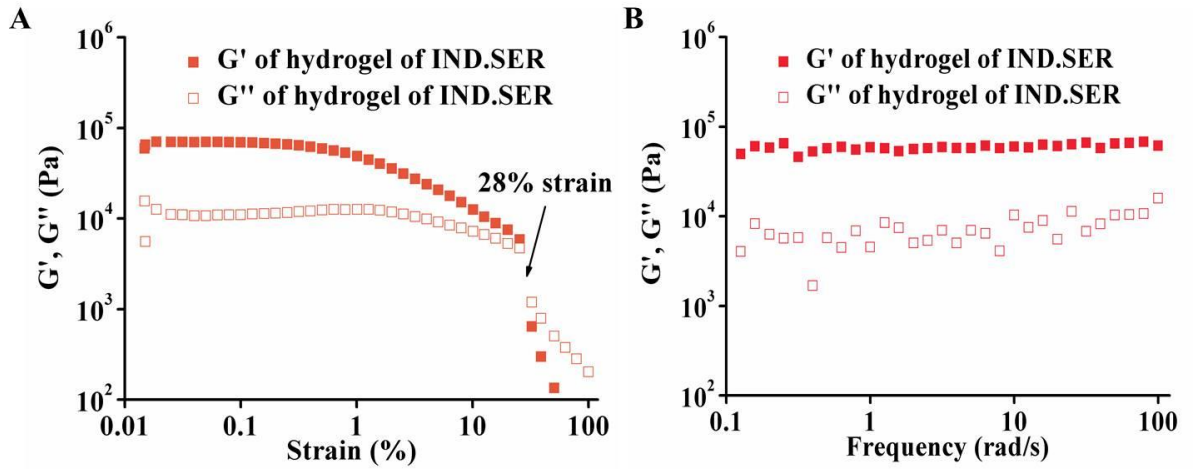

Figure S38: Different rheological responses: (A) oscillatory amplitude strain sweep and (B) oscillatory frequency sweep of H_2O : EtOH (9 : 1) gel of **IND.SER.TRIS.Zn**.

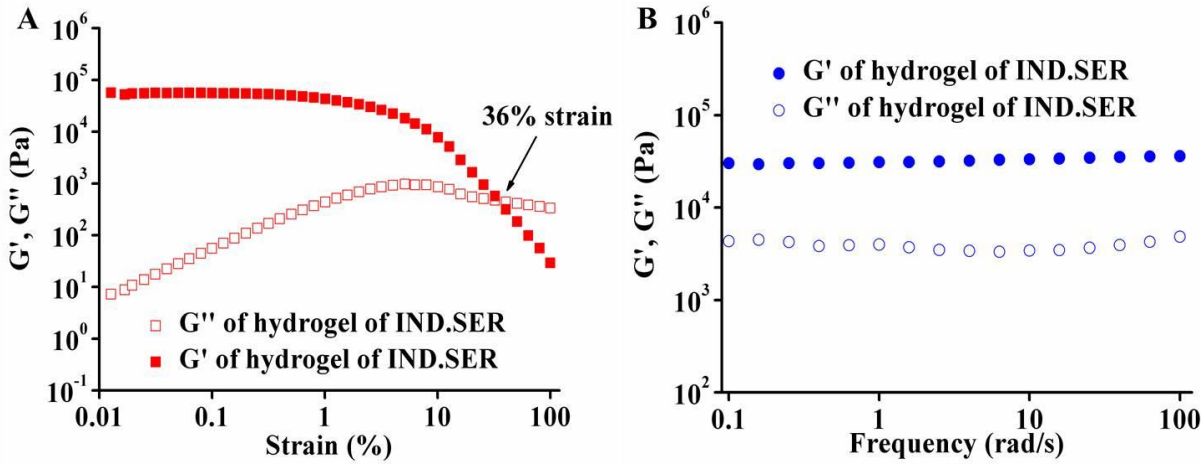

Figure S39: Different rheological responses: (A) oscillatory amplitude strain sweep and (B) oscillatory frequency sweep of H_2O : EG (9 : 1) gel of **IND.SER.TRIS.Zn**.

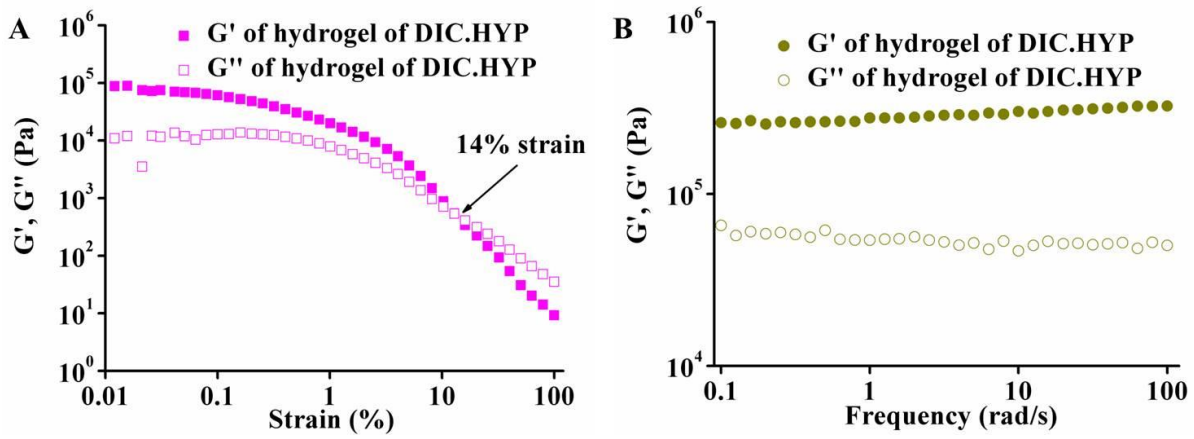

Figure S40: Different rheological responses: (A) oscillatory amplitude strain sweep and (B) oscillatory frequency sweep of H_2O : EtOH (9 : 1) gel of **DIC.HYP.TRIS.Zn**.

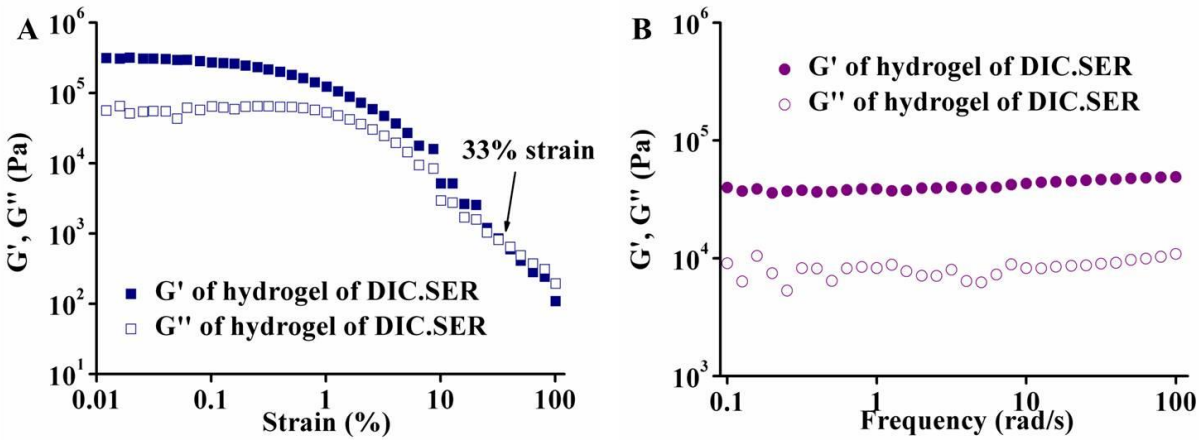

Figure S41: Different rheological responses: (A) oscillatory amplitude strain sweep and (B) oscillatory frequency sweep of H_2O : EG (9 : 1) gel of **DIC.SER.TRIS.Zn**.

As the **IND.SER.TRIS.Zn** in H_2O: EtOH (9:1) turned out to be gelator in all the possible 16 combinations of anions and organic salt:metal salt ratio, their detailed rheological responses were assessed. From the data it was concluded that the NO_3^- and AcO^- salts of Zn(II) were found to be stronger than the other two anions SO_4^{2-} and ClO_4^- and in most of the cases the 2:1 NSAID salt:metal salt ratio was found to be capable of forming better or comparable gels than 1:1 ratio in terms of storage or elastic moduli (G'). Again for the halides of Zn(II) (F^-, Cl^-, Br^- and I^-), the elastic moduli (G') of F^- and Cl^- were more than that of the Br^- and I^- salts and the 2:1 organic salt:metal salt ratio gels of F^- and I^- responded better in rheology than that of their 1:1 counterparts but the trends were reversed for the other two anions *e.g.* Cl^- and Br^-. Thus, the NSAID salt:metal salt ratio and variation of anionic counterparts play a very important role in the gel formation.

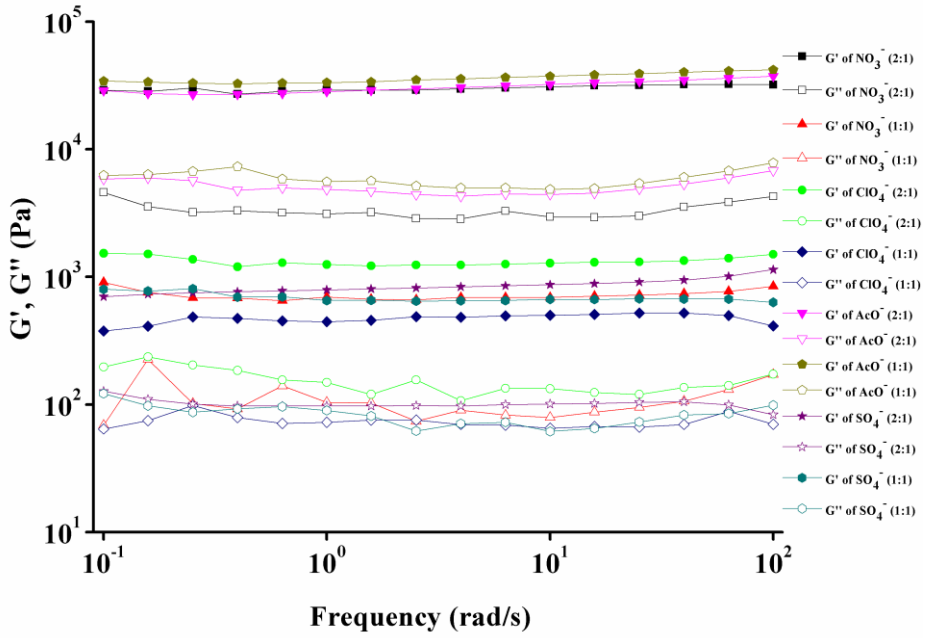

Figure S42: Frequency sweep experiments of H_2O : EtOH (9 : 1) gel of **IND.SER.TRIS.Zn** with different ligand : metal (L : M) ratio and with different anions of Zn(II) salts.

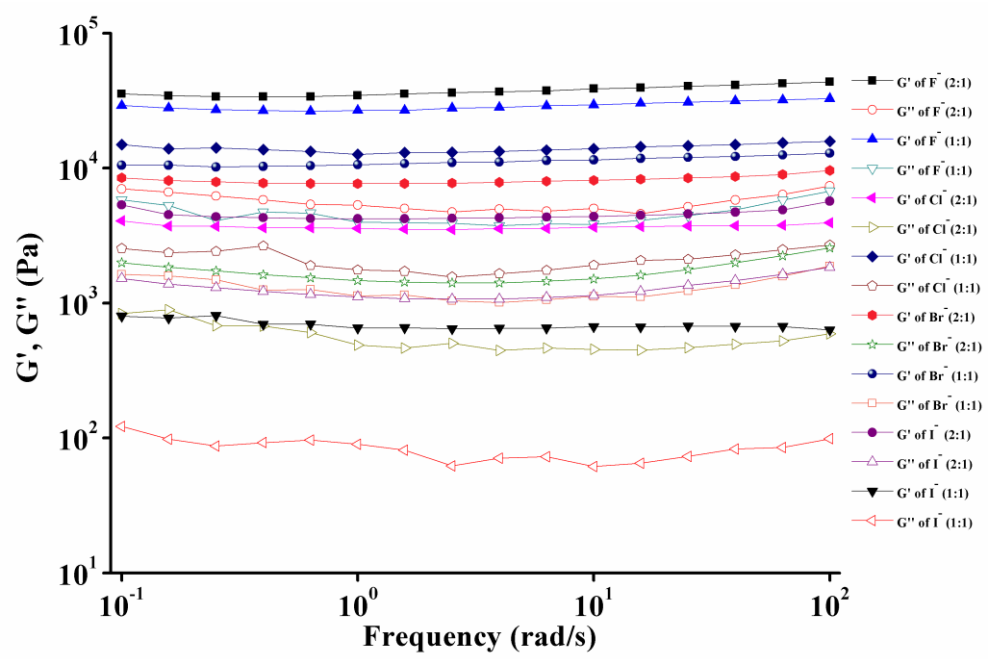

Figure S43: Frequency sweep experiments of H_2O : EtOH (9 : 1) gel of **IND.SER.TRIS.Zn** with different ligand : metal (L : M) ratio and with different halides of Zn(II) salts.

Single crystal X-ray diffraction

Single crystal data were collected using MoKα (λ = 0.7107 Å) radiation on a BRUKER APEX II diffractometer equipped with CCD area detector. Data collection, data reduction, structure solution/refinement were carried out using the software package of SMART APEX-II. All structures were solved by direct method and refined in a routine manner. Nonhydrogen atoms were treated anisotropically. All the hydrogen atoms were geometrically fixed. CCDC Numbers 1498320 [**(IND)$_2$.Zn**], 1498321 [**(FLR)$_2$.Zn**], 1498322 [**(IBU)$_2$.Zn**], 1498323 [**(TOL)$_2$.Zn**], 1498324 [**(SUL)$_2$.Zn**], 1498325 [**(DIC)$_2$.Zn**] and 1498326 [**(DIF)$_2$.Zn**] contain the supplementary crystallographic data for this paper. These data can be obtained free of charge via www.ccdc.cam.ac.uk/conts/retrieving.html (or from the Cambridge Crystallographic Data Centre, 12 Union Road, Cambridge CB21EZ, UK; fax: (+44) 1223-336-033; or deposit@ccdc.cam.ac.uk).

Table S4: Crystal data and structure refinement for the Zn-complexes.					
Identification code	**$(IND)_2$.Zn**	**$(DIC)_2$.Zn**	**$(TOL)_2$.Zn**	**$(IBU)_2$.Zn**	**$(FLR)_2$.Zn**
Empirical formula	$C_{40}H_{38}Cl_2N_2O_{10}Zn$	$C_{61}H_{60}Cl_8N_4O_{13}Zn_2$	$C_{86}H_{74}Cl_6N_6O_{14}Zn_3$	$C_{26}H_{20}O_6Zn$	$C_{30}H_{28}F_2O_6Zn$
Formula weight	842.99	1471.47	1824.32	493.79	587.89
Temperature/K	100	100	100	100	100
Crystal system	monoclinic	monoclinic	monoclinic	monoclinic	monoclinic
Space group	*C*2/c	$P2_1/c$	$P2_1/n$	*C*2/c	*C*2
a/Å	29.2403(13)	9.589(5)	14.3851(4)	9.8322(13)	9.9111(10)
b/Å	5.3028(2)	19.809(9)	11.1219(4)	5.9632(9)	6.1719(6)
c/Å	24.3344(11)	33.740(16)	25.0514(8)	45.904(6)	21.436(2)
α/°	90.00	90.00	90.00	90.00	90.00
β/°	90.895(3)	92.414(7)	97.523(2)	92.423(10)	91.592(8)
γ/°	90.00	90.00	90.00	90.00	90.00
Volume/$Å^3$	3772.7(3)	6403(5)	3973.5(2)	2689.0(7)	1310.8(2)
Z	4	4	2	4	2
$\rho_{calc}g/cm^3$	1.484	1.526	1.525	1.220	1.490
μ/mm^{-1}	0.855	1.148	1.171	0.947	0.995
F(000)	1744.0	3016.0	1872.0	1016.0	608.0
Crystal size/mm^3	0.76 × 0.06 × 0.04	0.23 × 0.2 × 0.19	0.29 × 0.21 × 0.04	0.25 × 0.14 × 0.04	0.26 × 0.16 × 0.04
Radiation	MoKα (λ = 0.71073)	MoKα (λ = 0.71073)	MoKα (λ = 0.71073)	MoKα (λ = 0.71073)	MoKα (λ = 0.71073)
2Θ range for data collection/°	2.78 to 51.36	2.38 to 52.1	3.1 to 47.46	3.56 to 46.5	5.7 to 50.04
Index ranges	-35 ≤ h ≤ 35, -6 ≤ k ≤ 6, -29 ≤ l ≤ 29	-11 ≤ h ≤ 11, -24 ≤ k ≤ 24, -41 ≤ l ≤ 41	-16 ≤ h ≤ 16, -12 ≤ k ≤ 12, -28 ≤ l ≤ 28	-10 ≤ h ≤ 10, -6 ≤ k ≤ 6, -50 ≤ l ≤ 48	-11 ≤ h ≤ 11, -7 ≤ k ≤ 7, -25 ≤ l ≤ 21
Reflections collected	22634	79263	40891	12737	7699
Independent reflections	3584 [R_{int} = 0.0674, R_{sigma} = 0.0467]	12525 [R_{int} = 0.0822, R_{sigma} = 0.0559]	6021 [R_{int} = 0.0336, R_{sigma} = 0.0216]	1945 [R_{int} = 0.1154, R_{sigma} = 0.0740]	2315 [R_{int} = 0.0667, R_{sigma} = 0.0806]
Data/restraints/parameters	3584/3/255	12525/12/811	6021/3/527	1945/0/150	2315/1/180
Goodness-of-fit on F^2	1.117	1.028	1.132	1.081	1.018
Final R indexes [I>=2σ (I)]	R_1 = 0.0418, wR_2 = 0.1038	R_1 = 0.0542, wR_2 = 0.1340	R_1 = 0.0325, wR_2 = 0.0885	R_1 = 0.0679, wR_2 = 0.1640	R_1 = 0.0690, wR_2 = 0.1766
Final R indexes [all data]	R_1 = 0.0740, wR_2 = 0.1361	R_1 = 0.0760, wR_2 = 0.1491	R_1 = 0.0402, wR_2 = 0.0975	R_1 = 0.0992, wR_2 = 0.1873	R_1 = 0.0794, wR_2 = 0.1869
Largest diff. peak/hole / e $Å^{-3}$	0.68/-0.67	2.40/-1.29	0.76/-0.39	0.96/-0.43	1.85/-0.53
Flack parameter	-	-	-	-	0.04(3)

Crystal data and structure refinement for the Zn-complexes.		
Identification code	**$(SUL)_2$.Zn**	**$(DIF)_2$.Zn**
Empirical formula	$C_{40}H_{42}N_8O_{14}S_2Zn$	$C_{26}H_{18}F_4O_8Zn$
Formula weight	988.31	599.77
Temperature/K	100	120
Crystal system	monoclinic	monoclinic
Space group	$P2_1/c$	$P2/c$
a/Å	14.4904(5)	30.098(2)
b/Å	10.3481(3)	5.2142(3)
c/Å	16.0712(5)	32.889(2)
α/°	90.00	90.00
β/°	112.233(2)	113.920(4)
γ/°	90.00	90.00
Volume/$Å^3$	2230.68(12)	4718.1(5)
Z	2	8
$\rho_{calc}g/cm^3$	1.471	1.689
μ/mm^{-1}	0.719	1.125
F(000)	1024.0	2432.0
Crystal size/mm^3	0.26 × 0.21 × 0.06	0.21 × 0.14 × 0.06
Radiation	MoKα (λ = 0.71073)	MoKα (λ = 0.71073)
2θ range for data collection/°	3.04 to 51.78	2.5 to 51.36
Index ranges	$-17 \le h \le 17$, $-12 \le k \le 12$, $-19 \le l \le 19$	$-33 \le h \le 36$, $-6 \le k \le 6$, $-40 \le l \le 40$
Reflections collected	34935	56691
Independent reflections	4317 [R_{int} = 0.0483, R_{sigma} = 0.0285]	8986 [R_{int} = 0.0996, R_{sigma} = 0.0715]
Data/restraints/parameters	4317/6/308	8986/0/712
Goodness-of-fit on F^2	0.897	1.050
Final R indexes [I>=2σ (I)]	R_1 = 0.0379, wR_2 = 0.0967	R_1 = 0.0726, wR_2 = 0.1988
Final R indexes [all data]	R_1 = 0.0546, wR_2 = 0.1103	R_1 = 0.1127, wR_2 = 0.2339
Largest diff. peak/hole / e $Å^{-3}$	0.48/-0.44	3.00/-1.11

Single crystal X-ray diffraction studies

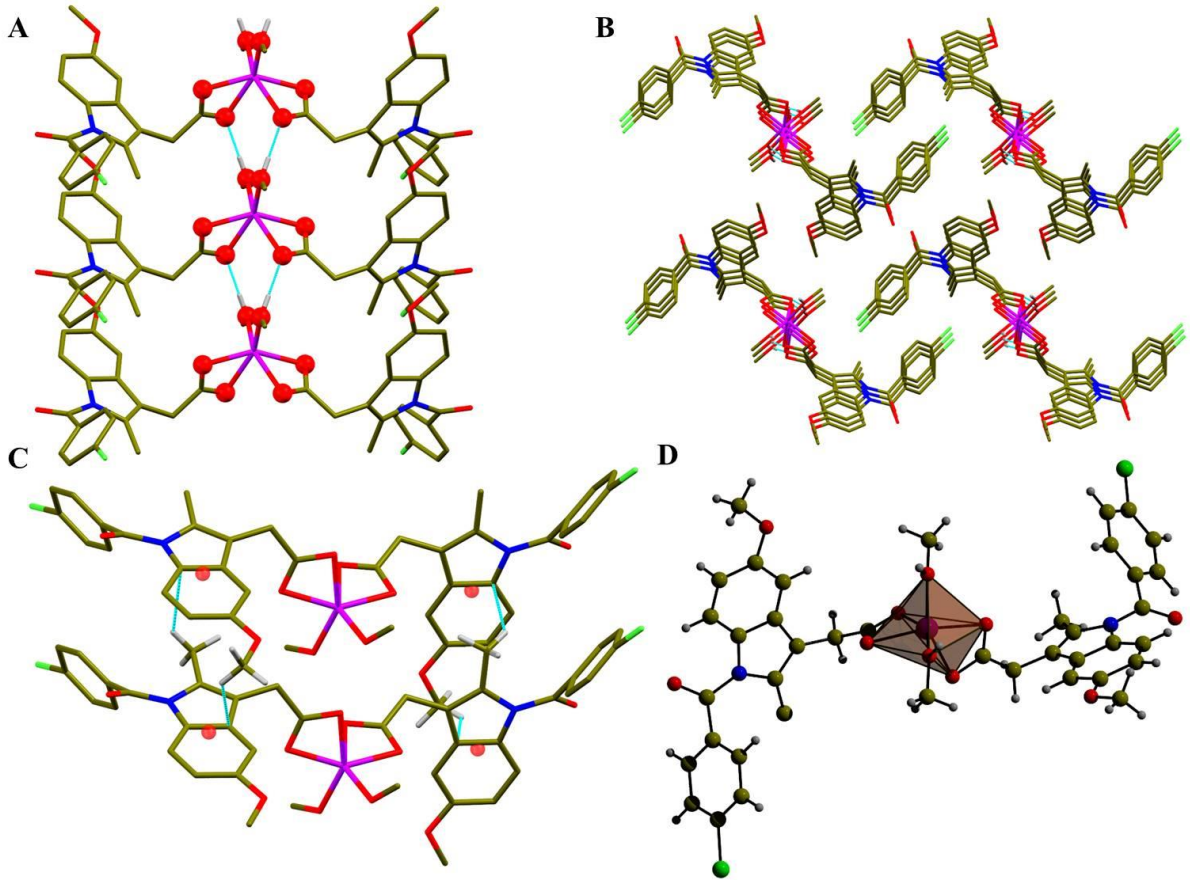

Figure S44: Single crystal structure of **$(IND)_2$.Zn**; (A) 1D HBN, (B) 1D parallel packing, (C) weak C-H•••π interactions and (D) geometry of metal center.

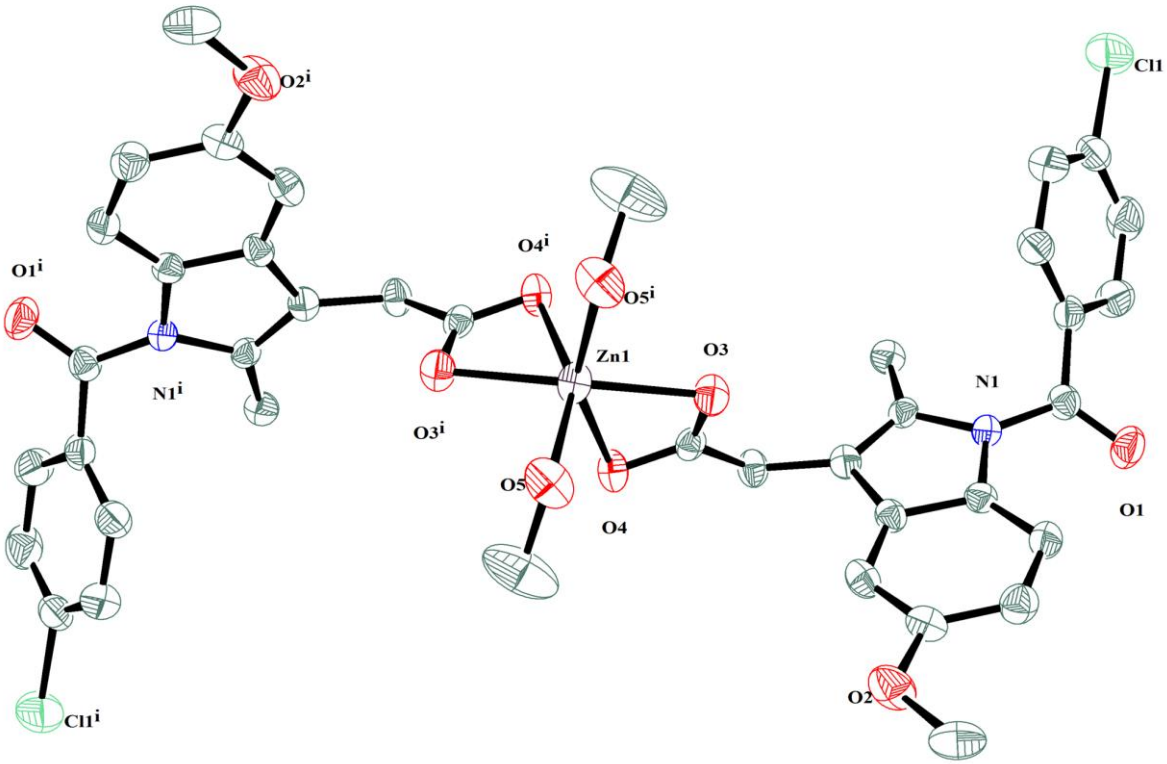

ORTEP Plot of **$(IND)_2$.Zn** (50% probability)

Table S5: Hydrogen Bonds for $(IND)_2$.Zn.						
D	**H**	**A**	**d(D-H)/Å**	**d(H-A)/Å**	**d(D-A)/Å**	**D-H-A/°**
O5	H5	O4[1]	0.856(9)	1.705(10)	2.559(3)	175(2)
C13	H13	O1	0.95	2.44	2.924(4)	111.7
C13	H13	O1[2]	0.95	2.58	3.504(4)	165.5
C18	H18B	O3[3]	0.99	2.66	3.598(4)	158.5
C12	H12A	Cl1[4]	0.98	2.93	3.605(4)	126.8
C20	H20B	Cl1[5]	0.98	2.83	3.674(6)	144.1

[1]+X,-1+Y,+Z; [2]3/2-X,3/2-Y,1-Z; [3]+X,1+Y,+Z; [4]3/2-X,-1/2+Y,3/2-Z; [5]-1/2+X,-1/2+Y,+Z

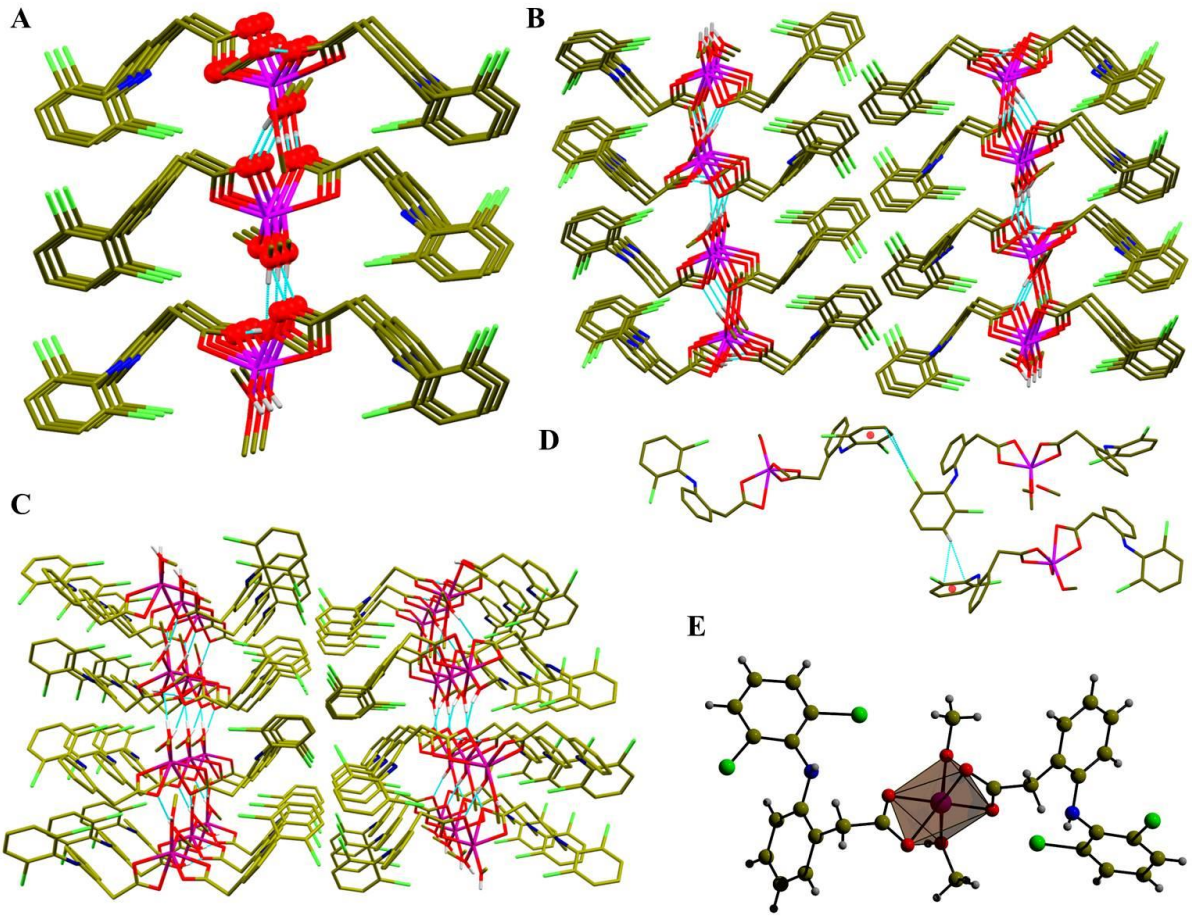

Figure S45: Single crystal structure of **$(DIC)_2$.Zn**; (A) 2D HBN, (B) 2D parallel packing, (C) tilted view of 2D HBN, (D) weak C-H•••π interactions and (E) geometry of metal center.

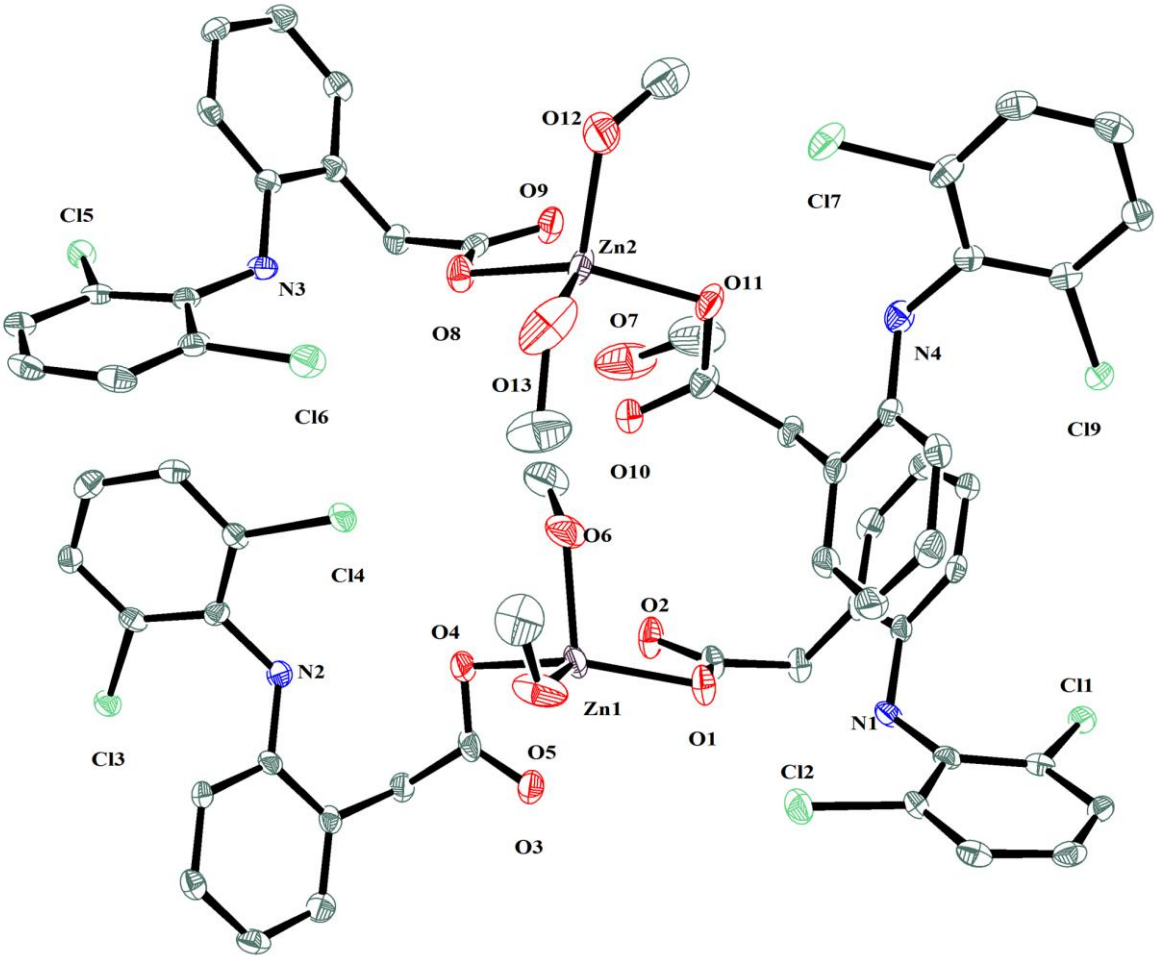

ORTEP Plot of **$(DIC)_2$.Zn** (50% probability)

Table S6: Hydrogen Bonds for $(DIC)_2$.Zn.						
D	**H**	**A**	**d(D-H)/Å**	**d(H-A)/Å**	**d(D-A)/Å**	**D-H-A/°**
O6	H6	O10	0.859(9)	1.800(11)	2.648(4)	169(4)
O12	H12A	O2[1]	0.857(9)	1.753(13)	2.586(5)	163(3)
O13	H13	O7[1]	0.853(9)	1.715(12)	2.544(6)	163(2)
O5	H5	O9[2]	0.852(9)	1.809(11)	2.646(5)	167(2)
O7	H7	O3[3]	0.82	1.81	2.619(5)	166.3
C1	H1B	O7	0.96	2.38	2.999(8)	121.9
C2	H2C	Cl7	0.96	2.75	3.432(6)	128.3

[1]1-X,1/2+Y,1/2-Z; [2]-1+X,+Y,+Z; [3]1+X,+Y,+Z

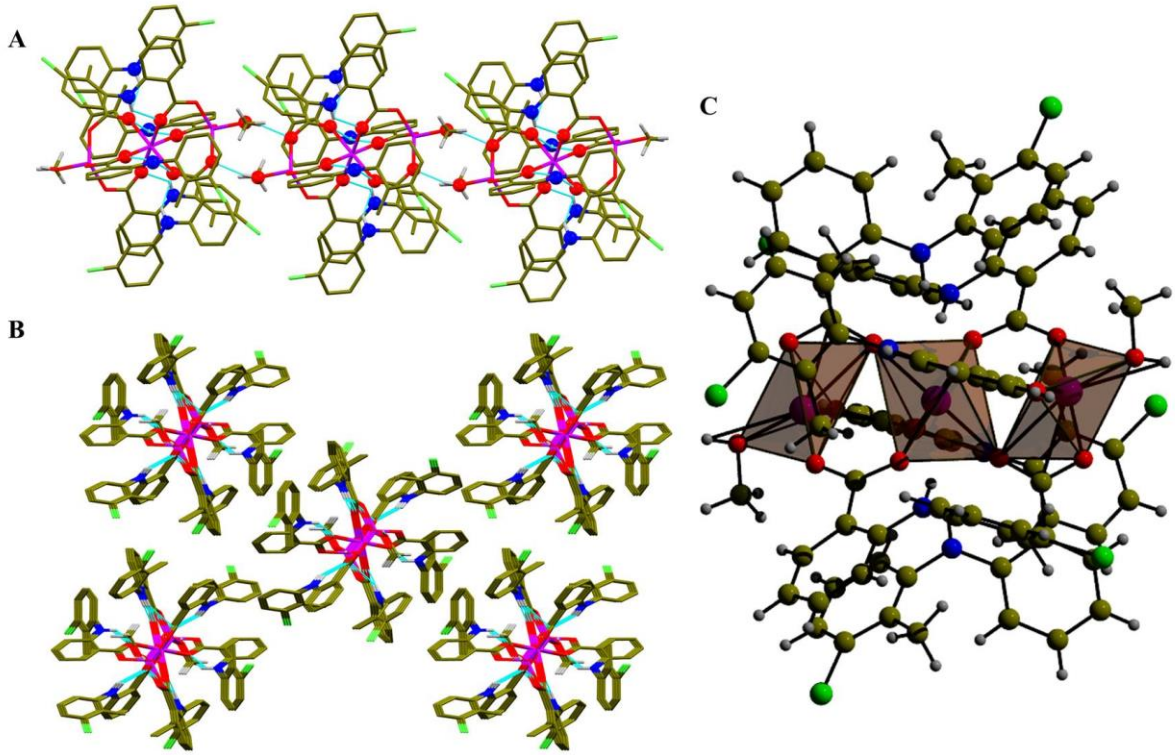

Figure S46: Single crystal structure of **$(TOL)_2$.Zn**; (A) 1D HBN of SBU, (B) 1D parallel packing of SBU and (C) geometry of metal center.

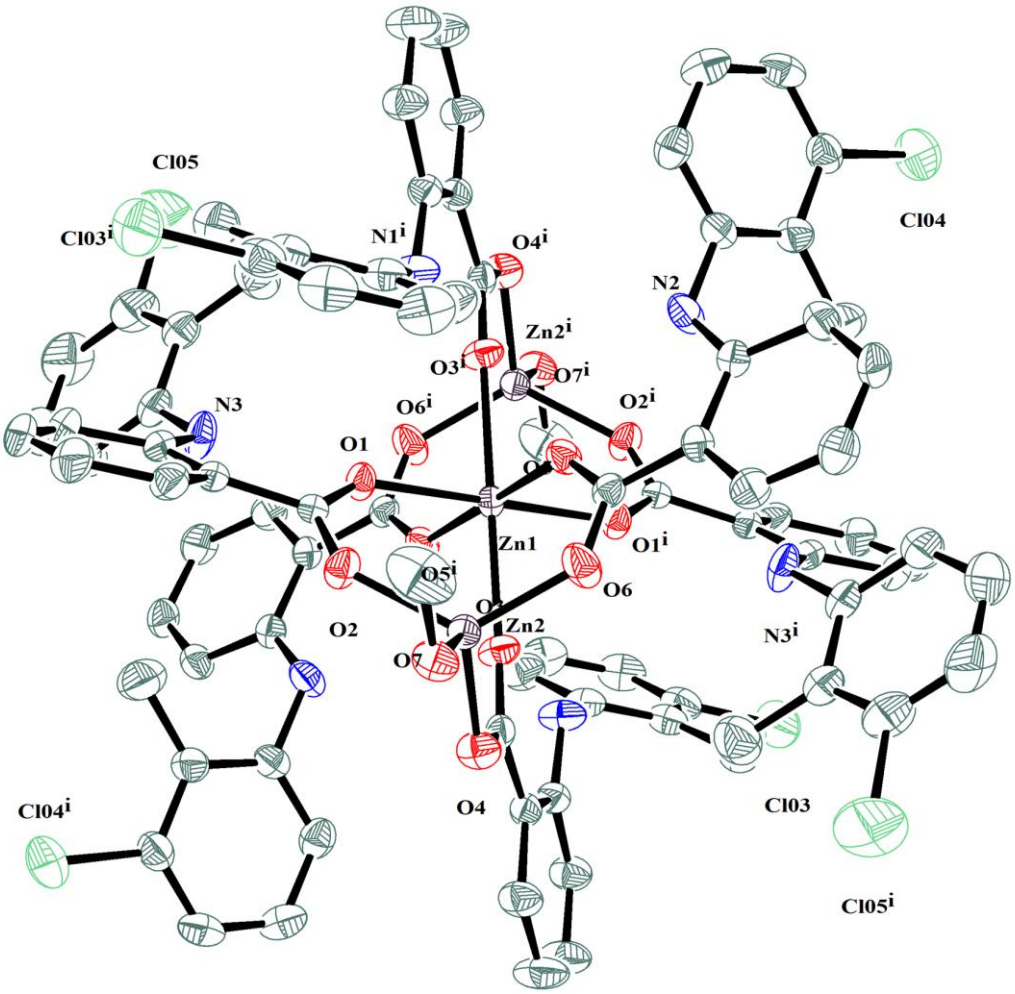

ORTEP Plot of **(TOL)$_2$.Zn** (50% probability)

Table S7: Hydrogen Bonds for (TOL)$_2$.Zn.						
D	**H**	**A**	**d(D-H)/Å**	**d(H-A)/Å**	**d(D-A)/Å**	**D-H-A/°**
O7	H7	O2[1]	0.856(9)	1.915(14)	2.746(3)	163(3)
N1	H1	O1[2]	0.88	2.49	3.234(3)	143.1
N1	H1	O3	0.88	2.03	2.704(3)	132.5
N3	H3	O1	0.88	2.05	2.730(3)	133.2
N2	H2	O5	0.88	2.02	2.687(3)	132.0
C43	H43A	Cl04[3]	0.98	2.95	3.777(4)	142.2

[1]1-X,2-Y,1-Z; [2]1-X,1-Y,1-Z; [3]+X,1+Y,+Z

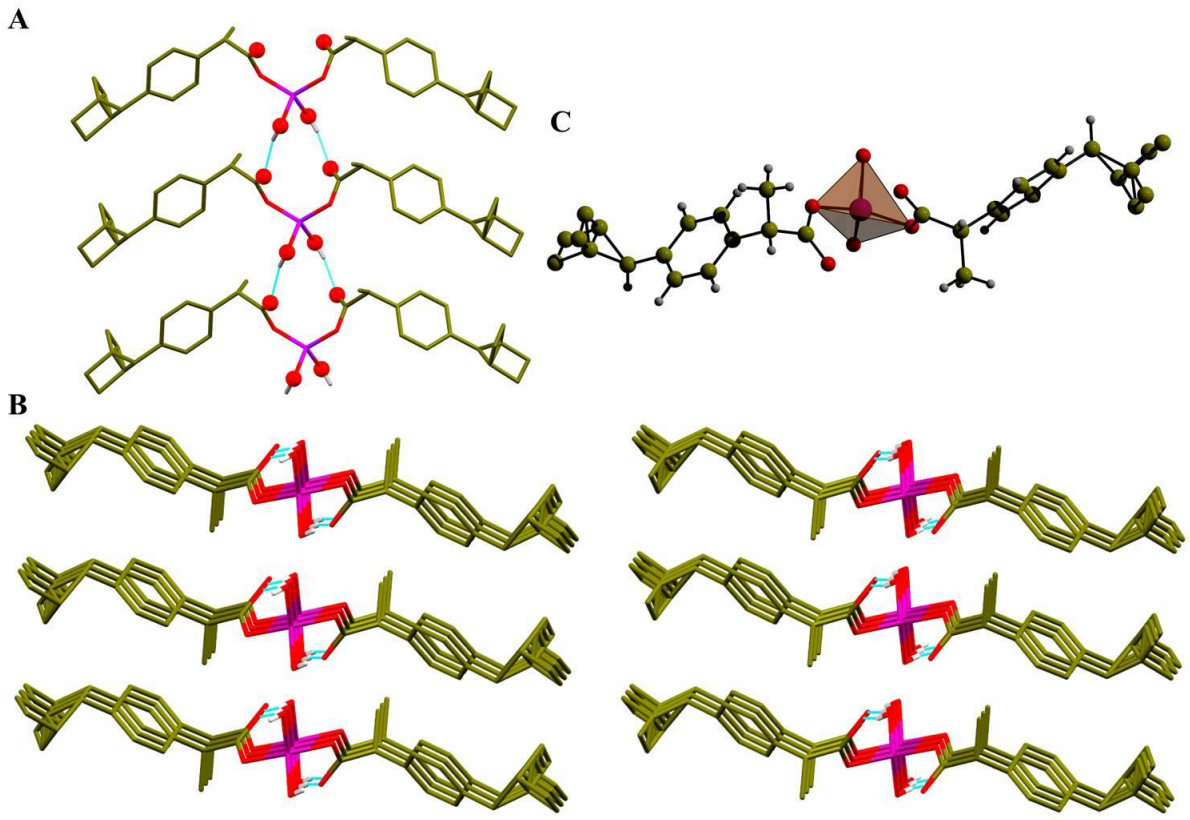

Figure S47: Single crystal structure of **$(IBU)_2$.Zn**; (A) 1D HBN, (B) 1D parallel packing and (C) geometry of metal center.

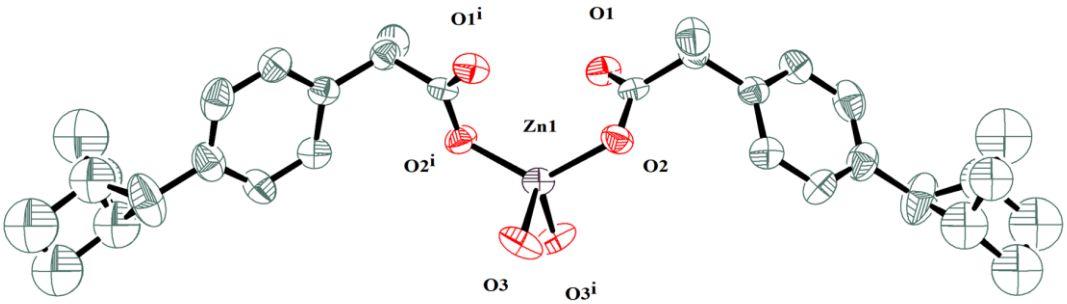

ORTEP Plot of **$(IBU)_2$.Zn** (50% probability)

Table S8: Hydrogen Bonds for $(IBU)_2$.Zn.				
D H A	**d(D-H)/Å**	**d(H-A)/Å**	**d(D-A)/Å**	**D-H-A/°**
O3 H3 O1[1]	0.84	1.86	2.665(6)	159.6

[1]1-X,-1+Y,1/2-Z

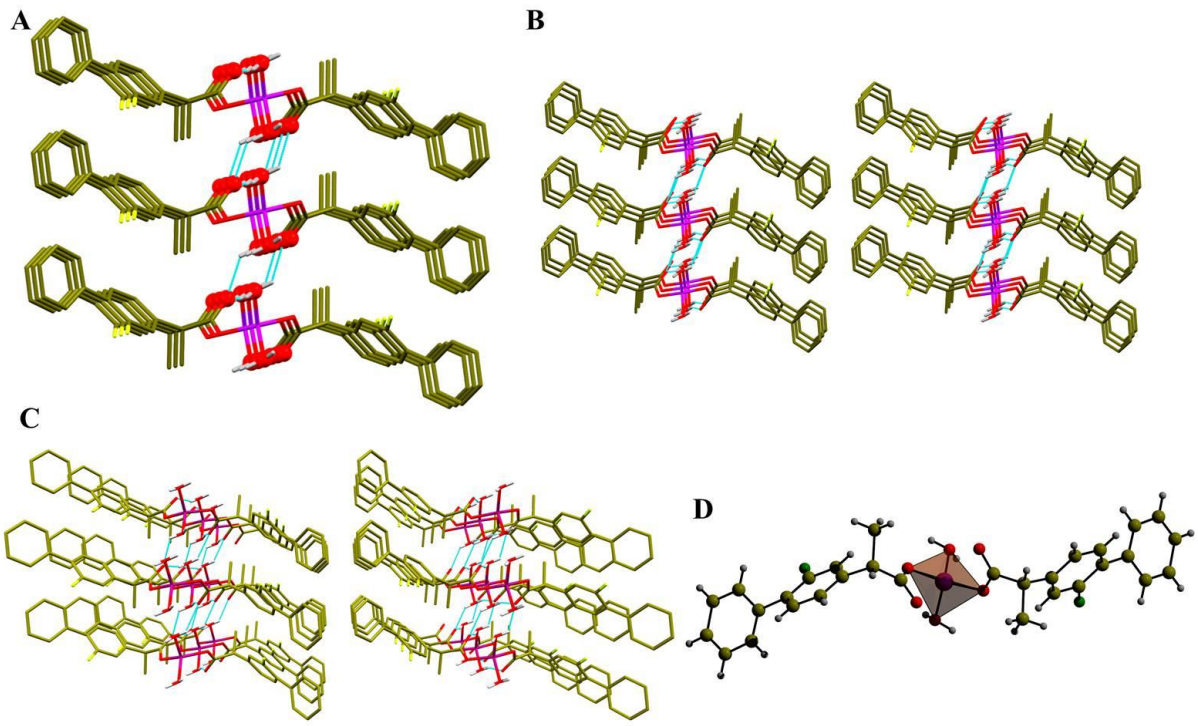

Figure S48: Single crystal structure of **$(FLR)_2$.Zn**; (A) 2D HBN, (B) 2D parallel packing, (C) tilted view of 2D HBN and (D) geometry of metal center.

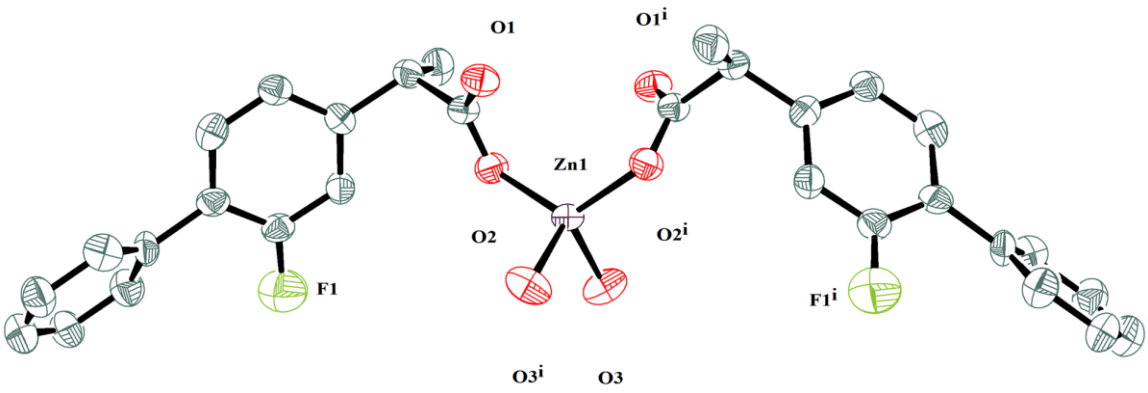

ORTEP Plot of **(FLR)$_2$.Zn** (50% probability)

Table S9: Hydrogen Bonds for (FLR)$_2$.Zn.				
D H A	**d(D-H)/Å**	**d(H-A)/Å**	**d(D-A)/Å**	**D-H-A/°**
O3 H3A O1[1]	0.87	2.13	2.690(8)	121.6
O3 H3B O1[2]	0.87	1.85	2.691(8)	161.6
C11 H11 O2	0.95	2.54	3.012(9)	110.7

[1]-1/2+X,-1/2+Y,+Z; [2]1-X,-1+Y,1-Z

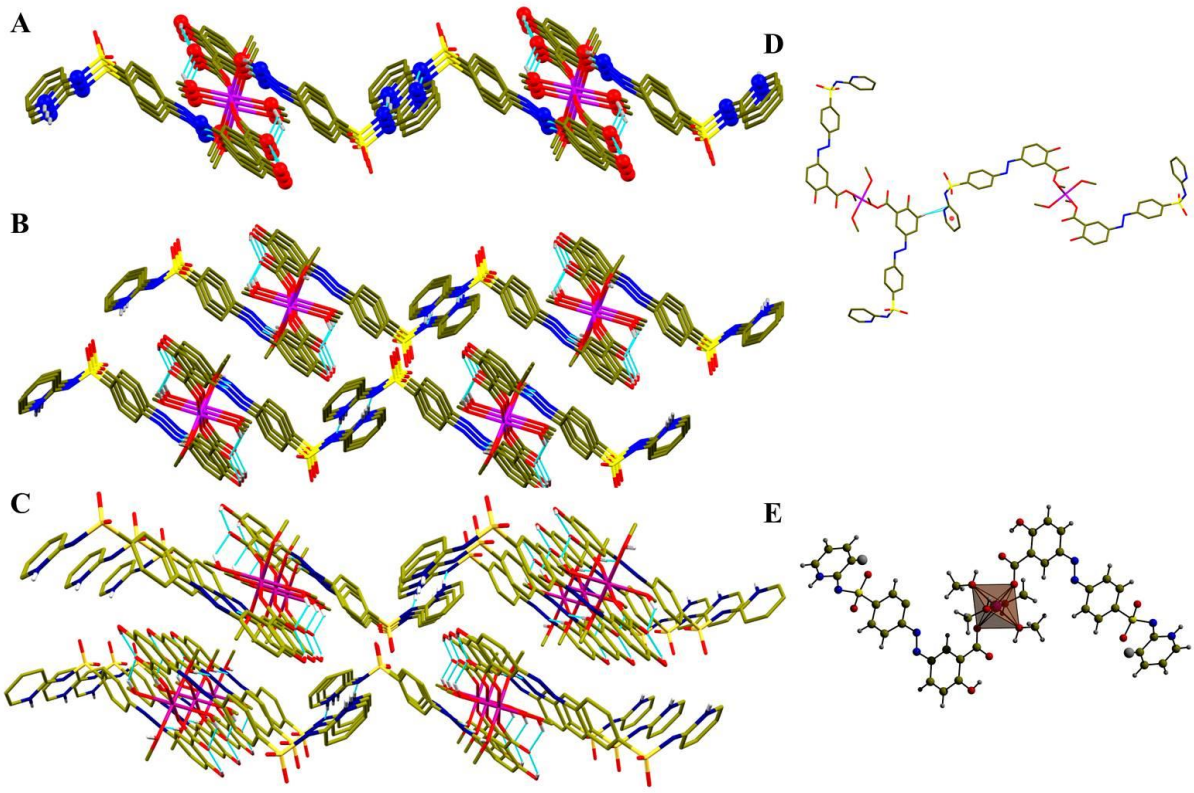

Figure S49: Single crystal structure of **$(SUL)_2$.Zn**; (A) 2D HBN, (B) 2D parallel packing, (C) tilted view of 2D HBN, (D) weak C-H•••π interactions and (E) geometry of metal center.

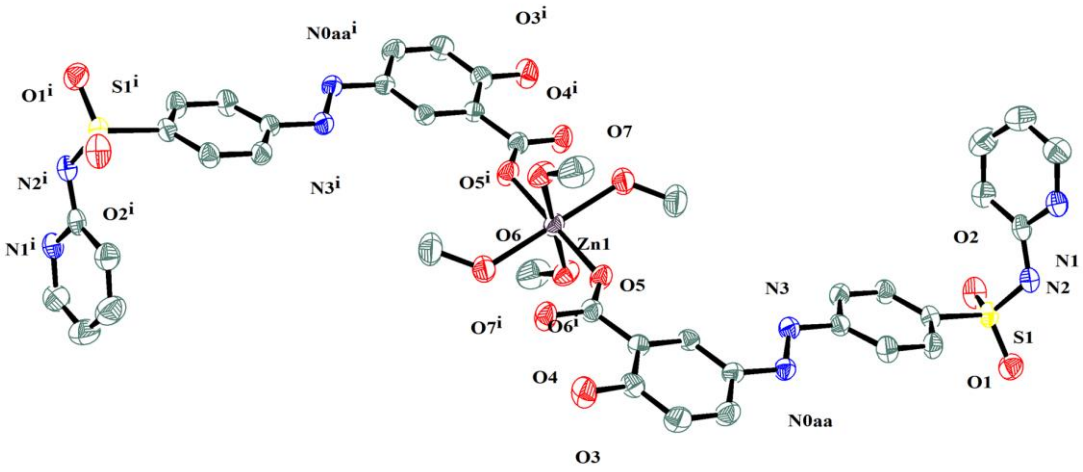

ORTEP Plot of **$(SUL)_2$.Zn** (50% probability)

Table S10: Hydrogen Bonds for $(SUL)_2$.Zn.						
D	**H**	**A**	**d(D-H)/Å**	**d(H-A)/Å**	**d(D-A)/Å**	**D-H-A/°**
O6	H6	N0AA[1]	0.883(9)	2.046(10)	2.922(3)	171(3)
O7	H7	O4[2]	0.886(9)	1.979(17)	2.709(3)	138.7(19)
C7	H7A	O1[3]	0.95	2.47	3.397(3)	166.6
C14	H14	N1[4]	0.95	2.53	3.474(3)	172.3
C1	H1A	O2[5]	0.95	2.32	3.094(3)	138.1
C1	H1A	O1[6]	0.95	2.51	3.146(4)	124.5

[1]+X,1+Y,+Z; [2]1-X,2-Y,-Z; [3]2-X,1/2+Y,1/2-Z; [4]-1+X,1/2-Y,-1/2+Z; [5]+X,1/2-Y,1/2+Z; [6]2-X,-Y,1-Z

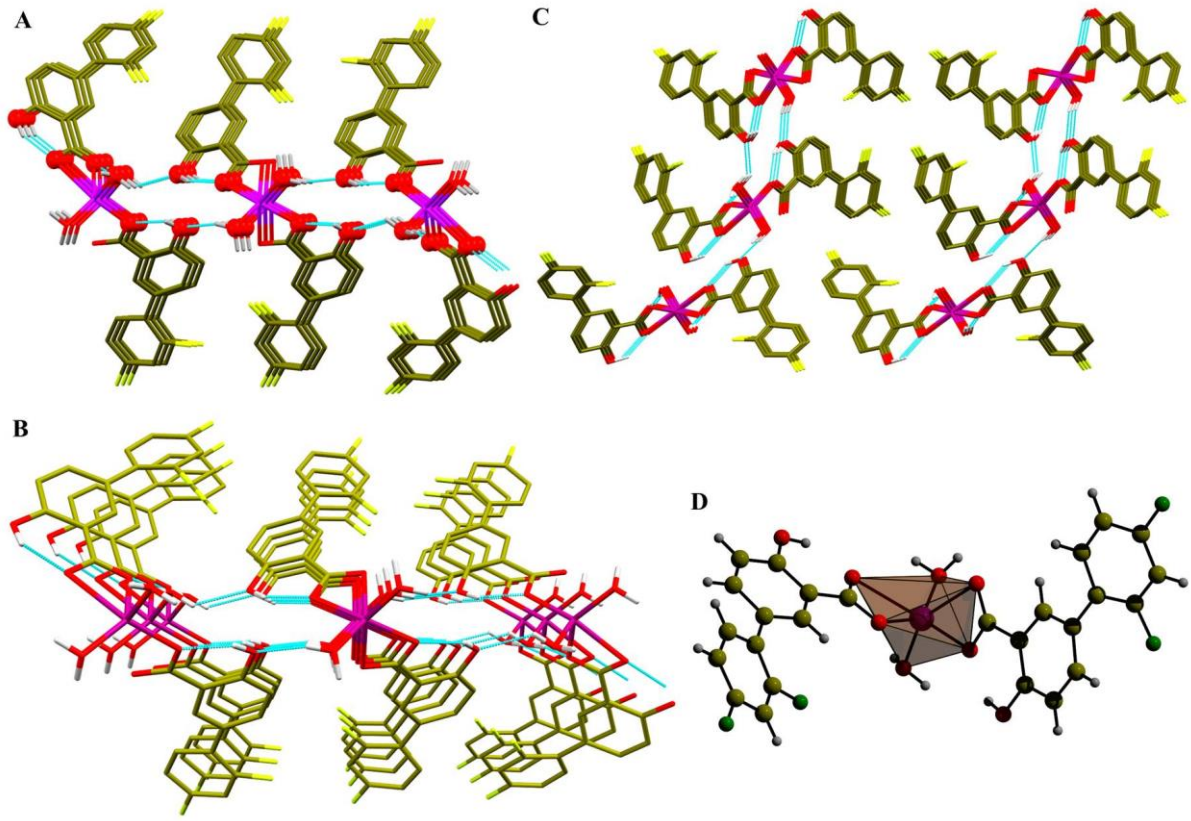

Figure S50: Single crystal structure of **$(DIF)_2$.Zn**; (A) 2D HBN, (B) 2D parallel packing, (C) tilted view of 2D HBN and (D) geometry of metal center.

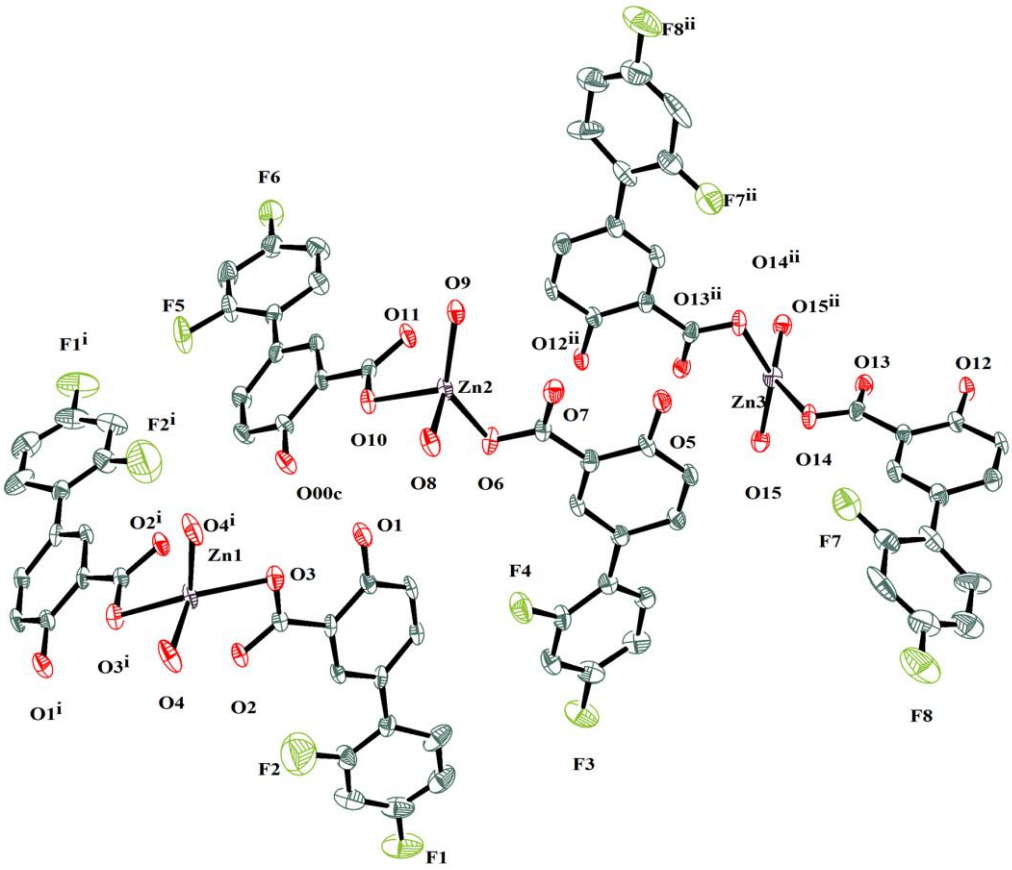

ORTEP Plot of **(DIF)$_2$.Zn** (50% probability)

Table S11: Hydrogen Bonds for (DIF)$_2$.Zn.						
D	**H**	**A**	**d(D-H)/Å**	**d(H-A)/Å**	**d(D-A)/Å**	**D-H-A/°**
O9	H9B	O12[1]	0.88	1.92	2.770(6)	161.2
O12	H12A	O13	0.84	1.86	2.589(6)	144.7
O5	H5	O7	0.84	1.80	2.545(6)	147.0
O00C	H00C	O10	0.84	1.80	2.539(6)	145.6
O8	H8A	O1[2]	0.88	2.10	2.694(6)	124.8
O8	H8B	O6[2]	0.88	1.79	2.647(6)	163.6
O15	H15A	F7[3]	0.88	2.31	3.160(7)	160.4
O15	H15B	O14[3]	0.88	1.82	2.699(6)	170.2
O1	H1	O3	0.84	1.80	2.538(6)	145.8
O4	H4B	O00C[4]	0.88	1.85	2.707(6)	163.4
C22	H22	O14[2]	0.95	2.65	3.538(8)	156.5
C19	H19	F6[5]	0.95	2.38	3.277(9)	157.4
C35	H35	O2[4]	0.95	2.45	3.366(8)	163.2
C6	H6	F1[6]	0.95	2.50	3.412(10)	159.8

[1]1-X,-2+Y,1/2-Z; [2]+X,-1+Y,+Z; [3]+X,1+Y,+Z; [4]-X,+Y,1/2-Z; [5]+X,2-Y,-1/2+Z; [6]-X,3-Y,-Z

It is very important to know the single crystal structures of the gelators studied herein as the design aspect of the peptide conjugate and normal organic salts was based on an assumption that various hydrogen bond functionalities such as amide•••amide and ammonium•••carboxylate would display different kind hydrogen bonding. We tried our best to crystallize all the zinc complexes and we are able to crystallize seven zinc complexes which were characterised thoroughly by CHN, FTIR, ^{1}H NMR and UV-vis spectroscopy (see Figure S2-S4). Nicely grown needle shaped yellow crystals from MeOH in solvothermal process (70 ^{o}C) of **(IND)$_2$.Zn** complex were diffracted and from the SXRD studies it was revealed that parallel 1D hydrogen bonding network (HBN) was present assisted by MeOH solvate with the adjacent carboxylate COO^- involving in O-H•••O H-bonding. Methyl C-H•••π weak interactions were present in the structure. For **(DIC)$_2$.Zn** complex, we had nice colorless block shaped crystals from MeOH by slow evaporation method in beaker and from the SXRD studies it was clear that intramolecular N-H•••O H-bonding was present in the crystal structure of **(DIC)$_2$.Zn** complex and MeOH solvate assisted 2D HBN was present involving two different kinds of O-H•••O H-bonding interactions. There were aromatic Cl•••π and C-H•••π weak interactions also present in the structure. SXRD mountable block shaped single crystals were grown from MeOH by slow evaporation method in beaker for **(TOL)$_2$.Zn** complex and here a trimeric metal cluster was formed containing three co-linear zinc metal-ions where the central metal-ion was found to be octahedral geometry and the terminal two were distorted tetrahedral. These secondary building units (SBUs) were reinforced by MeOH solvate supported O-H•••O H-bonding interactions. Colorless plate shaped single crystals of **(IBU)$_2$.Zn** complex were grown from MeOH-DMF (1:1) in long tube by slow evaporation method and here two carboxylates of two **IBU** molecules chelated zinc metal-ion which was in tetrahedral geometry having two solvent water molecules coordinated with the zinc metal center forming a O-H•••O 1D HBN involving the solvate

water and adjacent carboxylate anion. **$(FLR)_2$.Zn** complex was also crystallized in MeOH-DMF (1:1) in long tube by slow evaporation method as colorless plate shaped crystals and a 2D HBN was present in the structure due to O-H•••O H-bonding networks. For the **$(SUL)_2$.Zn** complex, the dark orange-yellow crystals were obtained from MeOH by slow evaporation method in beaker and a 2D HBN was present in the structure due to amide N-H•••N H-bonding and MeOH solvate supported O-H•••O H-bonding interactions with the adjacent carboxylate. Lastly for **$(DIF)_2$.Zn** complex, nice plate shaped colorless single crystals were grown from MeOH-DMF (1:1) in close tube by solvothermal method (70 ^{o}C) and the structure revealed the presence of a 2D HBN consisting of O-H•••O H-bonding involving solvate water and adjacent –OH group of **DIF**.

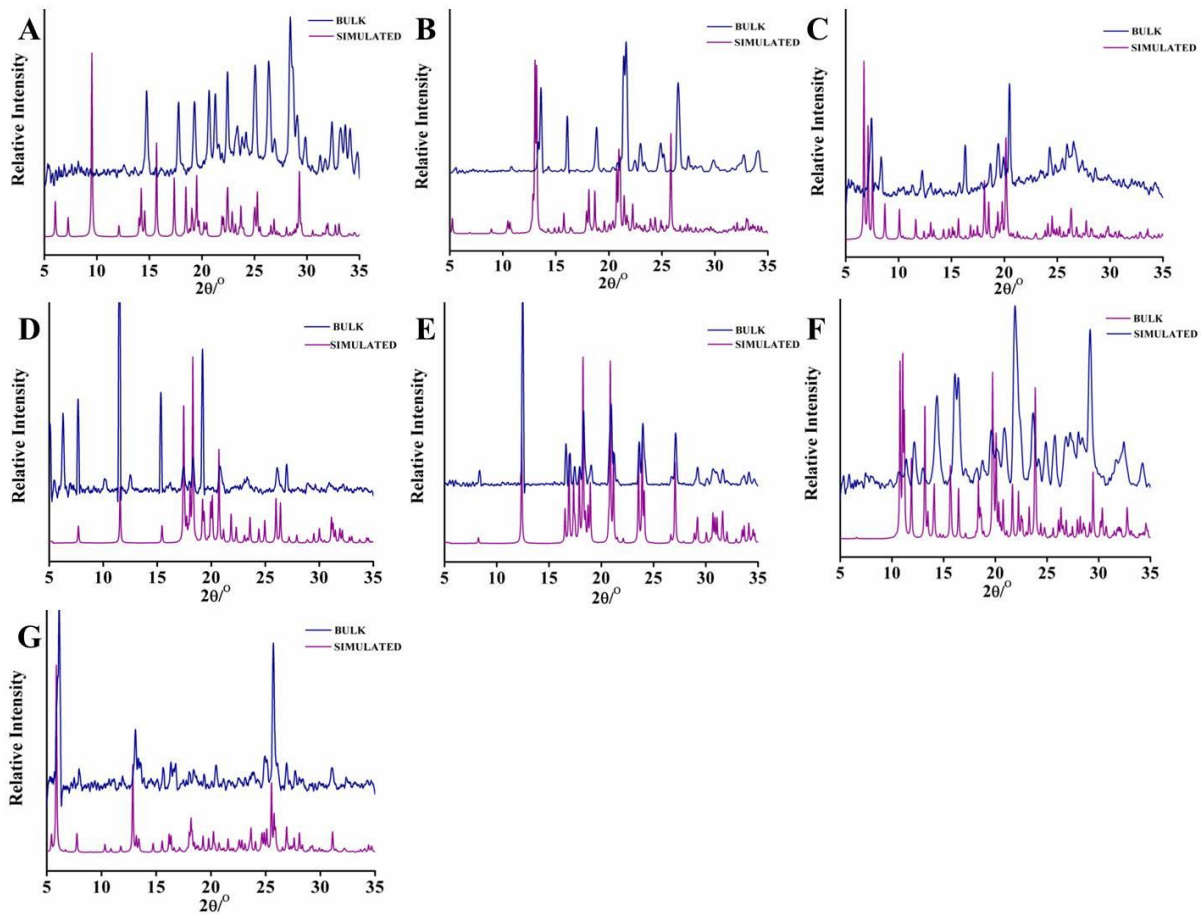

Figure S51: X-ray powder diffraction pattern of (A) **$(IND)_2$.Zn**, (B) **$(DIC)_2$.Zn**, (C) **$(TOL)_2$.Zn**, (D) **$(IBU)_2$.Zn**, (E) **$(FLR)_2$.Zn**, (F) **$(SUL)_2$.Zn** and (G) **$(DIF)_2$.Zn**.

Stability experiment

Incubation of the metallohydrogelator DIF.TRIS.Zn in PBS: The biostability of the metallohydrogelator was studied in near physiological conditions in aqueous buffer solutions (PBS) of pH 7.4 at 37 ^{o}C. After keeping 48h, the sample was subjected to UV absorbance which showed no degradation of the metallohydrogelator (see Figure S52).

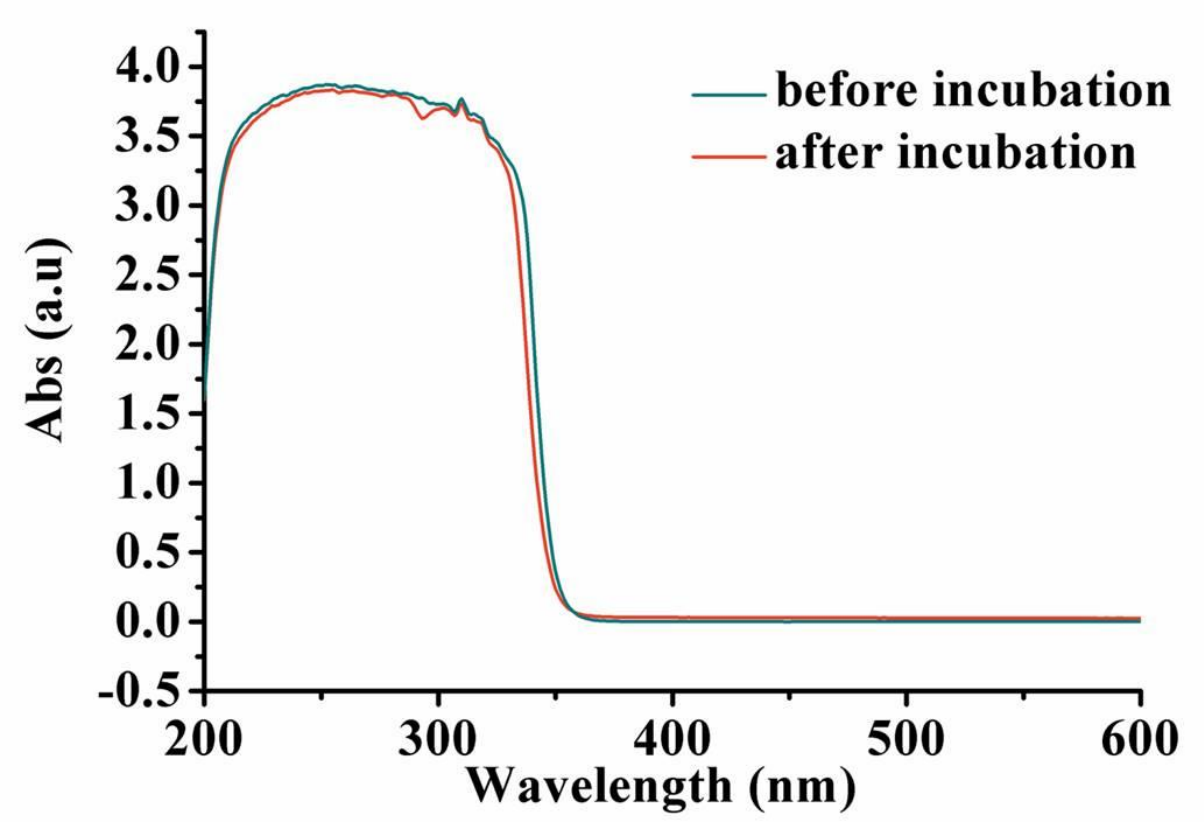

Figure S52: UV absorbance of the before and after PBS incubated metallohydrogelator of **DIF.TRIS.Zn**.

Solubility

Solubility studies were performed following literature procedure with minor modification (Higuchi T.; Connors, K. A. *Adv. Anal. Chem. Instru.* **1965**, *4*, 117-212). An excess of the metallohydrogelator was added to 5 mL of pure water taken in a glass flasks. The mixtures were then sonicated for 10 mins and heated for 2 minutes around 40^{o}-50 ^{o}C. The sample was then allowed to stand room temperature (25 ^{o}C) at least for 3 days to reach the equilibrium. After 3 days; the supernatant solution was filtered to ensure that that was free from any particulate matter. Concentration was determined by measuring absorbance after appropriate dilution and interpolation from the standard UV spectrophotometry calibration curve for the metallohydrogelator in pure water (see Figure S53).

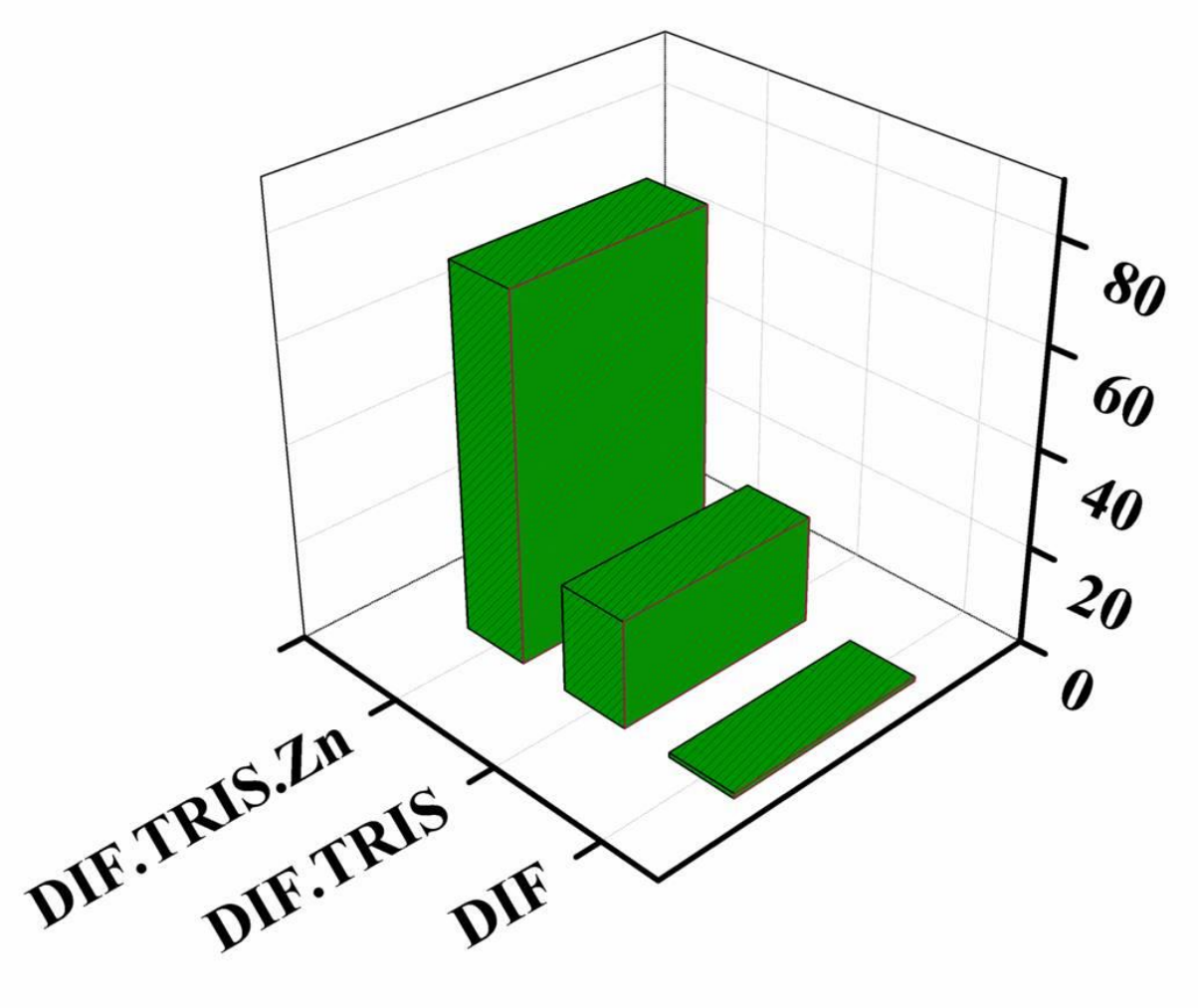

Figure S53: Increament of the water solubility of the metallohydrogelator **DIF.TRIS.Zn** with respect to **DIF.TRIS** salt and **DIF**.

Hydrogel leaching experiment

To demonstrate the sustained release of the metallohydrogelator **DIF.TRIS.Zn**, we placed 100 μl PBS (pH 7.4) over 100 μl 4 wt% metallohydrogel taken in a test tube; five such test tubes were incubated at 37 ^{o}C for various time intervals at 3h, 6h, 9h,12h and 24h and the concentration of the gelator in the PBS layer was measured in triplicate by spectrophotometric method after appropriate dilution and interpolation from previously standard UV spectrophotometry calibration curves at 264 nm for the metallohydrogelator **DIF.TRIS.Zn** in PBS (see Figure S54).

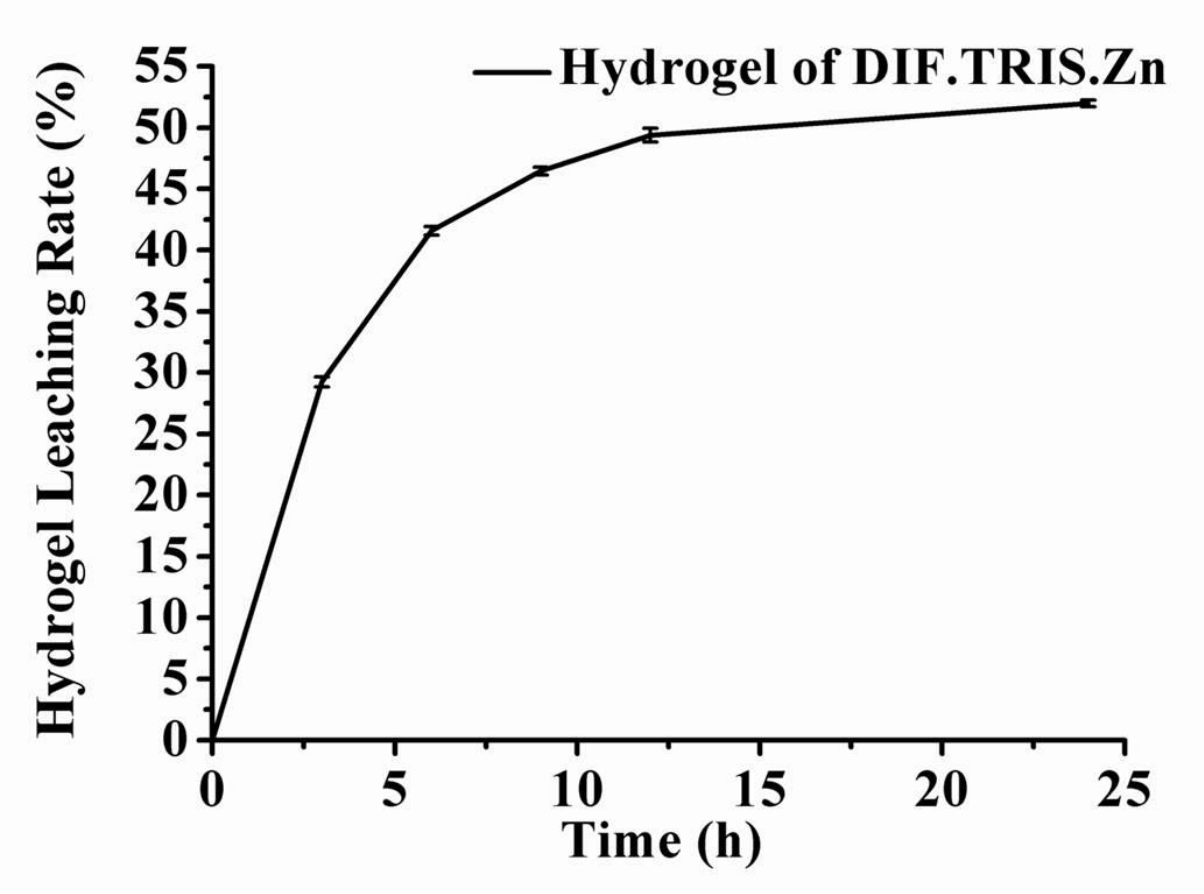

Figure S54: Sustained release of the metallohydrogelator **DIF.TRIS** in PBS (pH 7.4).

MTT Assay

The cytotoxicity of the metallohydrogelator was evaluated in RAW 264.7 cells using standard MTT (3-(4, 5-Dimethylthiazol-2-yl)-2,5-diphenyltetrazolium bromide) assay. The mouse macrophage RAW 264.7 cells were purchased from American Type Culture Collection (ATCC) and maintained following their guidelines. The cells were grown in Dulbecco's Modified Eagle's Medium (DMEM) supplemented with 10% Fetal Bovine Serum (FBS), 1% penicillin and streptomycin in a humidified incubator at 37 °C and 5% CO_2. The cells were seeded in 96-well plates at a density of 1×10^4 cells/well for 24 h. After 24 h of seeding, the cells were treated with various concentrations (upto 200 μM) of the compound or DMEM alone for 72 h in humidified incubator at 37 °C and 5% CO_2. Then, the culture medium was replaced with 100 μg of MTT per well and kept for 4 h at 37 °C. To dissolve the

formazan produced by mitochondrial reductase from live cells, DMSO (100 µL/ well) was added and incubated for 30 minutes at room temperature. The color intensity of the formazan solution, which is positively correlated to the cell viability, was measured using a multiplate ELISA reader at 570 nm (Varioskan Flash Elisa Reader, Thermo Fisher). The percentage of live cells in metallohydrogelator-treated sample was calculated considering DMEM-treated sample as 100%.

PGE_2 Assay

Production of PGE_2 was estimated according to a published protocol using 6-well plate and RAW 264.7 cell line. Approximately $1x10^6$ cells/well were seeded in 6-well plate (4 wells using 6-well plate) for 24 hrs. One of the wells was treated with 2 mL of DMEM only as control experiment, the rest three wells were treated with 1 µg/mL lipopolysaccharide (LPS) and 100 ng/mL interferon-gamma (IFN-γ); out of these LPS/IFN-γ treated wells, two well was treated with 50 µM (< IC_{50}) **diflunisal (DIF)**, **DIF.TRIS** and **DIF.TRIS.Zn** respectively in such a way that the total media (DMEM) volume in each well was 2 mL and all the wells were further incubated for 24 h. The culture media was diluted to 1:100 or 1:500 for measuring PGE_2 using Prostaglandin E_2 EIA Kit – Monoclonal (Cayman Chemicals, Ann Arbor, MI). This experiment was done in triplicate.

Cell imaging

Having successfully evaluated the biocompatibility of the hydrogel, it was applied in cell imaging. RAW 264.7 cells were cultured by using DMEM supplemented with 10% FBS and 1% penicillin–streptomycin on ethanol etched cover slips kept in a 35 mm tissue culture dishes. These were preserved in a humidified incubator at 37 ^oC overnight. Then the media was removed and fresh metallohydrogelator containing media was added (1mM). It was incubated for 15 minutes. After that, the media was removed and fresh PBS was added. The

cells were mounted on a confocal petridish and Carl Zeiss axio observer z1 fitted with Hamamatsu orca flash 4.0 was used to acquire the images.

Antibacterial studies

Determination of minimum inhibitory concentration (MIC)

A hot nutrient solution (1 L) containing peptone (5 g), agar (15 g) and yeast extract (3 g) in sterile water was poured into a hard glass test tube and kept it slanted at rt. to form gel (5 mL). A sterile wire loop was used to spread the corresponding bacteria (*E. Coli* or *B. Subtilis*) on the gel surface thus formed and incubated at 37 ^{o}C for 24 hrs. 5 mL sterile water was then poured into the test tube and swirled in order to make a suspension of the cultured bacteria, and 100 µL of the suspension was then diluted with 1.5 mL of sterile water and 100 µL of the diluted suspension was further diluted with 1.5 mL of sterile water. To attain the working concentration of the bacteria ($7.5x10^{7}$–$1x10^{8}$ cfu/mL for *B. Subtilis* and $3.75x10^{7}$–$7.5x10^{7}$ cfu/mL for *E. Coli*), 100 µL of the diluted suspension was then added to each of the 5 test tubes containing 5 mL of LB media. Keeping one of the test tubes as control, required amount of the corresponding drug (**DIF** or **DIF.TRIS.Zn**) was added in order to achieve four different concentrations of the corresponding drug (25, 50, 100 and 200 µg/mL). 100 µL of the control as well as drug treated bacterial suspension was then spreaded on 5 petri dishes (150 mm x 15mm) containing 5 mL nutrient gel and incubated at 37 ^{o}C for 24 hrs. One negative control was also performed wherein Triton X (50 µL in 5 mL LB media) was used. The bacterial colonies thus grown on the petri dishes were then counted. MIC (concentration of the drug that kills half of the colonies present in control experiment) of the corresponding drug was calculated by comparing the number of colonies present in nontreated (control) and treated petri dishes.

Determination of zone of inhibition

A hot solution containing 1 wt % gelator [comprising the solid components (peptone, agar and yeast extract) used in nutrient solution and gelatin in 2:1 (w/w) ratio] was prepared in PBS and required amount of the corresponding drug was added in order to achieve the corresponding MIC. To crosslink the gel network, glutaraldehyde (0.15 wt %, w/v) was added to this solution. 1 mL of this solution was poured into a 24 well plate. A control was performed wherein no drug was added. The well plate was then heated at 50 ^{o}C for 12 hrs to form thin films. The films were then treated with 0.1 mM glycine for 1 hour to block the remaining free aldehyde groups. The films were then washed for several time with sterile water to remove the excess glycine and then with PBS to neutralize the surface. The films so treated were again dried at 50 ^{o}C overnight and the sterilized using UV radiation. The thin films were then scooped out and placed at the center of petri dishes containing the corresponding bacteria grown on nutrient gel and incubated at 37 ^{o}C for 24 hrs. A ring of bacteria free zone centered around the thin film was observed in each case. The zone of inhibition was determined by subtracting the diameter of the thin film from the diameter of the bacteria free zone.

Table S12: Determination of MICs.

Bacterial stain	Compounds	MIC (µg/mL)
B.subtilis	**DIF**	**7.0**
	DIF.TRIS.Zn	**6.0**
E.coli	**DIF**	**75.0***
	DIF.TRIS.Zn	**23.0**

Eur. J. Med. Chem.*2003**, *38*, 1005-1013.

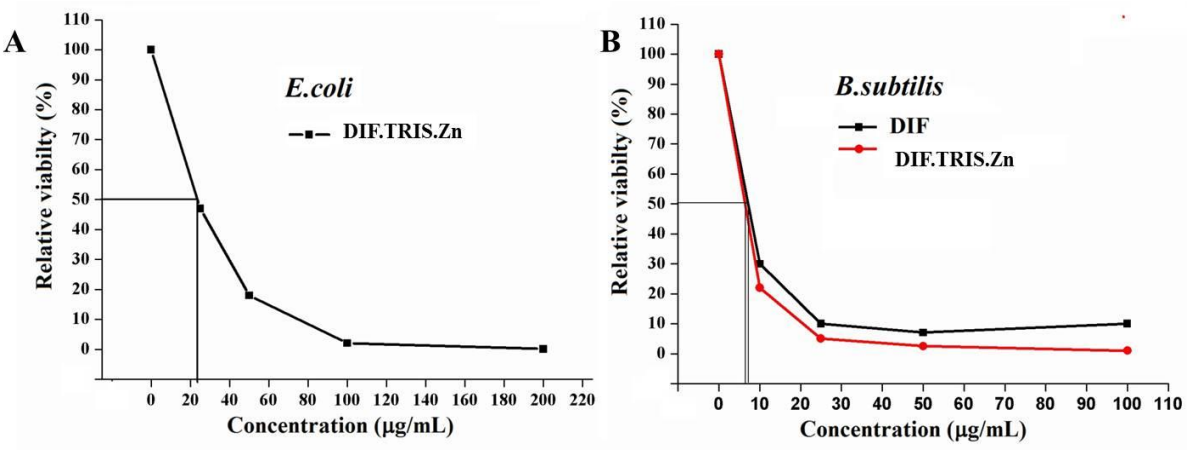

Figure S55: Relative viability of (A) *E.coli* and (B) *B.subtilis* after 6 h of incubation on the **DIF** and **DIF.TRIS.Zn** with concentration of the compounds. These were determined using the colony count method. The rectangles indicate the respective MIC values.

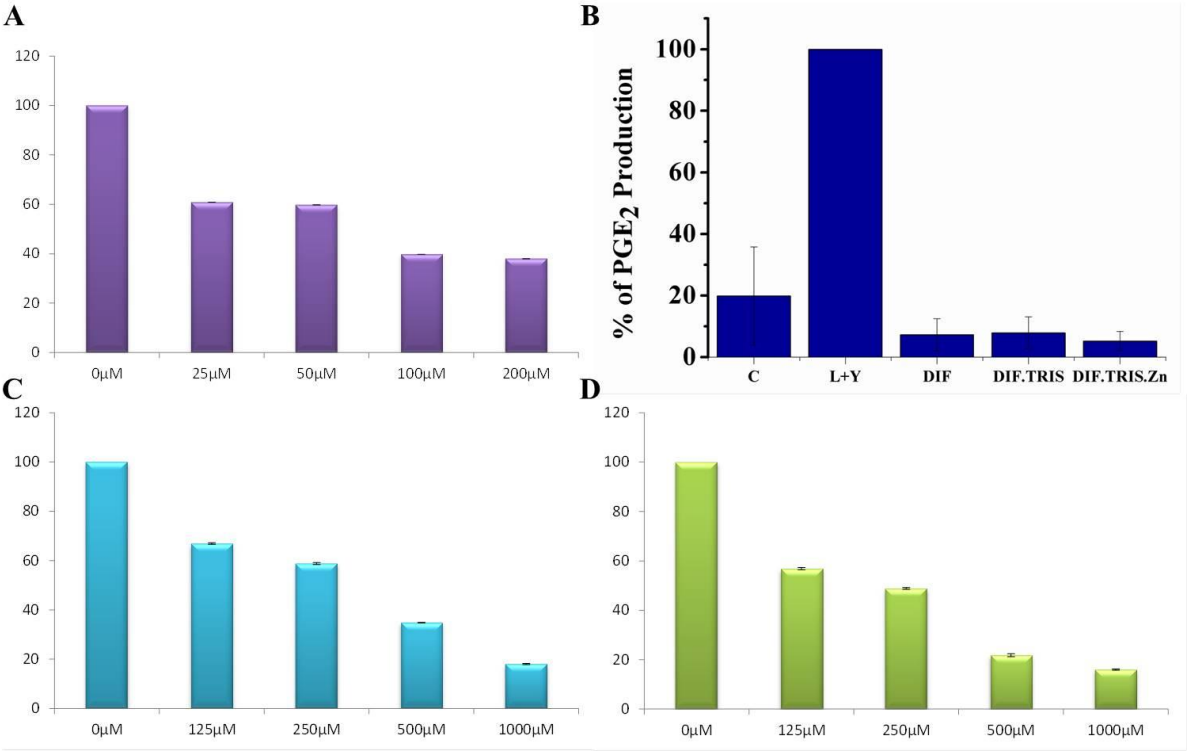

Figure S56: MTT assay of metallohydrogelator **(**A) **DIF.TRIS.Zn**, (C) **DIF**, (D) **DIF.TRIS** salt in RAW 264.7 cells for 72 h at 37 °C; (B) PGE_2 assay of **DIF**, **DIF.TRIS** salt and metallohydrogelator **DIF.TRIS.Zn**. Here DIF = Diflunisal, L = Lipopolysaccharide, Y= Interferon-γ.